MICROSEGREGATION IN NODULAR CAST IRON AND ITS EFFECT ON MECHANICAL PROPERTIES

by

G. Jolley, Dip.Tech. A.C.T.(Birm.).

A thesis submitted for consideration for the degree of Ph.D of The University of Aston in Birmingham.

March 1966

CONTENTS

SUMMARY

A review of the literature pertaining to the mechanical properties, solidification and segregation effects in nodular cast iron has been made. A series of investigations concerning the influence of microsegregation on mechanical properties of pearlitic, ferritic and austenitic nodular cast iron have then been reported.

The influence of section size on the tensile and impact properties of commercial purity and refined ferritic nodular cast iron has been studied. It has been shown that an increase in section caused a decrease in impact transition temperature of the commercial purity material without greatly affecting the impact transition temperature of the purer material. This effect has been related to increased amounts of segregation effects such as cell boundary carbides in heavier sections of the commercial purity material.

Microsegregation studies on the materials used in this thesis have been carried out using an electron probe microanalyser. This technique has shown that concentrations of chromium and manganese and depletions of nickel and silicon occurred at eutectic cell boundaries in nodular cast iron and were often associated with brittle carbides in these areas. These effects have been shown to be more prevalent in heavier sections.

The nature of segregation during the solidification of nodular cast iron has been studied by quenching samples of nodular iron during the solidification process. Micro-analysis of such samples has shown that segregation of manganese and chromium occurs by a gradual build-up of these elements at the solid/liquid interface.

The microstructures of the quenched specimens revealed carbide filaments connecting graphite nodules and areas of quenched liquid. These filaments have been used as evidence for a revised hypothesis for the solidification of nodular cast iron by a liquid diffusion mechanism.

A similar series of experiments has been carried out on two high nickel austenitic irons containing 0.5 per cent manganese and 4 per cent manganese respectively. In both these materials a decrease in elongation was experienced with increasing section. This effect was more drastic in the 4 per cent manganese material which also contained much greater amounts of cell boundary carbide in heavy sections.

Micro-analysis of samples of the 4 per cent manganese material quenched during solidification revealed that manganese concentrated in the liquid and that nickel concentrated in the solid during solidification. No segregation of silicon occurred in this material. Carbide filaments appeared in the microstructures of these specimens.

A discussion of all the above effects in terms of current concepts is included.

INTRODUCTION

In normal grey cast iron the graphitic carbon is in the form of flakes or lamellae, many of which are interconnecting. These create discontinuities in the metallic matrix and act as stress raisers thus rendering the material weak and brittle. Malleable cast iron contains more rounded graphite particles which are not connected, giving the material much superior strength and ductility. The process involves lengthy heat treatment however and cannot be applied to heavy-section castings. The announcement of nodular graphite iron produced in the as-cast state was thus received with great interest in the foundry industry.

Nodular graphite produced by treatment of the molten metal with cerium was announced by Morrogh and Williams[1] in March 1948. Pfeil[2] and Wickenden[3] later announced an alternative process involving magnesium treatment of the molten metal. The magnesium process has since been favoured for economic reasons. However, when irons contained certain trace elements, e.g. lead and bismuth, fully nodular structures were not always obtained by magnesium treatment. Morrogh[4] discovered that a small addition of cerium together with the normal magnesium addition offset the effect of these elements on the nodular graphite structure. It has since become industrial practice to combine cerium and mag-

nesium additions where harmful trace elements are expected to be present.

In the last eighteen years nodular cast iron has made substantial industrial progress and has replaced grey cast iron, non-ferrous alloys and cast or forged steel with advantage and economy for a number of applications. The material possesses high strength, ductility and toughness and by controlling the heat treatment and chemical composition the full range of matrix structures common to steel and flake graphite cast iron can be produced, giving the material a wide range of application and properties.

The invention of the electron probe micro-analyser by Castaing[5] in 1951 and its subsequent rapid development has enabled quantitative studies on the distribution of alloying elements in various metallic materials to be made on a micro scale. In the past few years a great deal of work has been published in this field. Nodular cast iron, although purer than commercial grey iron, usually contains a number of elements which might be expected to segregate during solidification. Very little work has been reported on the application of the micro-analyser to detect segregation in nodular cast iron although mention is often made in the literature of segregation and its subsequent homogenisation by heat treatment.

This thesis will describe investigations of the nature of microsegregation in nodular irons with ferritic and austenitic

matrices and its effect on mechanical properties. A review of the relevant literature will first be made describing the mechanical properties of these materials and the present state of knowledge of segregation in nodular cast iron including a description of the eutectic solidification process.

LITERATURE REVIEW

INTRODUCTION

Nodular cast iron can be produced in a full range of matrix structures resulting from alloying and heat treatment. This thesis is concerned with irons having pearlitic, ferritic and austenitic matrices.

Nodular cast irons are normally hypo-eutectic in composition, i.e. the carbon equivalent (carbon content + one third of the silicon content) is less than 4.3. The as-cast material usually possesses a pearlitic matrix (Fig. 1) or a mixture of ferrite and pearlite if the cooling rate is slower, i.e. in thicker sections. As-cast pearlitic nodular cast iron is characterised by high strength and hardness. Both of these properties are improved by a normalising treatment of holding in the austenitic region and air cooling. This refines the pearlitic matrix. Fig. 2 depicts the microstructure of a typical normalised nodular cast iron. When a pearlitic nodular cast iron is annealed the combined carbon is broken down and re-distributed as graphite around the graphite nodules leaving a ferritic matrix (Fig. 3). This material possesses increased toughness and ductility at the expense of tensile strength.

Alloying nodular iron with 20-30 per cent of nickel results in an austenitic matrix (Fig. 4). Austenitic irons are tougher

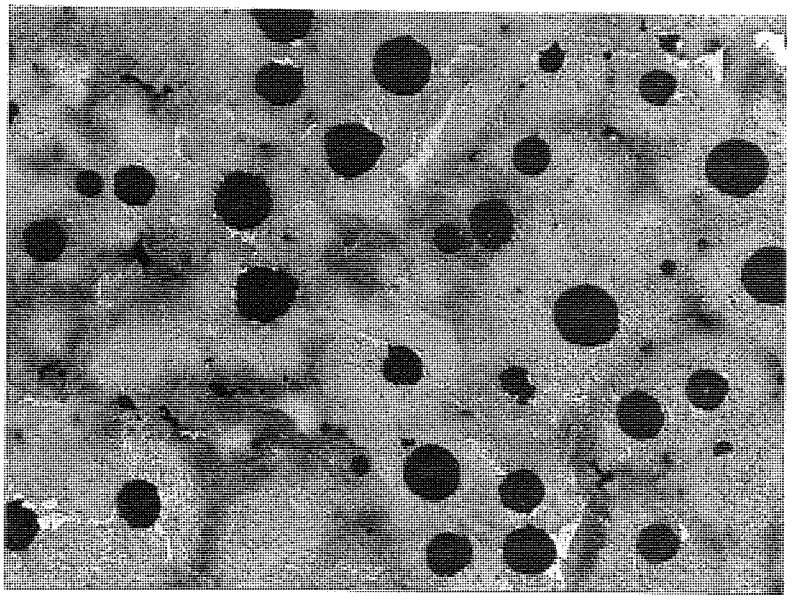

FIG. 1 Pearlitic nodular cast iron, as-cast.
Etched in 4% Picral x 100

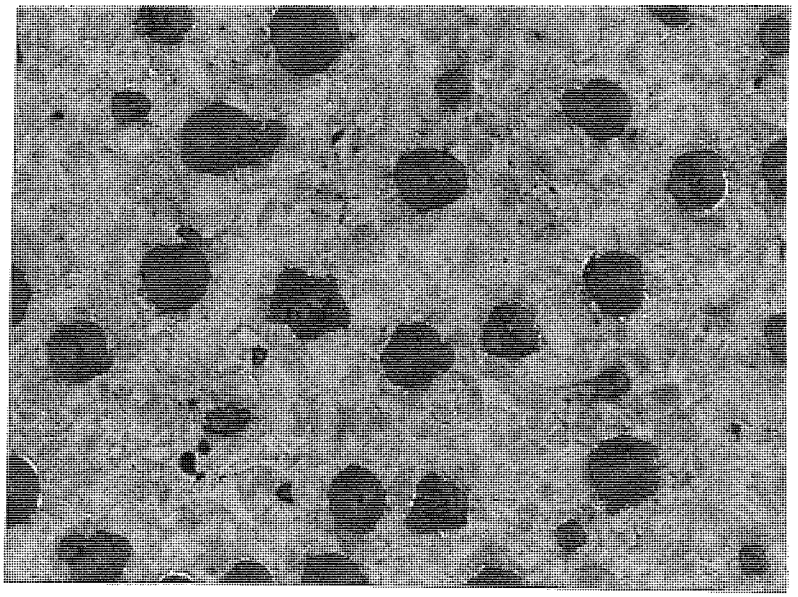

FIG. 2 Pearlitic nodular cast iron, normalised.
Etched in 4% Picral x 100

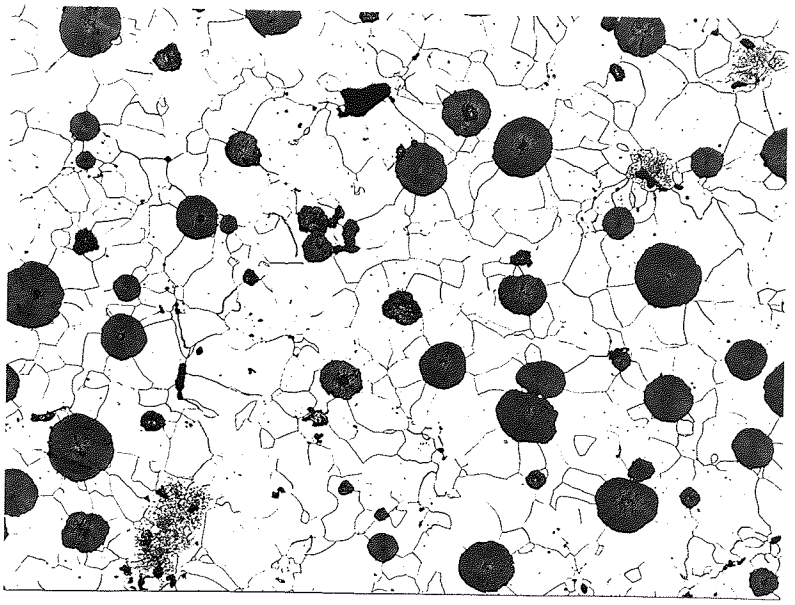

FIG. 3 Ferritic nodular cast iron.
Etched in 5% Nital x 100

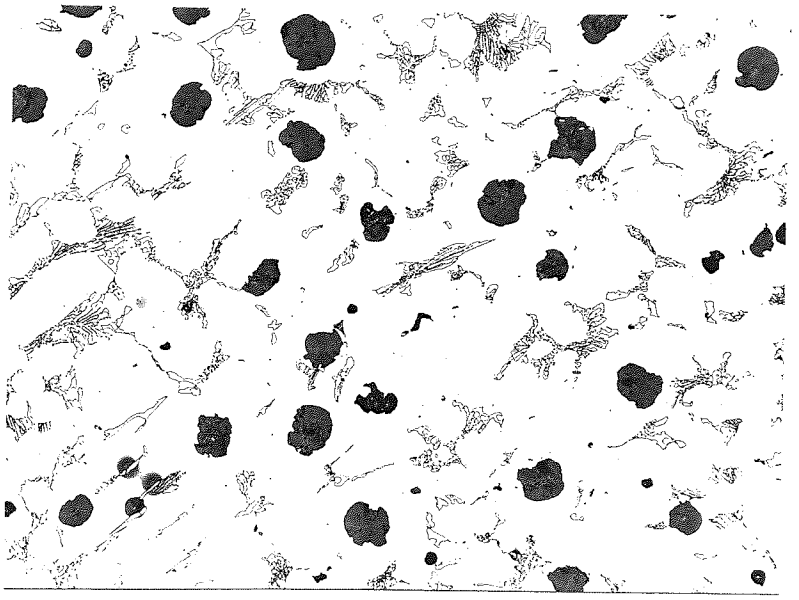

FIG. 4 Austenitic nodular cast iron.
Etched in 10% Nital x 100

and more ductile than ferritic irons and retain their properties over a much wider range of temperature. They also exhibit outstanding resistance to many types of corrosion and erosion.

In this review the literature relating to the mechanical properties of nodular cast iron will be surveyed. A separate section will be devoted to austenitic irons. The eutectic solidification process of nodular cast iron will be described and observations of segregation in nodular cast iron will be reviewed. Finally, the possible significance of segregation in nodular cast iron will be assessed.

MECHANICAL PROPERTIES OF NODULAR CAST IRON

General The mechanical properties of nodular cast iron vary widely depending upon the matrix structure and the properties associated with the different structures have been outlined above. In the next few paragraphs these properties are discussed in detail.

The stress-strain relationship of a nodular cast iron shows many similarities to that of a steel with a similar matrix structure. Gilbert[6] compared the stress-strain curves of a low carbon steel and a ferritic nodular cast iron. Fig. 5 shows the results of Gilbert's investigation. It can be seen that initially the ferritic iron showed elastic behaviour under stress but unlike the steel did not exhibit a yield point. The onset of plastic deformation was more gradual in the nodular iron than in the steel. The steel had a somewhat higher ultimate tensile strength

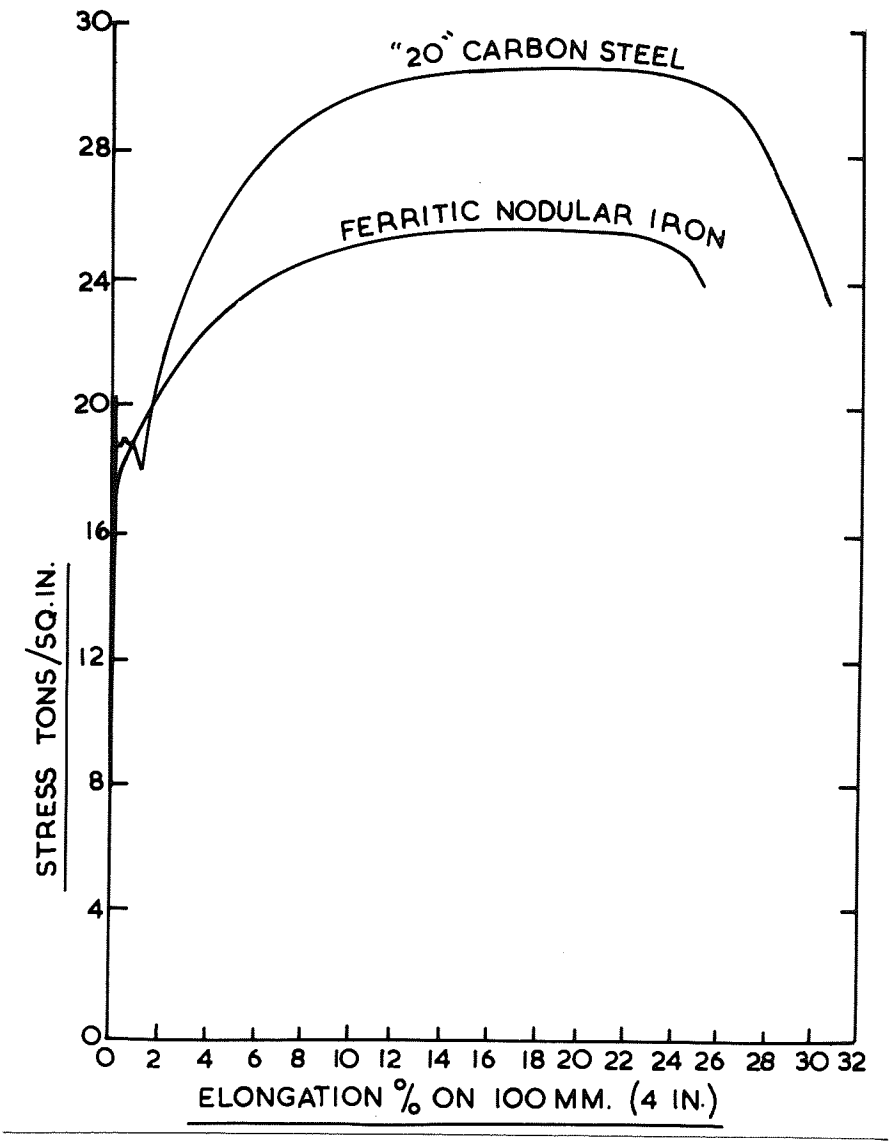

FIG. 5 Tensile curves for low carbon steel and ferritic nodular cast iron (after Gilbert[6]).

and elongation than the ferritic iron and also showed a much greater reduction in area. It was recommended that a proof stress value should be quoted for nodular cast iron as the material did not exhibit a yield point. Gilbert[7] augmented the results of these studies by a further investigation into the mode of deformation of nodular cast iron. By studying the microstructures of samples of nodular irons at progressive stages of the tensile test Gilbert was able to relate microstructural changes with stress-strain curves for pearlitic and ferritic nodular cast iron. He showed that during plastic deformation voids developed at the graphite/metal interface in pearlitic irons and at the primary graphite/secondary graphite interface in ferritic irons. In pearlitic irons the voids were not as far developed as in ferritic irons due to the fact that pearlitic material failed at a lower strain.

The mechanical properties of nodular cast iron are influenced by a number of variables. These include nodule size and number, ferrite grain size and the microconstituents present in the structure.

The effect of ferrite grain size on mechanical properties has been investigated by Gilbert[8]. By austenitising at various temperatures followed by a sub-critical anneal at 690°C Gilbert varied the grain size of a number of nodular irons of the same composition. He showed that as the ferrite grain size decreased the proof stress increased but the elongation decreased.

The size and number of graphite nodules would be expected to affect the mechanical properties by affecting the nature of void formation during plastic deformation. Graphite nodule size and number can be varied by varying the carbon content of the material. Reynolds, Adams and Taylor[9] tested a series of nickel free nodular irons with silicon contents of 3.13 per cent and carbon contents varying from 2.26-4.0 per cent. They found that increasing the carbon content resulted in a decrease in proof stress, elongation and ultimate tensile strength. Increasing the carbon content also resulted in an increase in nodule number and they concluded that the decrease in tensile properties were due to an effective decrease in matrix cross-sectional area brought about by the increase in carbon content. Gilbert[10] varied the carbon content of a series of 2 per cent silicon ferritic nodular irons and confirmed the results of the previous workers. He also showed that the impact value in the ductile range was higher in the case of low carbon material.

It has been shown that the mechanical properties of nodular cast iron are influenced by section size. Barton[11] investigated the mechanical properties of heavy section nodular iron castings and showed that the ultimate tensile strength and elongation of as-cast pearlitic and the elongation of annealed ferritic samples from a 12 in diameter bar were less than would be expected from smaller sections although the proof stress values were of the same order. Barton showed that the notched impact values of the heavy

section samples were slightly greater than would be found in smaller sections. During the course of this thesis Gilbert[12] investigated the effect of section size on the stress-strain properties of nodular cast iron. His results showed that ultimate tensile strength and elongation in as-cast and normalised material decreased with increasing section size while the proof stress values remained unchanged. Gilbert stated that these effects were associated with early failure of the larger section material on the stress-strain curve. The material used for this investigation was of commercial purity and the heavier sections contained a certain amount of cell-boundary carbides. The nodule size increased and the number decreased with increasing section. It has been shown that the latter factor could have an effect on mechanical properties but the presence of hard brittle carbides in the matrix which would undoubtedly act as stress raisers could also exert some effect on the stress-strain curve. However, as Gilbert pointed out the heavier section material only exhibited deleterious properties in the plastic range, therefore the engineering properties of importance to the designer do not deteriorate with increase in section.

Sandoz, Pellini and Bishop[13] have demonstrated the effects of microconstituents on the mechanical properties of nodular cast iron. These workers showed that increasing the amount of pearlite in a ferritic nodular cast iron resulted in an increase in the ultimate tensile strength and proof stress values with a corres-

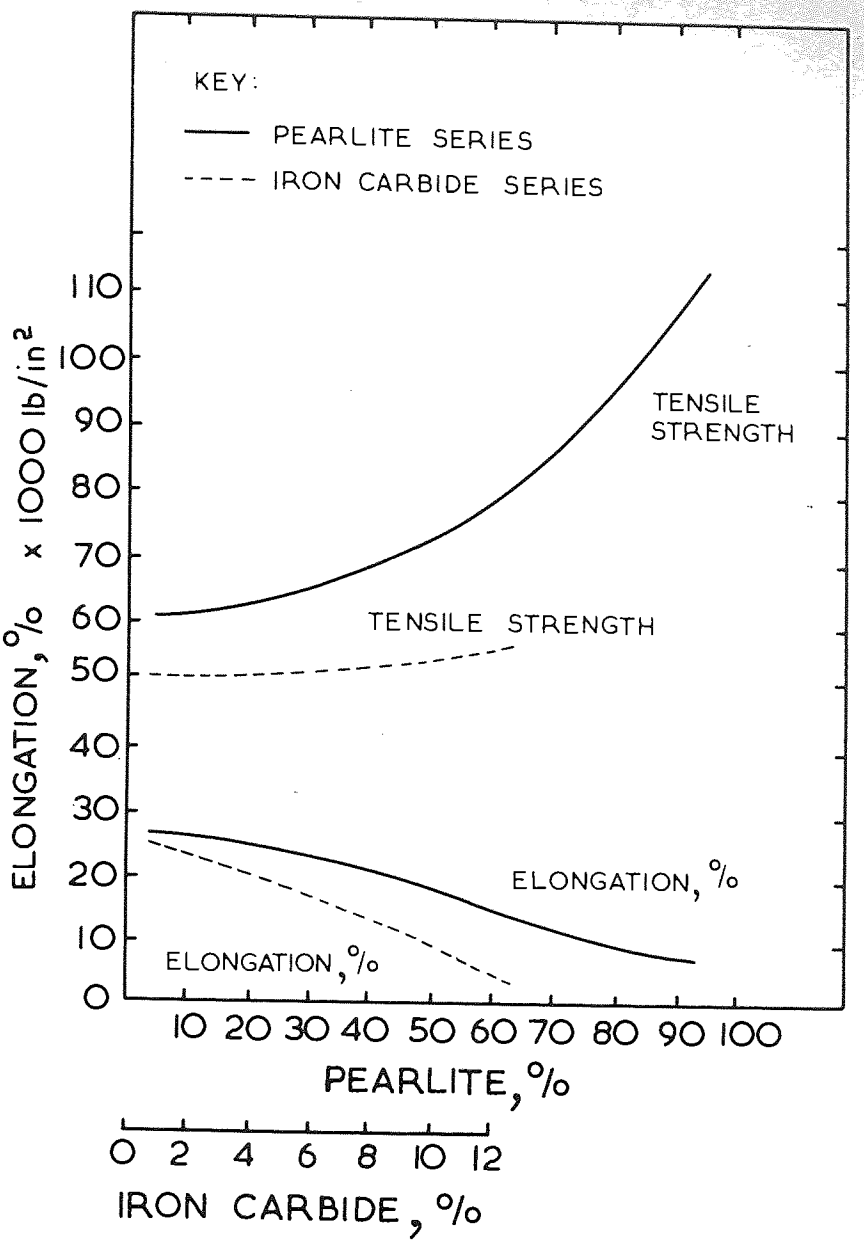

FIG. 6 Effect of pearlite and iron carbide on tensile properties of nodular cast iron (after Pellini, Sandoz and Bishop[13]).

ponding decrease in elongation (Fig. 6). Pellini, Sandoz and Bishop also showed that increasing amounts of carbide in the microstructure drastically reduced the elongation and caused a slight increase in proof stress and ultimate tensile strength.

The effect of segregation of various elements on the mechanical properties of nodular cast iron has not been studied directly. However, microconstituents such as cell-boundary carbides and retained pearlite can result from microsegregation of alloying elements in nodular cast iron. It has been shown that increasing the manganese and/or chromium contents increases the amount of cell-boundary carbide[14] and retained pearlite[15] in nodular cast iron.

Ductile-Brittle Transition in Nodular Cast Iron In 1953 Gilbert[16] and later Carr and Stevens[17] showed that ferritic nodular cast iron, like steel,[18] exhibited a ductile-brittle transition in the impact test. In the ductile range the fracture appeared dark and fibrous while brittle fractures were bright and faceted, typical of cleavage failure. Gilbert examined ductile and brittle fracture surfaces with a stereoscopic microscope and found that ductile fractures were covered with graphite nodules or spherical cavities left by the removal of nodules during fracture. Brittle fracture surfaces contained very few nodules and consisted of randomly oriented reflecting facets. Fig. 7 depicts microphotographs of ductile and brittle fractures taken from the work of Gilbert[16] showing the more direct route of the

FIG. 7 Photomicrographs of ductile and brittle impact fractures in ferritic nodular cast iron (after Gilbert[16]).

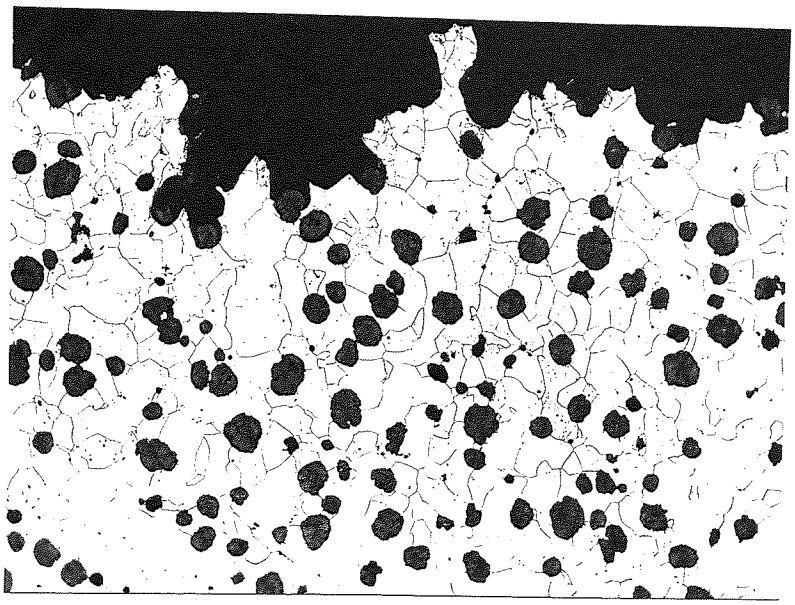

7(a) Ductile fracture.
Etched in 5% Nital x 100

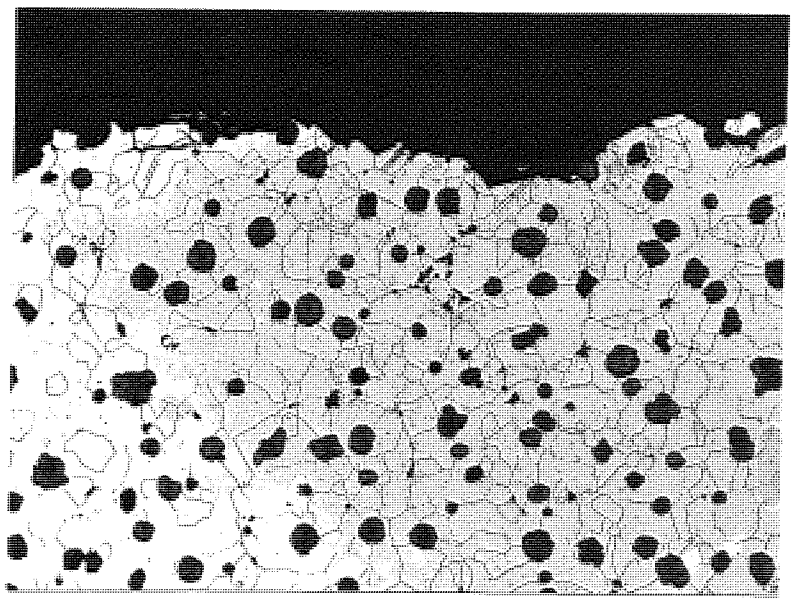

7(b) Brittle fracture.
Etched in 5% Nital x 100

brittle fracture which only occasionally passes through a graphite nodule. The appearance of graphite nodules on a ductile fracture is to be expected from the observations of Gilbert on the occurrence of voids around graphite nodules; fracture occurring by a linking up of these voids. In the same paper Gilbert produced results of notched and unnotched charpy impact and slow bend tests. He showed that silicon and phosphorus raised the ductile-brittle transition temperature in the impact test and by comparing the results obtained from slow bend and impact tests in notched and unnotched test pieces he deduced that the unnotched charpy test was a measure of the energy required to initiate a crack and the notched impact test was a measure of the crack propagation. However this comparison between results from slow bend and impact tests did not allow for the differences in strain rate involved between the two tests.

Pellini, Sandoz and Bishop[13] demonstrated the effect of chemical composition and microstructure on the notched impact transition of nodular cast iron and noted the harmful effect of silicon and phosphorus on impact transition temperature confirming the earlier work of Gilbert. They also found that the presence of pearlite above a limiting value of 10 per cent increased the impact transition temperature. Pearlite had no significant effect on the transition temperature of ferritic nodular cast iron below this limiting value (Fig. 8). The pre-

IMPACT TRANSITION CURVES FOR IRONS WITH INCREASING QUANTITIES OF PEARLITE. STANDARD 10 mm. SQUARE V NOTCHED SPECIMENS. (PELLINI)

FIG. 8

sence of carbide in the microstructure was also shown to raise the transition temperature markedly. One of the most interesting experiments reported in the same paper was a comparison between the notched impact properties of a high silicon ferrite having the same composition and structure as the matrix of a ferritic nodular cast iron and an ordinary ferritic nodular iron. Fig. 9, taken from the work of Pellini, Sandoz and Bishop, shows the results of these tests. The authors suggested that the superior impact transition properties of the nodular iron were a result of the graphite nodules interfering with brittle crack propagation and showed photomicrographs of brittle cracks terminating at nodules to support this theory. The inferior ductile impact properties noticed in the nodular iron can be explained by assuming that the nodules act as stress raisers and create voids at the graphite/metal interface, thus lowering the energy requirements for the nucleation and propagation of a ductile crack.

The effect of nodule size and number on impact properties was investigated by Gilbert[10]. The nature of the experiment has been described earlier (p.7). Increase in nodule number was found to lower the impact transition temperature slightly and cause a significant lowering in the ductile impact value which would be expected from the arguments previously put forward.

In 1955 Gilbert[19] showed that annealing nodular cast iron beneath the critical temperature resulted in a sub-boundary

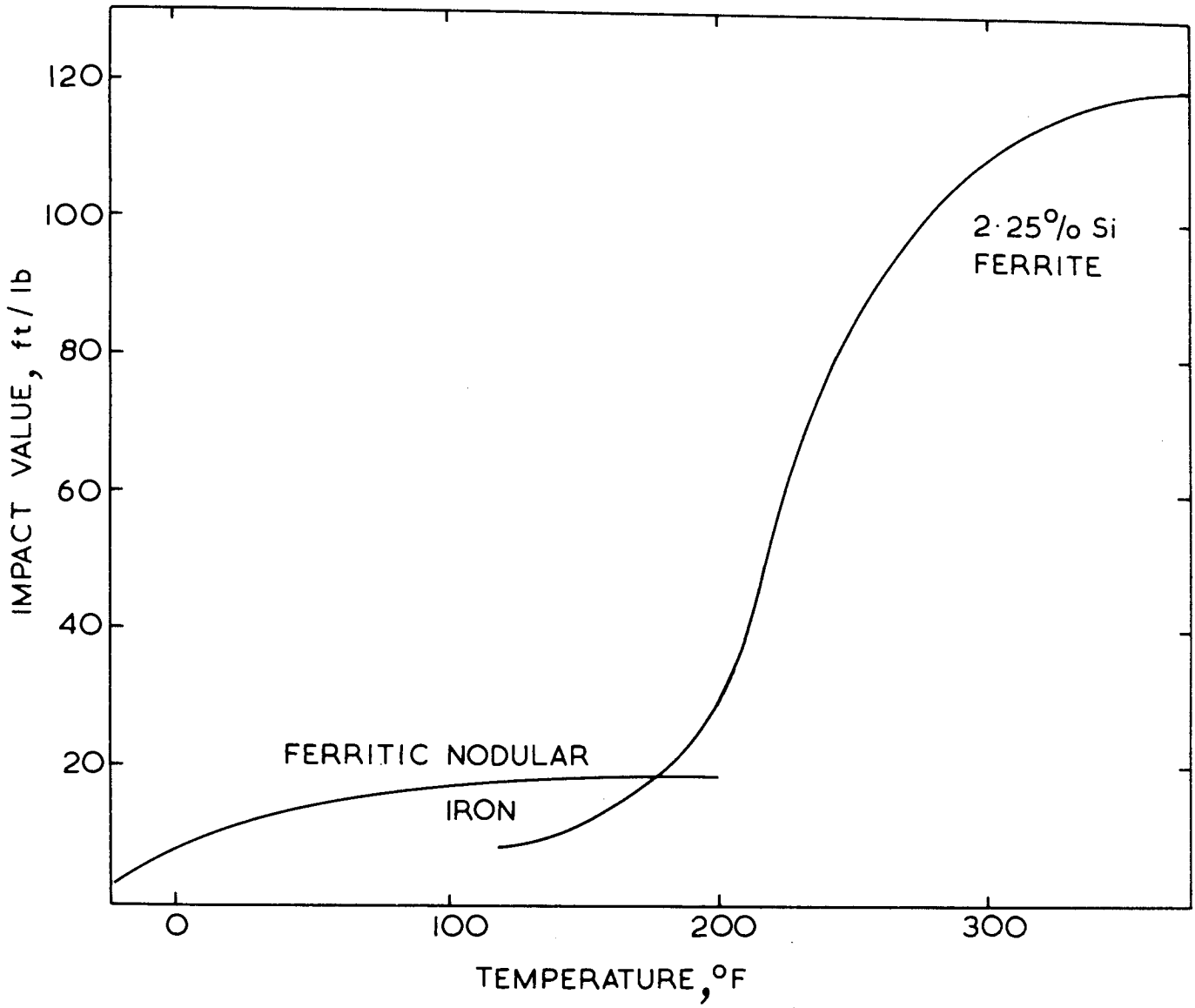

FIG. 9 Impact transition curves for a ferritic nodular cast iron and a 2.25 per cent silicon ferrite. (after Sandoz, Pellini and Bishop[13])

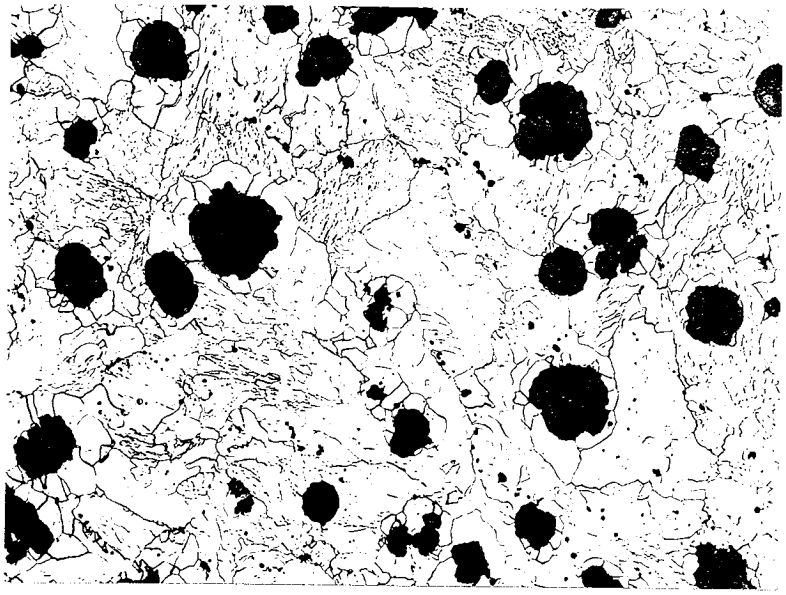

FIG. 10 Sub-boundary ferrite structure in a sub-critically annealed nodular cast iron (after Gilbert[19]).
Etched in 5% Nital x 100

ferrite structure (Fig. 10) which had a higher transition temperature and lower impact value in the ductile range than a ferritic nodular iron given a two stage annealing treatment, i.e. held in the austenitic range (900°C) before cooling to a sub-critical temperature. Satisfactory ferritic structures were also obtained after air cooling from 900°C before reheating to a sub-critical temperature. In a later paper[8] Gilbert demonstrated the effect of ferrite grain size on the impact transition temperature of nodular cast iron and showed that decreasing the ferrite grain size of a nodular cast iron caused a lowering of the impact transition temperature but no significant change in the ductile impact value was noticed.

Nodular cast iron also shows a ductile-brittle transition in tension which was first noticed by Gilbert and Palmer[20]. It will be shown below that this effect is related to the impact transition in this material.

Theory of Brittle Fracture The problem of brittle fracture has received considerable theoretical and experimental attention. For the purpose of this review it is deemed sufficient to outline the more modern concepts and show how they can be applied to the known behaviour of nodular cast iron.

A ductile-brittle transition occurs mainly in metals having a body-centred cubic structure. These metals, due to the effect of impurities, exhibit a yield point on a load-extension curve. There is considerable evidence to show that the ductile-brittle

transition is associated with a yield phenomenon[22]. Yielding is accompanied by the release or production of an avalanche of dislocations which are able to run together and form a micro-crack. If the crack spreads too rapidly to allow relaxation to occur by slip in neighbouring regions brittle fracture will result. There are therefore three important stages in the fracture process, namely yielding when slip can occur, crack nucleation by dislocation movement and finally crack propagation leading to fracture.

The applied stress to produce yielding, σ_y, is given by the Petch[21] equation which was first applied to the yield point of iron and steel by Hall[57] and has since been adopted by Petch:-

$$\sigma_y = \sigma_o + Kyd^{-\frac{1}{2}}$$

where

σ_o = the lattice friction stress impeding the motion of dislocations.

Ky is the unpinning stress for impurity-locked dislocations which depends on the thermally activated tearing of dislocations from their impurity atmospheres (as proposed by Cottrell[22]).

d is the grain diameter.

However considerable experimental data suggests that the yield point in iron and steel is not due to the thermally activated tearing of dislocations from their interstitial atmospheres. It has been pointed out by Conrad[23] that the yield point in iron and steel may be of the type proposed by Johnson and Gilman[24] for

the yield point in lithium fluoride whereby yielding occurs by a sudden multiplication of dislocations. He stated that there is strong evidence to suggest that in iron and steel Ky is not a measure of the stress required to unpin "atmosphere-locked" dislocations. At the present time there is insufficient evidence to be specific as to the exact nature of Ky but it has been shown that Ky is relatively independent of temperature and strain rate in the range of 100-300°K[25,26,27].

Once yielding has occurred moving dislocations are able to run together to form a microcrack. A number of mechanisms by which plastic deformation by slip could nucleate a crack have been devised[28,29,30,31], some of which are illustrated in Fig. 11. Where plastic deformation occurs by twinning, cracks may also be nucleated by twin intersections providing the plane of intersection is the cleavage plane[32,33].

Cottrell[34] and Petch[35] have both concluded that crack propagation is the difficult step in the fracture process. Both Cottrell and Petch assume the Griffith concept that a crack will propagate when:-

$$\sigma > \sqrt{E\gamma/C}$$

where σ is the applied normal stress, E is Youngs Modulus, C is one half the crack length and γ is the surface energy of the fractured faces. Cottrell[34] combined the Griffith and Petch equations and derived the following criterion for brittle crack propagation.

Fracture will occur if:-

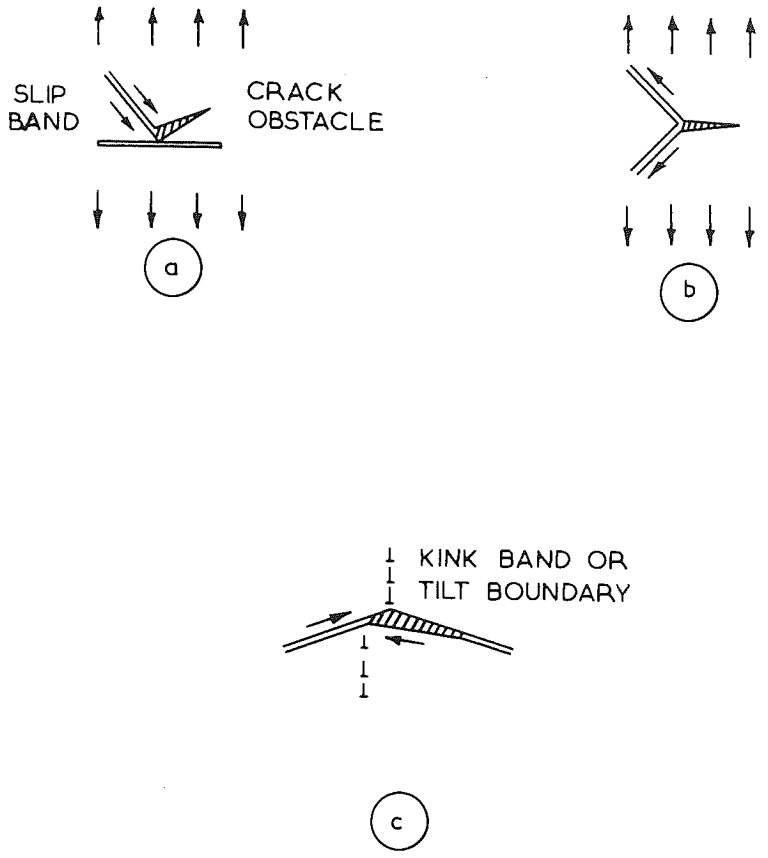

FIG. 11 Models for crack nucleation by slip (after Cottrell[30]).

$$\sigma_y > \frac{\beta \mu \gamma}{K y d^{\frac{1}{2}}}$$

where μ is the shear modulus and β is the ratio of shear stress to normal stress for the particular conditions of loading. Petch[35] derived a similar expression for a notched bar and stated that brittle fracture will occur in a notched bar when:-

$$\sigma_y > \frac{4 \mu \gamma}{K^* d^{\frac{1}{2}}}$$

where K^* is the slope of the ductile fracture stress versus $d^{-\frac{1}{2}}$ curve.

In both of these equations the right hand side varies only slightly with temperature while the yield stress increases with decreasing temperature thus accounting for a ductile-brittle transition. Any factor which increases the yield stress is therefore likely to raise the ductile-brittle transition temperature of a particular material the only anomalous factor being the grain size which is incorporated in both sides of the equations. This is due to the fact that grain boundaries act as barriers to a propagating crack and although from the Petch equation decreasing the grain size raises the yield stress, the corresponding increase in grain boundary area inhibits brittle crack propagation, causing a lowering in the transition temperature.

Nodular cast iron does not exhibit a yield point on a load-extension curve but 2 per cent silicon ferrite, the matrix material of nodular iron shows a pronounced yield point. The presence of

graphite nodules in nodular iron obviously masks any yield point as do the cementite lamellae in pearlitic steels. However, a ductile-brittle transition is noticed in both materials.

The effect of silicon and phosphorus in raising the ductile-brittle transition temperature in nodular cast iron is related to their effect of increasing the lattice friction stress, σ_i, and thereby increasing the yield point.

The rate of straining applied to a material affects the ductile-brittle transition. Impact transition temperatures are known to be much higher than tensile transition temperatures. Pugh, Chang and Borwick[36] investigated the effect of strain rate on the tensile properties of pure iron from -196 to +200°C and showed that the higher ductile-brittle transition temperatures noticed with higher strain rates were related to a corresponding increase in the yield point. The relationship between transition temperature and yield point has been discussed above. This work underlines the relationship between the tensile and impact transition in nodular cast iron and suggests that the fundamental mechanism is the same.

The presence of a notch in a specimen creates a state of triaxial stress thereby increasing the yield point resulting in an increase in the ductile-brittle transition temperature.

The above theories indicate that segregation of alloying elements is likely to affect the ductile-brittle transition in a material for the following reasons:-

1. Segregation may result in an increase in the yield point in a localised area.
2. The surface energy, γ, of that area may be lower than the rest of the matrix due to the different composition.
3. Segregation may result in hard grain boundary particles such as carbides which would act as stress-raisers and have a similar effect to a notch.

Austenitic Cast Irons Nickel austenitic nodular cast irons comprise a group of highly alloyed irons containing 18-36 per cent nickel plus manganese and/or chromium depending upon the properties required. Kraft and Flynn[37] investigated the interrelation of mechanical properties, casting size and microstructure of chromium-free and 1.5 per cent chromium austenitic nodular irons containing 20 per cent nickel. These workers showed that chromium-containing irons had poorer ductility and impact resistance than chromium-free irons which they concluded was due to the presence of cell-boundary carbides in chromium-containing irons. They also showed that the ultimate tensile strength and elongation decreased with increasing section and suggested that this may be due to the lower combined carbon content of the heavier sections. Sefing[38] in 1960 published a comprehensive list of data on various types of austenitic cast iron. He pointed out that chromium-containing irons should be used where good corrosion and erosion resistance were required rather than ductility and chromium-free irons used where good ductility and impact resistance were required. This

thesis is only concerned with the chromium-free irons where mechanical properties are of prime importance. Sefing recommended a 20 per cent nickel, 2 per cent manganese iron, designated D-2C by International Nickel Limited, for applications where maximum ductility was required. This material was shown[38] to have high tensile strength, elongation and impact resistance. Franson and Schelling[39] studied the effect of composition and section size on austenitic nodular cast iron and showed that an increase in section resulted in a decrease in mechanical properties in a chromium-containing iron, confirming the work if Kraft and Flynn. Unfortunately no data on the effect of as-cast section size on the mechanical properties of chromium-free irons were given. By increasing the manganese content from 1.1 to 3.55 per cent in a 20 per cent nickel chromium-free iron, Franson and Schelling showed an increase in ultimate tensile strength from 25.6 to 31.3 tons/in^2 and an increase in per cent elongation from 18.0 to over 40. They also noticed that strain-induced martensite often formed near cell-boundary carbide regions in chromium-containing irons during the tensile test, considerably lowering the ductility. Electron probe micro-analysis of these regions showed that segregation had resulted in depletions of nickel and concentrations of chromium and manganese. The authors concluded that the strain-induced martensite had formed adjacent to carbide areas because these regions were depleted in nickel and

the austenite would therefore be more unstable than the rest of the matrix under stress. Although this is undoubtedly true, it is felt that the stress concentration caused by the hard carbide particles must have contributed to the comparative instability of the surrounding regions.

Austenite has a face-centred cubic structure and so austenitic nodular cast iron does not undergo a ductile-brittle transition. The material is therefore finding increased application for cryogenic purposes. However the D-2C alloy which possessed the best ductility was found to have a comparatively unstable matrix at low temperatures. Rickard[40] showed that increasing the manganese content of the D-2C alloy to 4 per cent made the material stable at least as low as -196°C. This material was designated "D-2C modified" by International Nickel Limited.

The temperature at which austenite starts to transform to martensite, which is usually termed "Ms", is given by a formula[41] of the type:-

$$Ms(°C) = 561 - 474(\%C) - 33(\%Mn) - 17(\%Ni) - 17(\%Cr) - 21(\%Mo)$$

The beneficial effect of manganese in promoting austenite stability is shown in this equation.

It is quite apparent that should microsegregation occur then the Ms temperature will vary throughout the section of a casting resulting in premature austenite breakdown in some areas. Increasing the section may well exaggerate these effects. Abbot and Colleggi[42] have shown that increasing the section size of

chromium-containing austenitic irons results in an increase in cell-boundary carbide content with a corresponding decrease in mechanical properties. The D-2C modified alloy contains 4 per cent of manganese which may well segregate in high concentrations at cell boundaries promoting carbide formation in heavier sections. As the alloy is recommended for heavy section applications a study of the behaviour of the material in heavy sections would seem to be very necessary. The formation of carbide in this material would be expected to lower the ductility. Segregation would also cause a variation in the Ms temperature throughout the section. The microsegregation of this material, particularly in heavy section castings, would therefore seem to be worthy of some study.

SOLIDIFICATION OF NODULAR CAST IRON

Segregation in nodular cast iron occurs during the eutectic solidification process. A description of the solidification sequences is therefore relevant to any work concerning segregation in nodular cast iron.

The eutectic solidification is a nucleation-and-growth process. There is some difference of opinion as to the nature of nucleation of the eutectic but as segregation is a result of the growth process, the following discussion will be devoted to the growth of the nodular cast iron eutectic from the liquid phase. This stage of the process can be studied by quenching samples of nodular cast iron at various stages during the solidification process. Experiments of this kind have been carried

out by several investigators[43,44,45,46,47,48,49] and the results of these investigations have contributed to the present theory of eutectic solidification which is described below.

Fig. 12 taken from the work of Hughes[50] illustrates the solidification of a eutectic nodular cast iron. Solidification of a hypo-eutectic iron starts with the formation of austenite dendrites. Nodular graphite eutectic cells are nucleated close to the austenite dendrite/liquid interface[43] and begin to grow when the eutectic temperature is reached. Each cell consists of a graphite nodule within a sphere of solid austenite. Growth proceeds by radial diffusion of carbon to the nodule from the liquid phase via the austenite envelope concurrent with austenite deposition on the surface of the envelope. The growth of the graphite nodule must occur by the deposition of carbon atoms at its surface and the withdrawal of iron and silicon atoms from the austenite-graphite interface[51]. Solidification then proceeds by the growth of austenite-graphite eutectic cells. As the cells grow the diffusion distance for carbon atoms will increase and solidification will become more difficult[44]. The eutectic arrest in nodular cast iron takes place over a more extended range of temperature than in flake graphite cast iron illustrating the fact that cell growth rate in nodular iron is insufficient to maintain the arrest at a constant temperature. Solidification is completed by the mutual impingement of growing austenite-graphite eutectic cells leaving the last liquid to

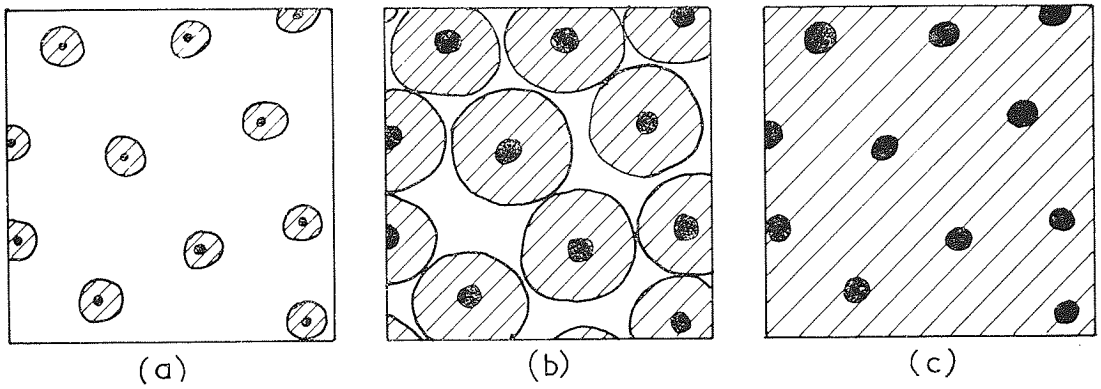

FIG. 12 Growth of a eutectic nodular cast iron from the liquid (after Hughes[50]).

solidify as a fine network between them. Any segregation effects will be manifested in this cell boundary region which marks the end of solidification particularly at the interstices of the austenite-graphite eutectic cells.

The above theory explains satisfactorily the appearance of the nodular graphite eutectic. It differs from the normal theories of eutectic solidification, however, in so far as it relies on a substantial amount of solid state diffusion to take place in order that solidification of the nodular iron eutectic can proceed.

Hillert[52] has shown by a mathematical treatment that the diffusion of carbon in liquid iron is twenty times greater than diffusion of carbon in austenite at the same temperature and concluded that wherever geometrically possible cast irons would solidify by liquid diffusion of carbon. With this knowledge Tiller[53] has stated that the austenite envelopes seen on quenching nodular irons during solidification are a result of the quenching treatment and are formed from areas of low-carbon liquid surrounding the graphite nodules.

SEGREGATION IN NODULAR CAST IRON

Evidence of segregation in nodular cast iron was first observed by Wittmoser[49] who noticed that cell boundary areas in as-cast pearlitic irons tended to etch darker than the rest of the matrix. He attributed this to cellular segregation in these regions. Gilbert and Palmer[20] found that after normalising an

as-cast iron this differential etching effect was removed. They concluded that the normalising treatment had homogenised the matrix and removed the segregation effects. Gilbert and Palmer stated that this homogenisation had contributed to the lowering of the impact transition temperature brought about by normalising. However, microstructures of hardened and tempered irons[54] reveal darker-etching grain boundaries after similar austenitising treatments to those given to the normalised specimens of Gilbert and Palmer.

The effects of segregation have also been shown in heavy-section castings. Barton[11] found that 12 in diameter castings contained cell-boundary carbides in the microstructure indicative of heavy segregation. Annealing these castings was difficult due to the fact that pearlite was retained in these cell boundary areas.

The sub-boundary ferritic structures resulting from sub-critically annealing nodular cast iron have been attributed by Gilbert to an inhomogeneity of the metallic matrix. Gilbert argued that a treatment in the austenitic region would remove this inhomogeneity resulting in a good ferritic structure on further treatment beneath the critical range.

Attempts have been made to assess microsegregation in nodular cast iron by specialised etching techniques. Luderung[55] has shown silicon depletions in cell boundary areas in ferritic nodular cast iron by potentiometric etching of samples in cold sodium

hydroxide solution. Charbonnier and Margerie[56] showed that a ferritic nodular iron, which appeared to have a homogenous matrix, showed strong differential etching effects in sodium metabisulphite, which etched the cell boundary areas much more strongly than the rest of the matrix. These investigators used X-ray micro-analysis to obtain a quantitative analysis of the silicon and manganese content of the cell boundary regions and reported silicon and manganese analyses of 1.486 and 0.334 per cent respectively in the deeply etched regions while the rest of the matrix contained 2.778 per cent silicon and 0.223 per cent manganese. These figures were reported in a material which had been heat treated and possessed a seemingly homogenous microstructure. In as-cast materials or in heavy-section materials which reveal segregation effects such as cell-boundary carbides the micro-segregation could be expected to be more marked.

Micro-analysis has also been employed to study microsegregation in austenitic cast iron. Franson and Schelling[39] found depletions of nickel and concentrations of chromium and manganese in cell boundary regions in chromium-containing irons.

SUMMARY

Several workers have shown that microsegregation occurs in nodular cast iron but at present there is a lack of quantitative data. It has also been shown that segregation effects in heavy sections are likely to be more pronounced although there is no published work on the effect of section size on microsegregation

in nodular cast iron.

Little work has been carried out on the effect of micro-segregation on the mechanical properties of nodular cast iron. It has been stated by Gilbert that the sub-boundary structure noticed in sub-critically annealed ferritic nodular cast iron could have been caused by segregation of alloying elements. The same author suggested that the increased mechanical properties obtained by normalising an as-cast pearlitic cast iron (p.23) could be associated with an homogenisation of the segregated as-cast structure. No experimental evidence is available to support either of these two suggestions. The work of Barton on heavy sections (p.23) showed that large cell-boundary carbides were dispersed throughout the microstructure of a 12 in diameter bar of nodular cast iron. The ultimate tensile strength and elongation of this material were less than would be expected from a smaller section of the same material. Impact tests revealed that, in the annealed condition, the heavy-section material also had inferior transition properties to smaller-section material. The role of cell boundary carbides in influencing the mechanical properties of this material is difficult to assess from Barton's results as other variables such as graphite nodule size and number are affected by change in section. However, it is to be expected that cell-boundary carbides would lower the ductility of a material and from the theory of brittle fracture discussed above carbides might be expected to increase the ductile-

brittle transition temperature. The retention of pearlite in cell boundary areas after annealing is often noticed. This is caused by the large diffusion distance between the cell boundary and the graphite nodule surface and also any carbide-forming elements which tend to segregate will stabilise pearlite in these regions. Charbonnier and Margerie[57] have shown that manganese and chromium, both carbide stabilisers, tend to segregate to cell boundaries in flake graphite cast iron.

It can therefore be seen that there is, at present, some need for a study of segregation in nodular cast iron using X-ray micro-analysis. Such a study could include an investigation of the effects of section size and heat treatment on microsegregation. The importance of microsegregation effects in influencing mechanical properties could then be assessed by carrying out appropriate mechanical tests from the materials under investigation.

In austenitic materials segregation is important because of its possible effect upon martensite transformation. The tests that Rickard carried out on the "D-2C modified" austenitic material were all on sections of 3 in or less. It is possible that the effects of segregation may become more pronounced in heavier sections.

It was therefore decided to cast a series of varying section sizes in commercial purity nodular cast iron and carry out X-ray micro-analysis and mechanical tests on samples from each section

in the as-cast condition and after various heat treatments. The results of this investigation should give some indication of the nature of microsegregation in nodular cast iron and the way in which it is affected by heat treatment and change in section. In order to assess the effect of microsegregation on mechanical properties, the mechanical test results would be compared with results obtained from similar sections of refined nodular cast iron where a minimum amount of segregation would be expected.

In austenitic irons the major alloying elements, i.e. nickel, will be expected to segregate and the effect of microsegregation on mechanical properties will be more difficult to assess. However, an investigation of microsegregation effects in a series of section sizes of austenitic irons with appropriate mechanical tests could greatly add to the present knowledge concerning these materials.

Having obtained some indication of the importance of microsegregation in nodular cast iron from the investigations described above, a series of quenching experiments would be carried out to obtain samples of nodular iron quenched at progressive stages of the eutectic solidification process. Micro-analysis of these samples would provide information regarding the nature of microsegregation during the solidification process. Furthermore, a knowledge of the distribution of alloying elements in these quenched microstructures would provide some information on the eutectic solidification process.

EXPERIMENTAL PROCEDURE

MELTING AND HEAT TREATMENT

Four materials were produced for the purpose of this investigation. A commercial purity nodular cast iron and a refined iron were produced in a series of section sizes. Two austenitic irons of 0.5 per cent and 4 per cent manganese were also produced. It is proposed to consider the former two materials under the general heading "ferritic" irons although, of course, in the as-cast and normalised conditions the commercial purity material possessed a pearlitic matrix.

Ferritic Cast Irons Two ferritic irons were produced, one of commercial purity, which was pearlitic in the as-cast state, the other being produced from more refined base materials.

Commercial purity iron A charge of 550 kg was melted in a 600 kg capacity induction furnace. The charge was made up of commercial pig iron to which 32 kg of steel scrap was added in order to adjust the carbon content of the melt to 3.50 per cent. Additions of 2.25 kg of 80 per cent silicon ferrosilicon and 2.50 kg of 80 per cent manganese ferromanganese were made to the charge to adjust the silicon and manganese levels to 2.0 per cent and 0.40 per cent respectively. The melt was treated at 1 400°C in the ladle with 2.55 kg of a nickel-magnesium alloy containing 17 per cent magnesium. When the reaction had subsided 0.5 per cent silicon, as 80 per cent ferrosilicon and 75 g of cerium Mischmetall

TABLE 1

ANALYSIS OF MATERIALS USED

Material	T.C. %	Si %	Mn %	S %	P %	Ni %	Cr %	Mg %
Commercial Purity Material	3.50	1.96	0.37	0.016	0.028	0.78	0.10	0.065
Refined Material	3.53	2.02	<.02	0.010	0.012	0.82	0.01	0.069
Low Manganese Austenitic Iron	2.33	2.11	0.52	0.017	0.023	24.4	0.01	0.11
4% Manganese Austenitic Iron	2.47	2.51	3.64	0.011	0.027	22.1	<.01	0.11

were added.

Castings in a variety of section sizes were produced from this melt; one 12 in diameter bar, one 6 in diameter bar, ten $1\frac{3}{4}$ in keel blocks and several $\frac{1}{2}$ in keel blocks cast in moulds incorporating a steel base plate for the purpose of producing white iron in this section.

The analysis of the material is given in Table 1. The cast samples were sectioned to allow mechanical tests to be carried out on each section in the as-cast condition and after a variety of heat treatments. Fig. 13 shows the method employed in the sectioning of the 12 in and 6 in diameter bars. In each case the top 9 inches of these bars were discarded to remove any unsoundness. The remaining sections were 9 inches long. A 1 in wide slice was cut across the diameter of each bar from which microspecimens were prepared, so that the microstructure throughout the section of the bars could be examined. In the case of the keel blocks the heads were removed and only the bottom portions were used for mechanical tests.

The heat treatments adopted for various sections and the mechanical tests carried out are given in Table 2.

"Refined" iron The melting and casting procedure for the commercial purity iron was repeated with a charge of oxygen blown Vantit pig iron and high purity Swedish pig iron. No addition of ferromanganese was made. The analysis of the material is given in Table 1. Tensile and impact test piece blanks from all

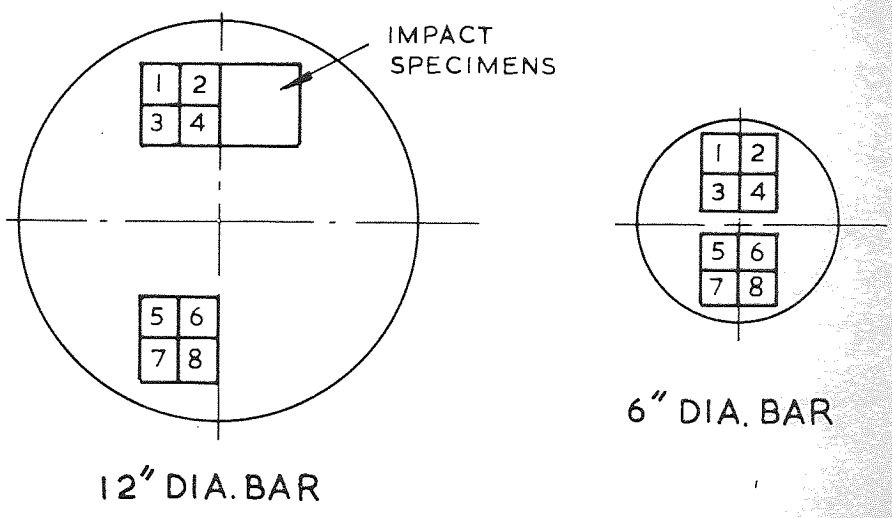

FIG. 13 Method of sectioning 12 in diameter and 6 in diameter bars.

TABLE 2

Treatment No.	Type of Treatment	Samples Undergoing Treatment	
		Section	Mechanical Tests
1	As-cast.	12 in bar 6 in bar 1¾ in keel ½ in keel	T† + I* T T + I
2	Double Anneal: 900°C for 16 hours. Furnace cooled to 690°C, then 690°C for 48 hours. Air cooled.	12 in bar 6 in bar 1¾ in keel ½ in keel	T + I T T + I
3	Normalise: 900°C for 6 hours. Air cooled.	12 in bar 6 in bar 1¾ in keel ½ in keel	T + I T T + I
4	Single Anneal: 690°C for 48 hours. Air cooled.	12 in bar 6 in bar 1¾ in keel ½ in keel	T + I T T + I
5	Spheroidizing Anneal: 900°C for 48 hours. Furnace cooled to 690°C, then 690°C for 100 hours. Air cooled.	12 in bar 1¾ in keel	I I

† T = tensile test
* I = impact test

sections were subjected to treatment 2 in Table 2. No ½ in chill keels were produced from this material.

Austenitic Irons Two austenitic irons of approximately 0.5 per cent and 4 per cent manganese respectively were cast. In each case one 12 in diameter bar, one 6 in diameter bar and ten 1¾ in keels were produced from a 550 kg melt. The melts were inoculated in the ladle at 1 400°C with 2.90 kg of nickel-

magnesium alloy and 0.5 per cent silicon as 80 per cent ferro-silicon. The analyses of these materials are given in Table 1.

MECHANICAL PROPERTIES

Tensile and impact test specimens were machined from the treated materials to enable comparisons between section size, heat treatment and mechanical properties to be made in the various materials which had been prepared.

In all cases 0.798 in diameter tensile bars with 2.82 in gauge length were machined from the 12 in and 6 in bars while 0.564 in diameter bars and 0.398 in bars with 2 in gauge length were produced from the $1\frac{3}{4}$ in and $\frac{1}{2}$ in keel blocks respectively.

Notched and unnotched Charpy impact specimens conforming to BS 131, part II 1959 were also produced from all sections.

Tensile tests were carried out on an Amsler 25 ton universal testing machine.

A Hounsfield extensometer was used for proof stress determinations. Impact tests were carried out on an Amsler impact testing machine with a striking force of 120 or 240 ft lb. Variation in testing temperature for the purpose of transition curve determinations was effected by employing several different mediae. Table 3 shows the media employed over various temperature ranges.

METALLOGRAPHY

Microspecimens of all materials in the as-cast condition were prepared from the 12 in and 6 in bars and a 1 in wide, $\frac{3}{8}$ in

TABLE 3

ENVIRONMENTS USED FOR DIFFERENT TEMPERATURES IN IMPACT TRANSITION DETERMINATIONS

Temperature	Environment used
200°C +	Furnace
100°C - 200°C	Oil bath
Room temp. - 100°C	Water bath
-76°C - room temp.	Petroleum spirit + solid CO_2
-150°C - -76°C	Isopentane bath cooled by liquid O_2
-186°C	Liquid oxygen bath

thick slice passing through the centre of each bar was cut 9 inches from the base to allow a series of microspecimens from the edge to the centre of the bar to be prepared. Microspecimens of all the materials in the various heat treated conditions were machined from the threaded ends of the broken tensile specimens. The recommended polishing procedure for nodular cast iron has been described elsewhere by Turner[58].

MICROHARDNESS DETERMINATIONS

Microhardness measurements were carried out on a Leitz "Miniload" microhardness tester using a 25 g load. With this small load the accuracy of the instrument is rather limited due to the extremely small indentations produced especially in hard carbides. The microhardness tests, however, were carried out merely to indicate the relative hardness of cell boundary carbides and it was felt that some inaccuracy in the technique could be tolerated.

MICRO-ANALYSIS

Microsegregation determinations were carried out with the aid of a Cambridge Microscan electron probe X-ray micro-analyser[59] (Fig. 14). The micro-analyser can be used for quantitatively analysing elements on regions as small as 1 micron over the surface of a specimen. It functions by recording the intensity of the characteristic X-radiation for each element that is excited in the specimen by bombardment from a beam of electrons focussed into a probe of less than 1 micron in diameter. The intensity of the characteristic X-ray line of an element emitted by the

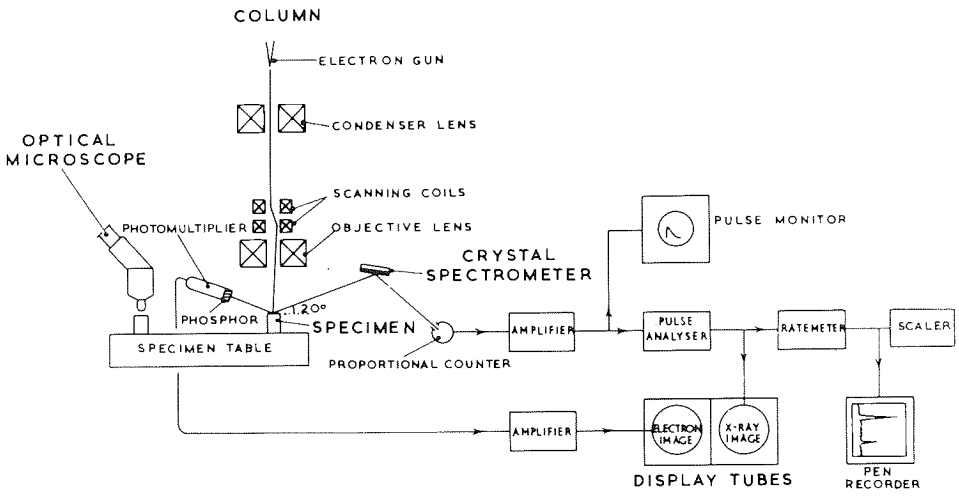

FIG. 14 Microscan electron probe micro-analyser - schematic diagram.

specimen is compared with the intensity of the same line emitted from a pure metal standard. The weight fraction of that element in the specimen is given to the first approximation by the ratio of these two intensities. This electron probe can either be static and directed on to a particular point of interest or it can be made to scan a raster of up to $\frac{1}{2}$ mm square. X-radiation for a particular element is selected by means of a spectrometer incorporated in the instrument which can be set at the Bragg angle for the X-radiation of that element. The Cambridge instrument can also be adjusted to scan a line across an area for a particular element. Thus a quantitative measure of the distribution of that element across a field of interest can be made.

This assumes that the electron probe current is constant throughout all the tests. In the Cambridge Microscan instrument the electron probe current is not continuously recorded and must be periodically checked on a Faraday cage. The graphite nodules absorb electrons like the aperture in a Faraday cage. The ratio of the currents obtained on graphite nodules and a Faraday cage were compared and found to be 4.65 : 5.00. Thereafter, the probe current was checked on graphite nodules in the specimen under investigation thus ensuring a regular check on probe current.

Micro-analyser specimens, $\frac{1}{4}$ in diameter discs, $\frac{1}{8}$ in thick, were machined from the threaded ends of broken tensile test

pieces and polished on one face to a normal metallographic finish. It was therefore possible to examine microsegregation in samples of known mechanical properties.

Segregation determinations were carried out by extensive use of the line scan technique. In order to assess the microsegregation in each cell scans for various elements were carried out from the edge of a graphite nodule, assumed to be a cell centre, to the cell boundaries which were indicated by segregation effects such as darker etching and cell boundary carbides.

Certain corrections may be necessary in order to obtain accurate quantitative data from micro-analysis results[60-65]. When the electron beam strikes the metal under examination electrons diffuse into the metal and excite characteristic X-rays. The depth of electron penetration decreases with heavier elements. Furthermore, some electrons are back scattered at the specimen surface, the effect being greater in the heavier elements. Corrections are therefore necessary if large atomic number differences exist between the component metals of an alloy. Fortunately most of the elements examined in these investigations were of similar atomic weights to the base metal, iron.

It can be seen that most X-rays are generated from below the surface of the metal. Transmission of these X-rays through the solid sample will involve some absorption which must be included in correction calculations. In an alloy the absorption coefficients of the elements for each measured radiation must therefore be known and utilised in absorption corrections.

When more than one element is present in a sample primary X-rays from one element may excite secondary X-rays from another element, thus increasing the X-ray intensity of the latter element and giving an erroneous result. This fluorescent effect occurs only between elements that are very close together (two or three atomic numbers) in the periodic table.

Of the elements investigated in this thesis the atomic number correction was only necessary for the silicon results where the method of Poole and Thomas[64] was used. Absorption corrections using Birk's[61] method were performed on nickel and silicon analyses while corrections for fluorescence were only required for chromium analyses. Duncumb[66] has produced a fluorescence correction factor for chromium in iron which was used for all chromium analyses in this thesis.

QUENCHING EXPERIMENTS

Quenched samples of a commercial purity nodular cast iron and a "D-2C modified" austenitic iron were obtained during the solidification process in order to further investigate the nature of segregation in these materials. The techniques involved in obtaining these samples are similar to those described by Gittus and Hughes[67] and are described below.

Melting Procedure For both alloys a 100 kg charge of metal was melted in a 135 kg induction furnace. The melting techniques were similar to those described previously (pp.28 and 30) for these materials. The test casting was an 8 in long, 2 in diameter bar, cast vertically and gated below the central parting line in greensand

moulds. Analyses of the two materials are given in Table 4.

TABLE 4

ANALYSIS OF MATERIALS USED IN QUENCHING EXPERIMENTS

	T.C. %	Si %	Mn %	S %	P %	Ni %	Cr %	Mg %
Commercial Purity Material	3.30	1.99	0.64	0.017	0.026	0.84	0.21	0.064
4% Manganese Austenitic Material	1.99	2.33	4.10	0.008	0.024	21.4	0.015	0.057

Thermal Analysis From the melts two taps of 25 kg and 75 kg were taken. From the smaller tap a cooling curve was taken on the first casting which contained a platinum/platinum - 13 per cent rhodium thermocouple at the mid-radius position in the mid-length cross section plane. The thermocouple was connected to a high speed recorder. From the cooling curve obtained the holding times prior to quenching for five further castings taken from the second tap were assessed in order to provide suitable samples showing progressive stages of the eutectic solidification process.

Quenching Technique Castings 2-6 were knocked from the moulds at pre-determined intervals into a tank of agitated cold water. They were then sectioned through the mid-length positions and samples for micro-analysis were machined from mid-radius positions. Micro-analysis line traces for a series of elements were carried out across the solid/liquid interface in these samples.

RESULTS

It has been shown above that basic differences exist between irons of ferritic and austenitic matrices. In this section, therefore, the results obtained from the two materials will be presented separately.

FERRITIC NODULAR CAST IRON

Metallography Figs. 15-17 illustrate the microstructures of the various sections of the commercial purity iron in the as-cast condition. The microstructures of the as-cast material, with the exception of the chilled specimens, all revealed nodular graphite structures with pearlitic matrices. The size of the graphite nodules decreased while their number increased with decreasing section size. The $\frac{1}{2}$ in keel specimen (Fig. 17) revealed a typical white iron microstructure with small graphite nodules dispersed throughout the pearlite.

Cellular segregation effects were shown in all but the $\frac{1}{2}$ in chilled specimen by the darker appearance of the cell boundaries with respect to the rest of the matrix. Segregation was most marked in the 12 in section (Fig. 15) with evidence of cell boundary carbides. Microhardness determinations on these carbides gave results varying from 900-1 100 D.P.N. In the $1\frac{3}{4}$ in keel section much smaller amounts of these carbides were just visible. More detailed examination of the cell boundary regions in these materials revealed that the pearlite lamellae were much more closely spaced

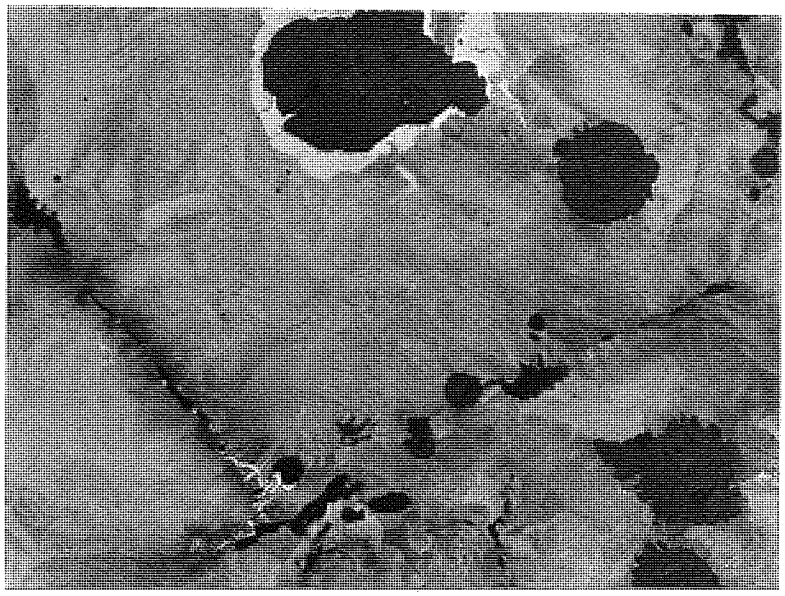

FIG. 15 12 in section of commercial purity nodular iron as-cast.
Etched in 4% Picral x 100

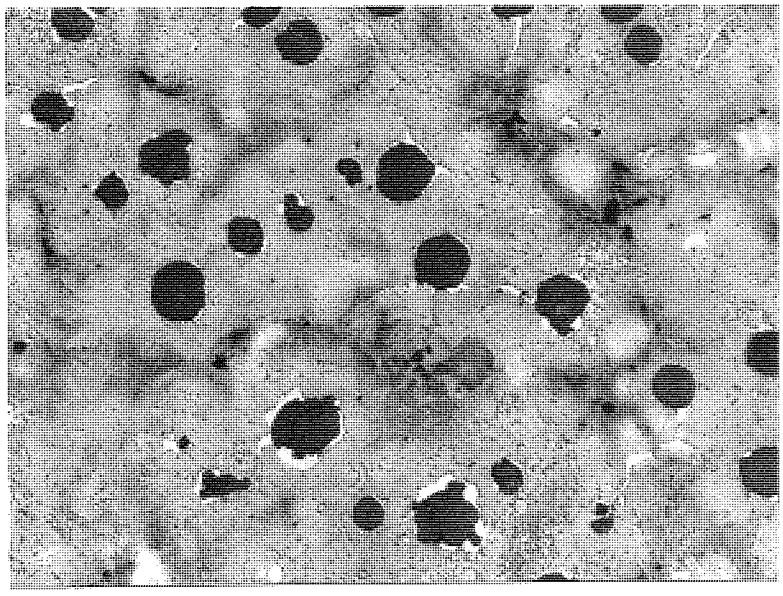

FIG. 16 1.75 in keel of commercial purity nodular iron as-cast.
Etched in 4% Picral x 100

in cell boundary areas than in the rest of the matrix which caused the cell boundaries to appear darker at lower magnification.

Figs. 18-20 illustrate the microstructures of the commercial purity material in the double-annealed condition. Microstructures of the 12 in, 6 in and $1\frac{3}{4}$ in sections consisted of ferritic matrices which contained areas of retained pearlite in cell boundary regions. Undissolved massive carbides were associated with areas of retained pearlite in the 12 in and 6 in sections (Fig. 19). No undissolved carbide was noticed in the $1\frac{3}{4}$ in section. The microstructure of the $\frac{1}{2}$ in keel contained no retained pearlite or carbide.

Figs. 21 and 22 show the microstructures of the normalised commercial purity material. The cell boundary areas in these specimens did not appear darker than the rest of the matrix and examination of the pearlite lamellae revealed no discernible difference in interlamellar spacing between the matrix and cell boundary areas due to the refining action of the normalising treatment. Cell boundary carbides, however, were still present in the 12 in, 6 in and $1\frac{3}{4}$ in sections.

The microstructure of the single-annealed material is shown in Fig. 23(a). These samples were essentially similar to the double-annealed samples apart from the ferrite grains which revealed large amounts of the sub-boundary structure reported previously by Gilbert (p.11). A sample of as-cast material was deeply etched to investigate the possibility of a relationship

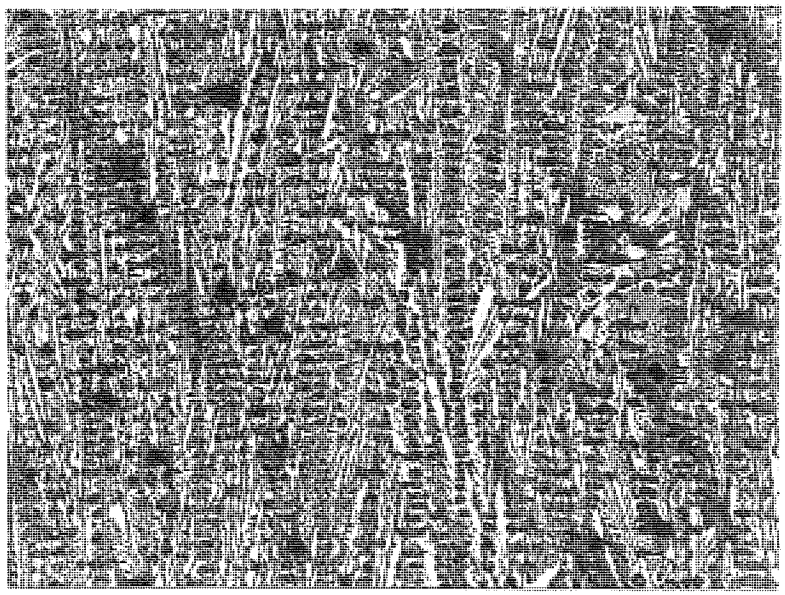

FIG. 17 0.5 in keel specimen as-cast.
Etched in 4% Picral x 100

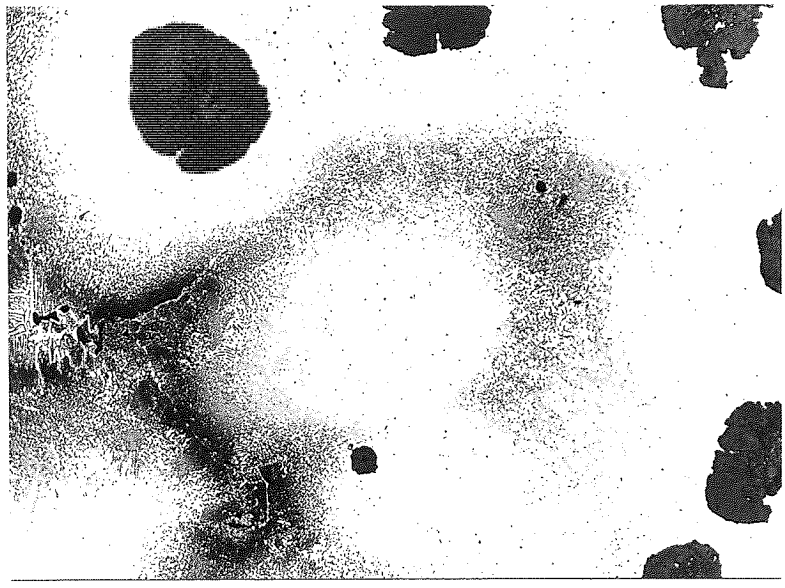

FIG. 18 12 in section of commercial purity nodular iron double annealed.
Etched in 4% Picral x 100

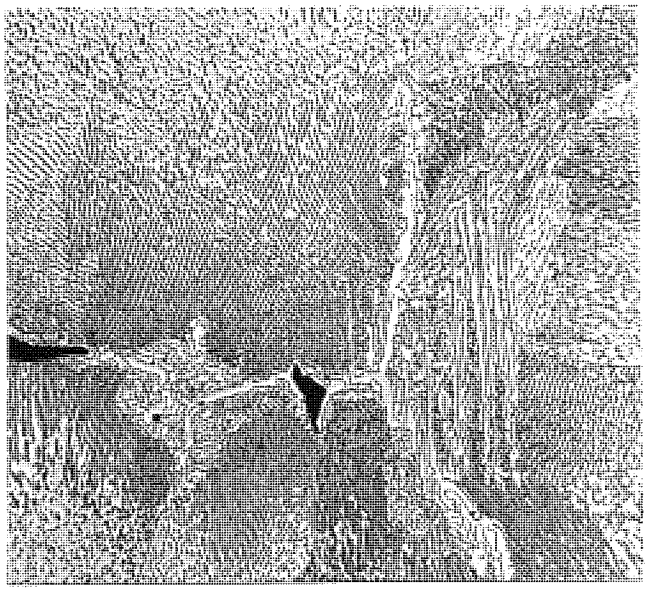

FIG. 19 Undissolved massive carbide in 12 in double annealed sample.
Etched in 4% Picral x 600

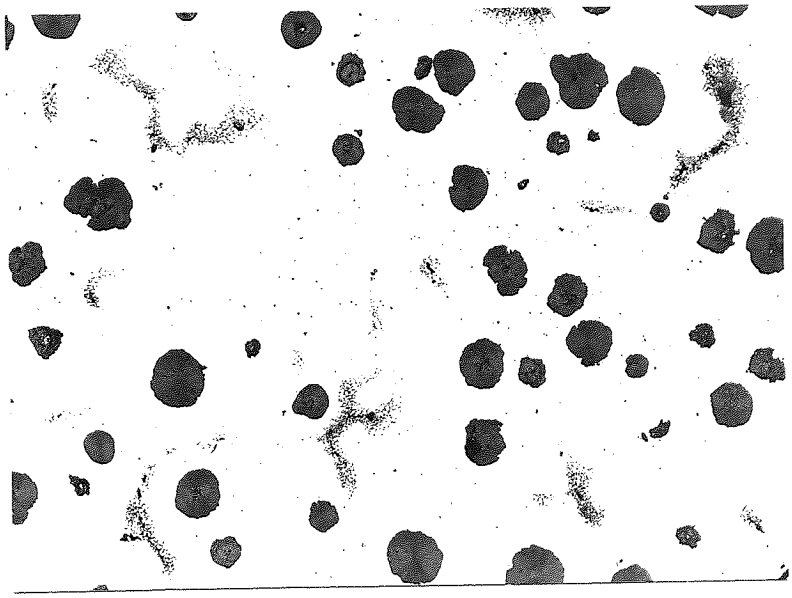

FIG. 20 1.75 in keel specimen double annealed.
Etched in 4% Picral x 100

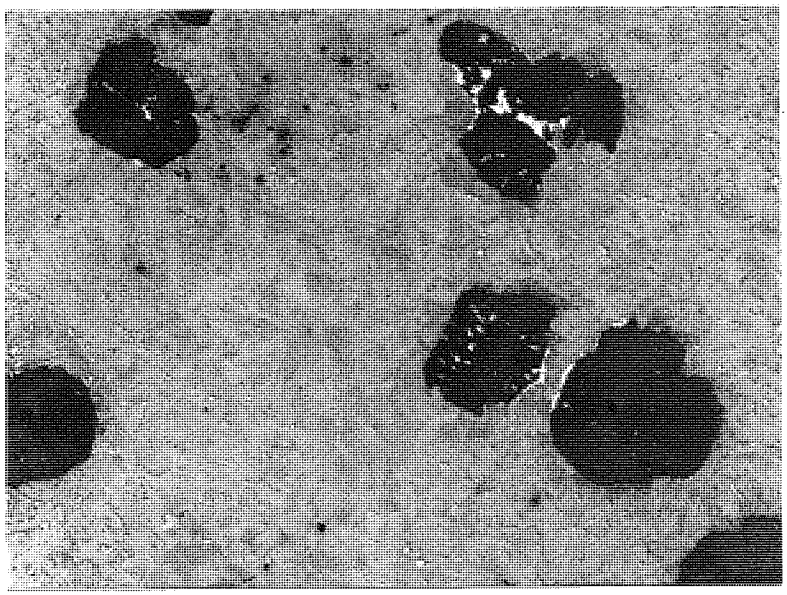

FIG. 21 12 in section of commercial purity material normalised.
Etched in 4% Picral x 100

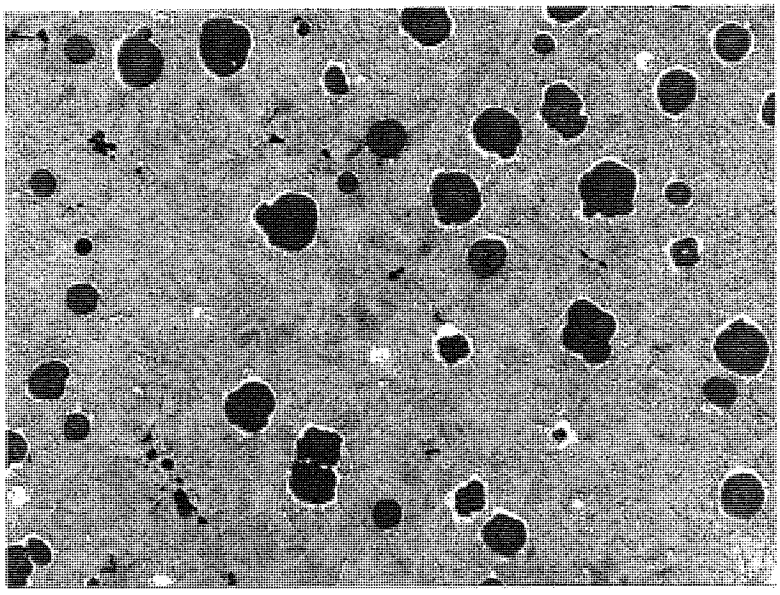

FIG. 22 1.75 in keel specimen normalised.
Etched in 4% Picral x 100

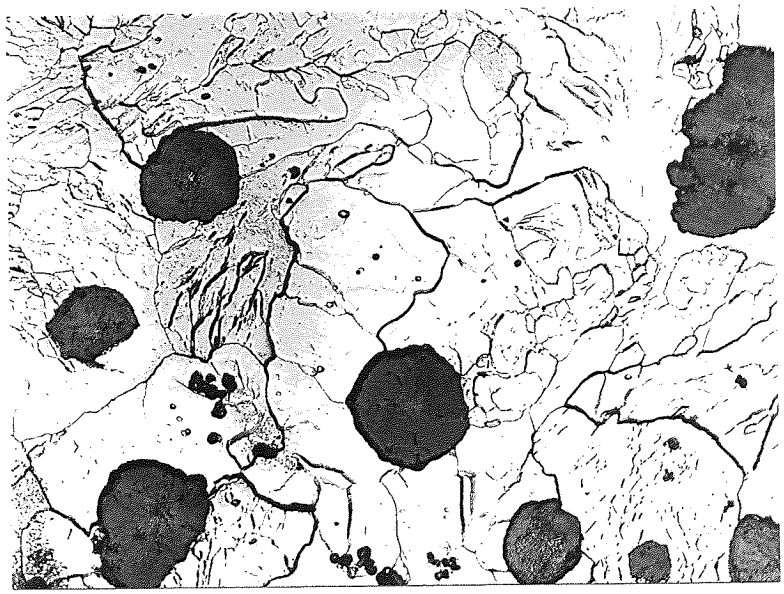

FIG. 23a 12 in specimen single annealed showing sub-boundary ferrite structure.
Etched in 4% Nital x 100

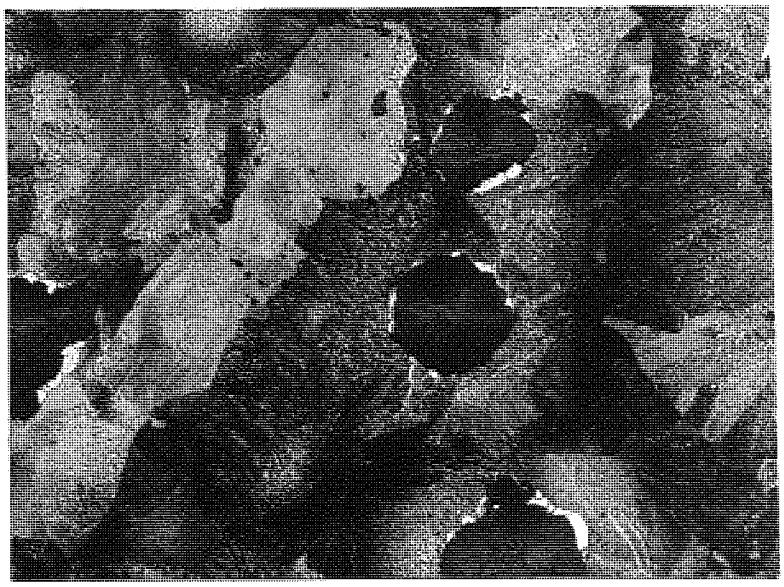

FIG. 23b 12 in specimen as-cast deeply etched to show sub-boundary structure within pearlite grains.
Etched in 5% Nitric acid in acetone x 100

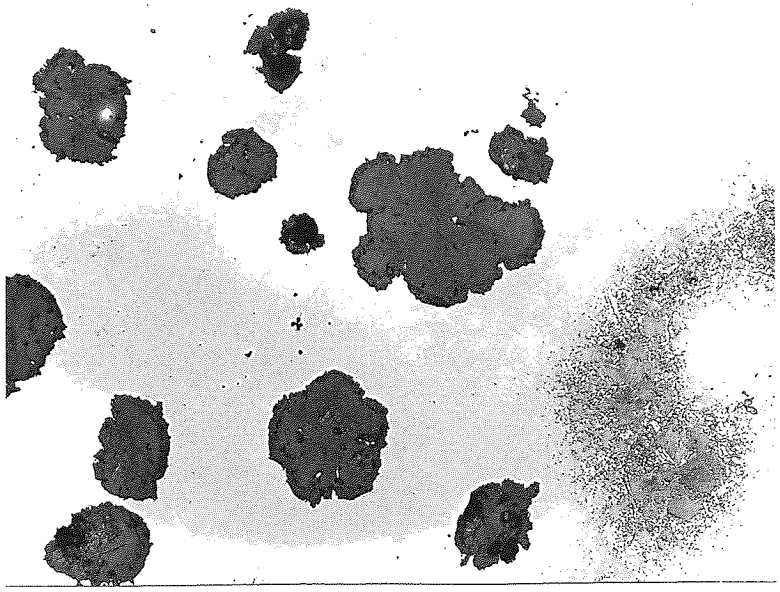

FIG. 24 12 in section commercial purity material after spheroidise anneal treatment.
Etched in 4% Picral x 100

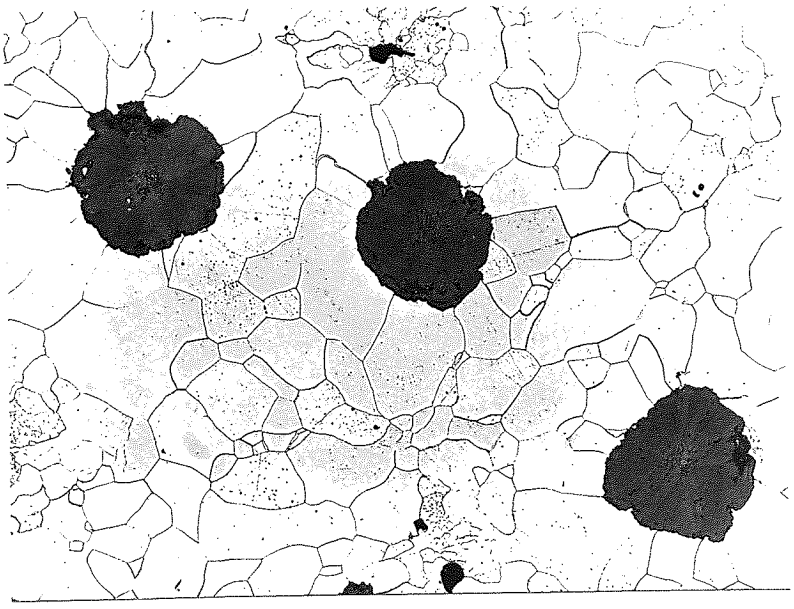

FIG. 25 12 in section refined ferritic material double annealed.
Etched in 5% Nital x 100

TABLE 5

EFFECT OF SECTION SIZE ON FERRITE GRAIN SIZE OF DOUBLE ANNEALED MATERIALS

Material	A.S.T.M. grain size *
Commercial purity material	
12 in section	4
6 in section	4
$1\frac{3}{4}$ in section	$4\frac{1}{2}$
Refined material	
12 in section	4-$4\frac{1}{2}$
6 in section	$4\frac{1}{2}$
$1\frac{3}{4}$ in section	5

* A.S.T.M. designation E112

between the structure of pearlite in an as-cast material and ferrite produced by sub-critically annealing an as-cast sample. Fig. 23(b) illustrates the microstructure obtained by deeply etching a sample of the 12 in as-cast material which revealed marked evidence of a sub-structure within the pearlite grains. Fig. 24 illustrates the microstructure of the 12 in section material after the spheroidise anneal treatment. Substantial carbide breakdown had occurred but some globular cell boundary carbide remained associated with small amounts of retained pearlite.

Fig. 25 shows the microstructure of the refined ferritic material in the double-annealed condition. The structures consisted of graphite nodules in a ferritic matrix which contained no cell boundary carbides or retained pearlite.

Ferritic grain size measurements were made on all the double-annealed samples of commercial purity and refined material. The results of these tests are given in Table 5.

Mechanical Properties Tensile specimens were machined from the treated samples; 0.798 in diameter specimens from the 12 in and 6 in sections, 0.564 in diameter specimens from the $1\frac{3}{4}$ in keel sections and 0.399 in diameter specimens from the $\frac{1}{2}$ in keel sections. The results of the tensile tests are listed in Table and illustrated graphically in Figs. 26 and 27.

Fig. 26 illustrates the marked effect of section size on the ultimate tensile stress of the normalised and as-cast samples while the annealed samples were relatively unaffected. The

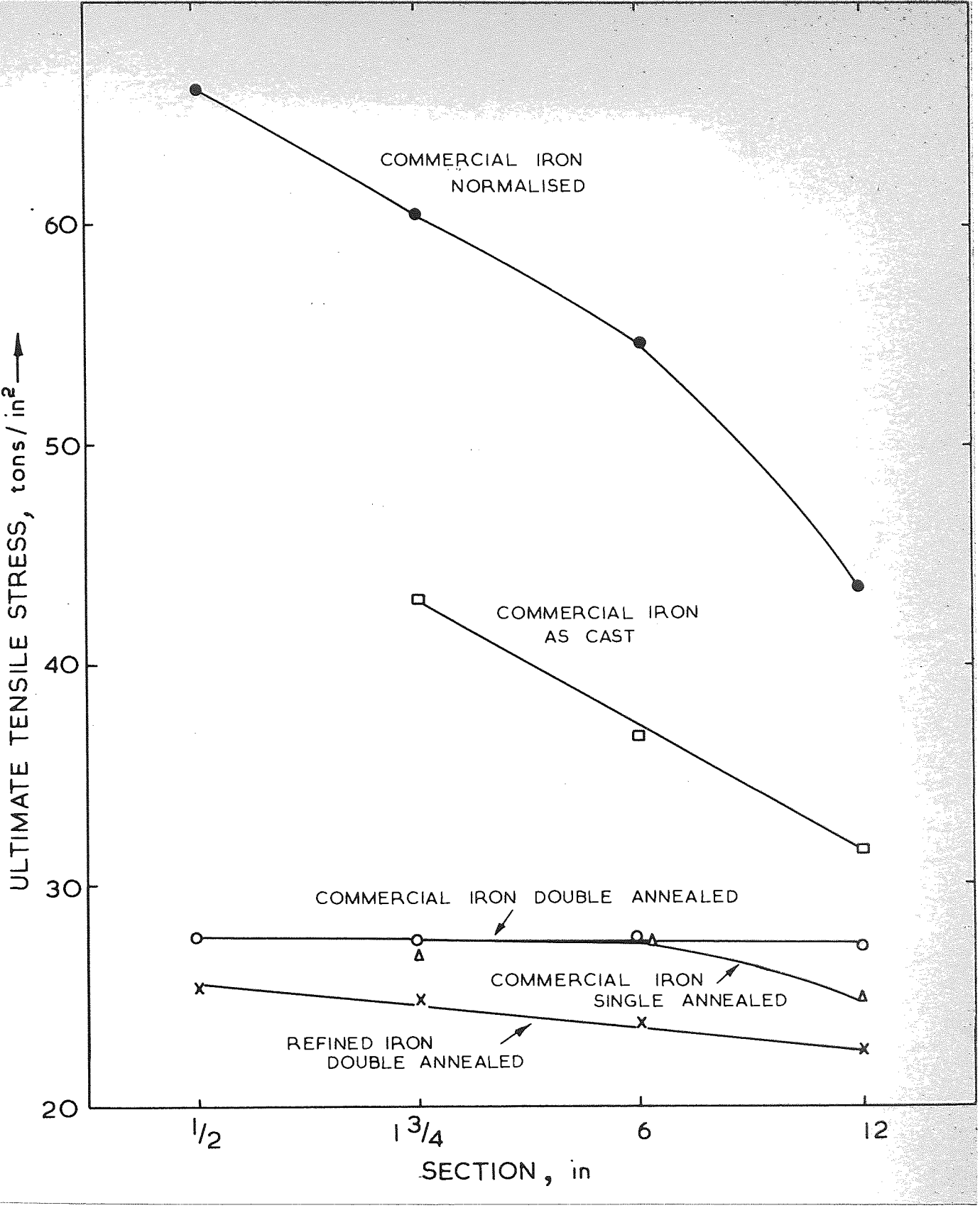

FIG. 26 Effect of section size on ultimate tensile stress values.

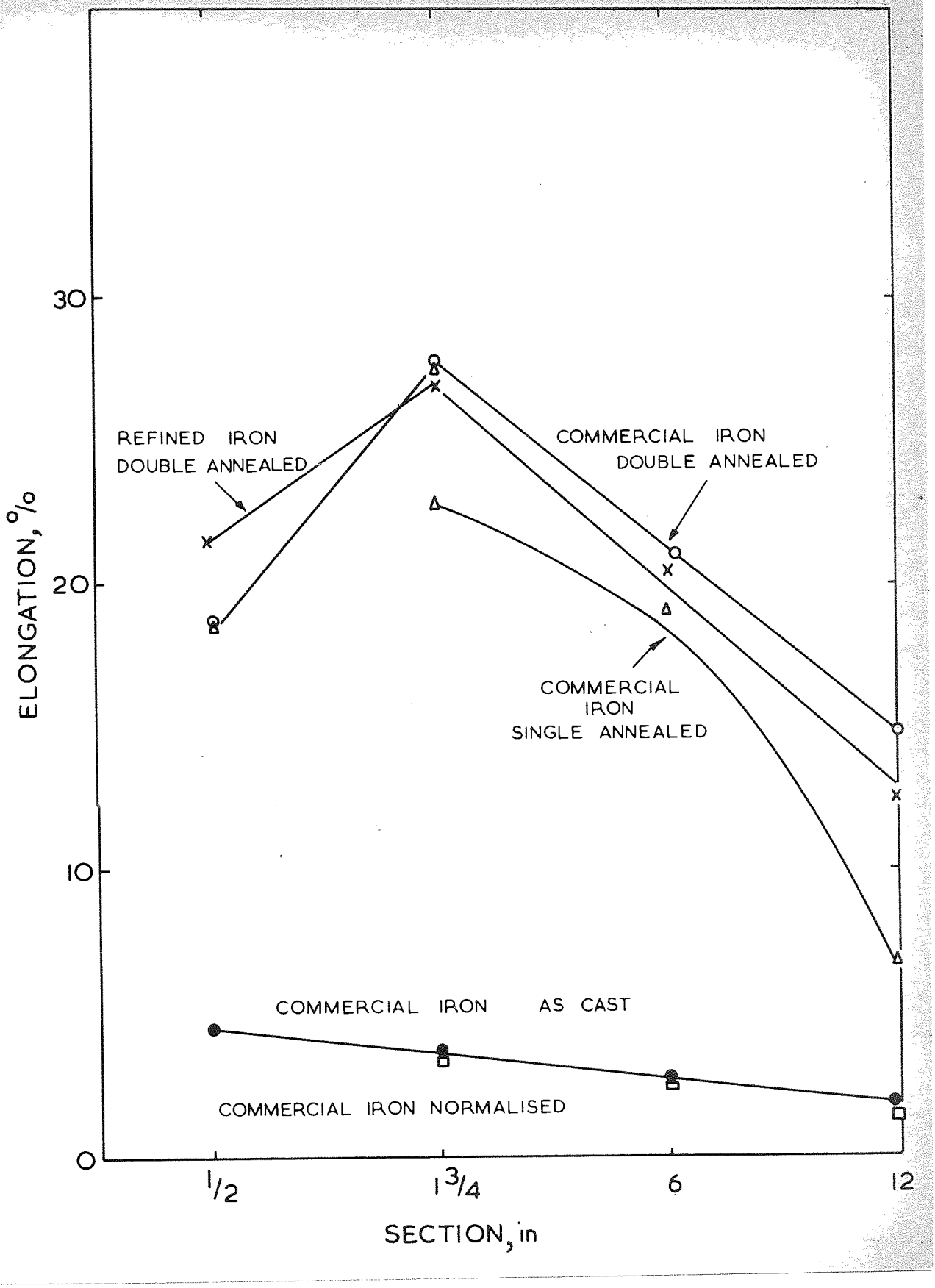

FIG. 27 Effect of section size on per cent elongation values.

elongation values of annealed samples (Fig. 27) of commercial purity iron deteriorated with increase in section. Proof stress values in all materials remained fairly constant over the series of section sizes. The effect of section on the double-annealed refined material differed slightly. Increase in section size in this material resulted in a significant decrease in proof stress and ultimate tensile stress. The effect of increase in section on the elongation of the double-annealed refined material was almost identical to the effect found in the double-annealed commercial purity material.

Unnotched and notched (45°-006) Charpy impact specimens, 10 x 10 x 55 mm, were prepared from the samples shown in Table 2. Impact transition curves were determined on these samples. The results of these tests are shown in Figs. 28-37. Fig.31 demonstrates the effect of heat treatment on the unnotched impact properties of the commercial purity material confirming the work of Gilbert. The effect of variation in section on the as-cast unnotched impact properties of the commercial purity material is shown in Fig. 28 which shows the higher transition temperature and lower impact value in the ductile range, of the 12 in bar. This difference persisted after each heat treatment.

The effect of segregation on the notched and unnotched impact properties of ferritic nodular cast iron is demonstrated in Figs. 32-37. Fig. 32 illustrates the effect of section size on the unnotched impact properties of the double-annealed commercial purity material. It can be seen that increase in section

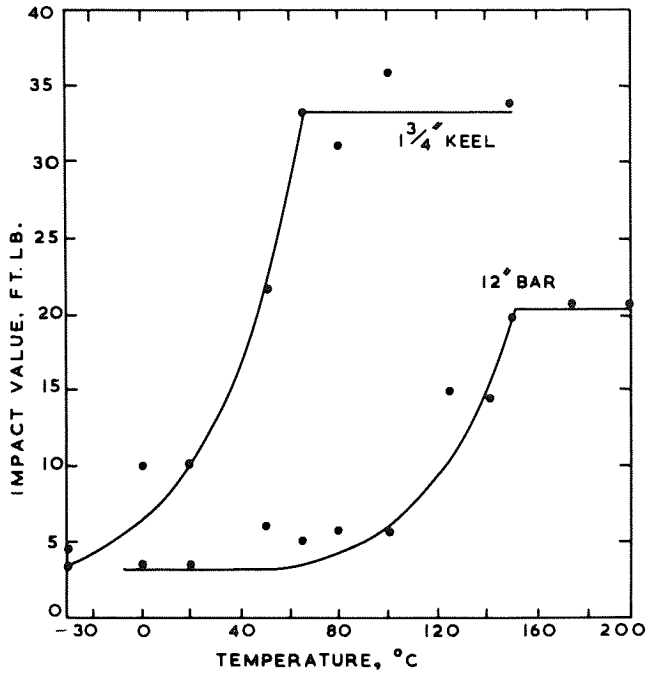

FIG. 28 Effect of section size on unnotched impact values of as-cast commercial purity material.

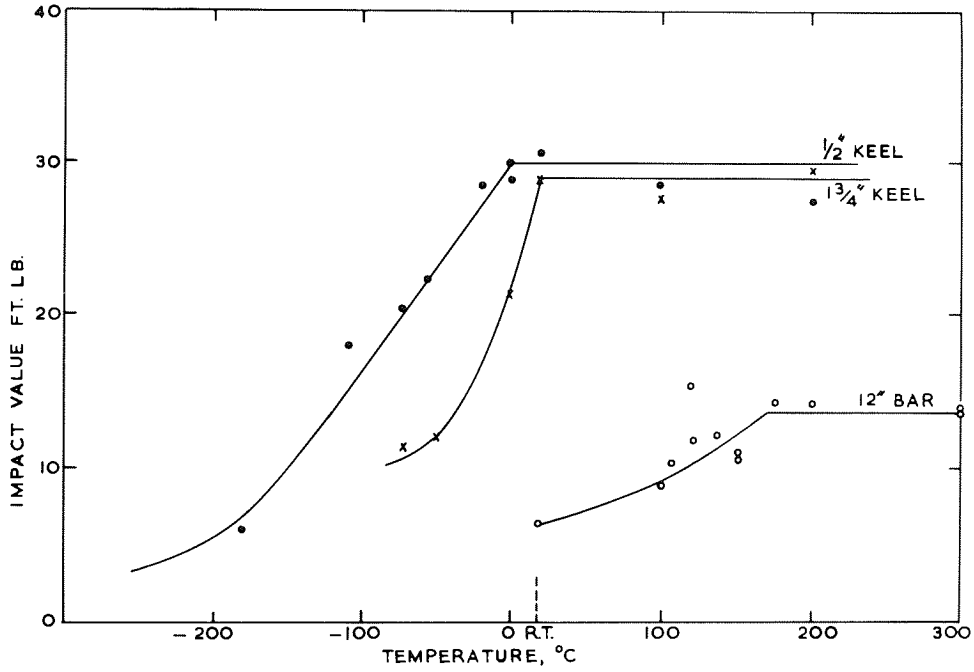

FIG. 29 Effect of section size on unnotched impact values of normalised commercial purity material.

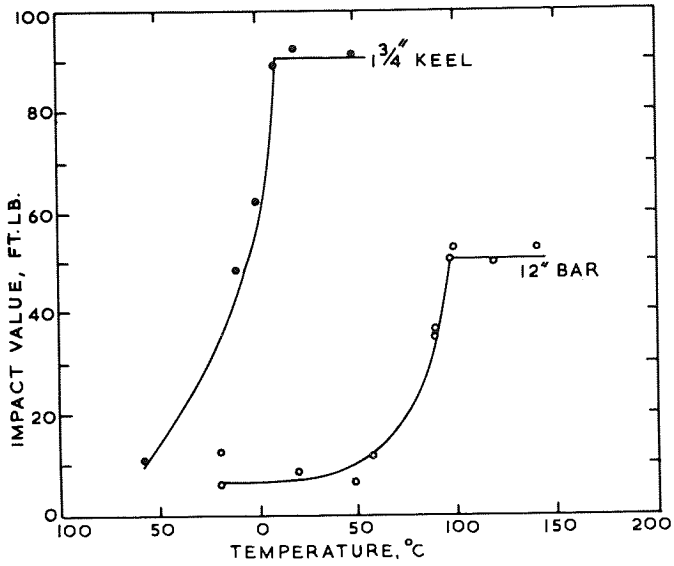

FIG. 30 Effect of section size on unnotched impact values of single-annealed commercial purity material.

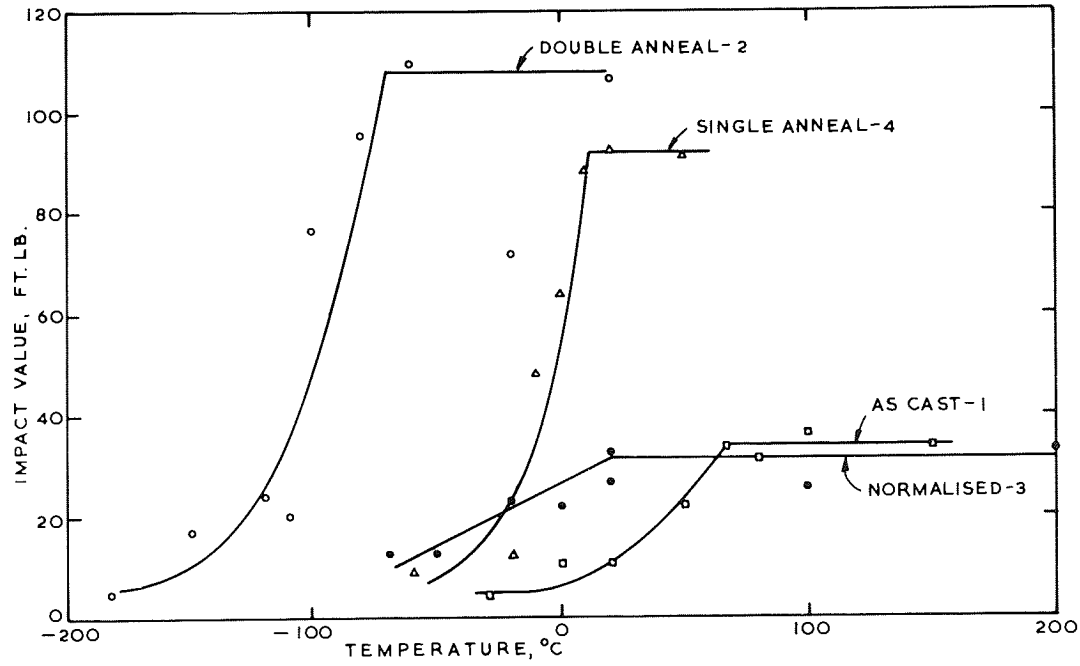

FIG. 31 Effect of heat treatment on unnotched impact values of 1.75 in keel material.

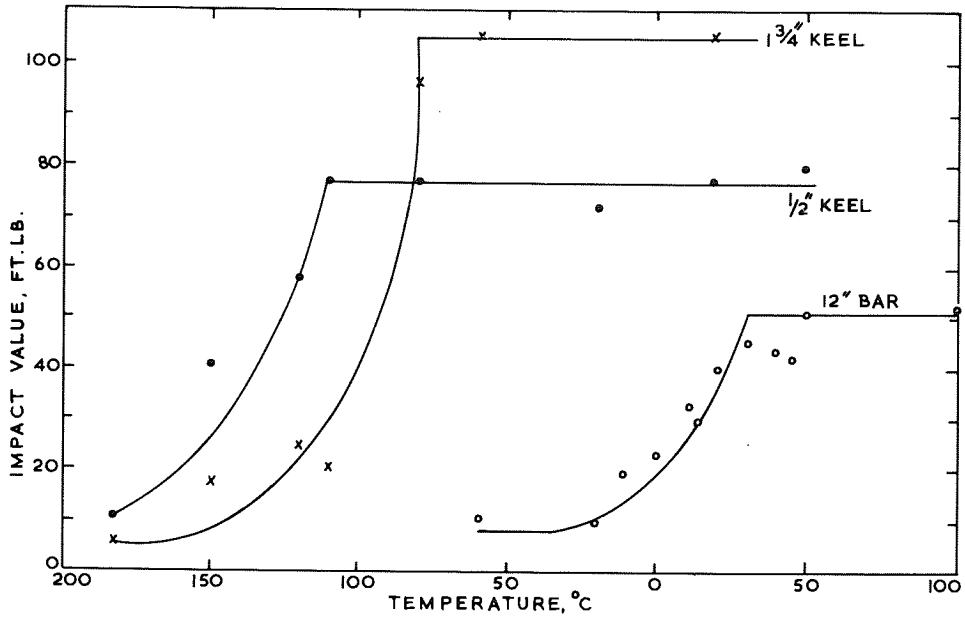

FIG. 32 Effect of section size on unnotched impact values of double annealed commercial purity material.

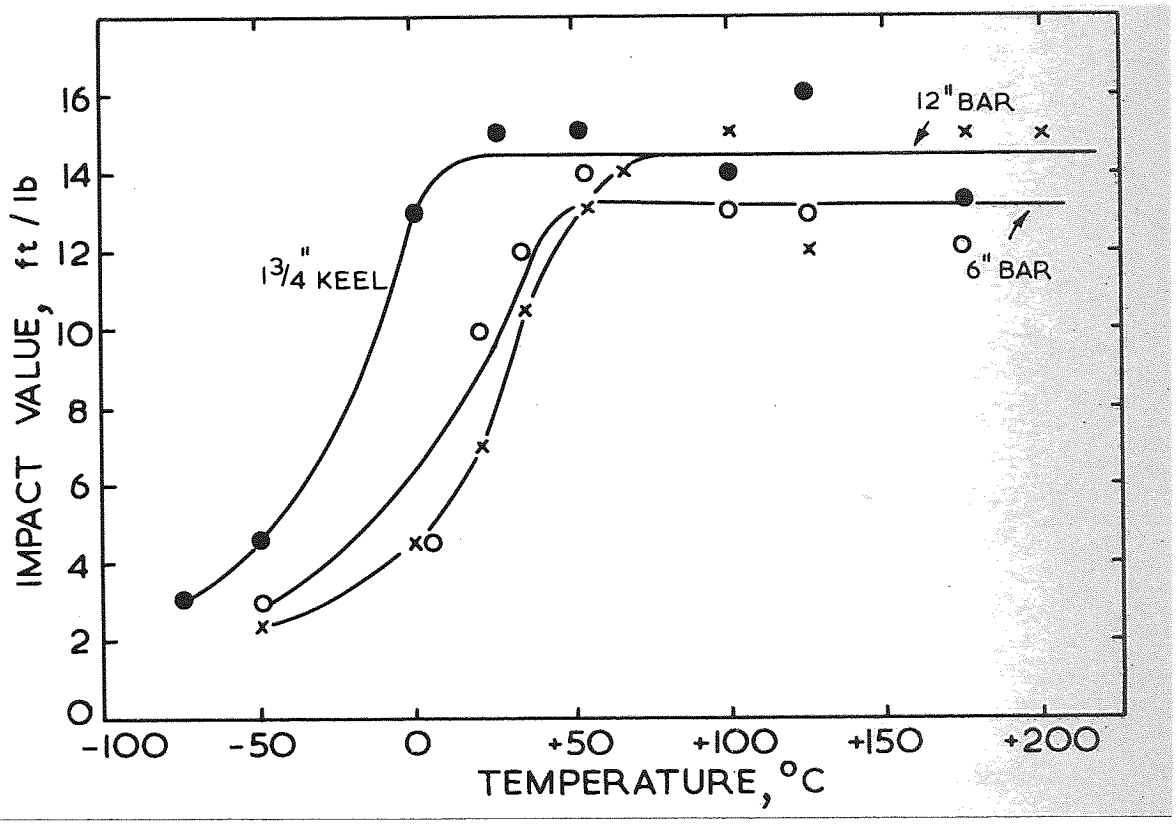

FIG. 33 Effect of section size on notched impact values of double annealed commercial purity material.

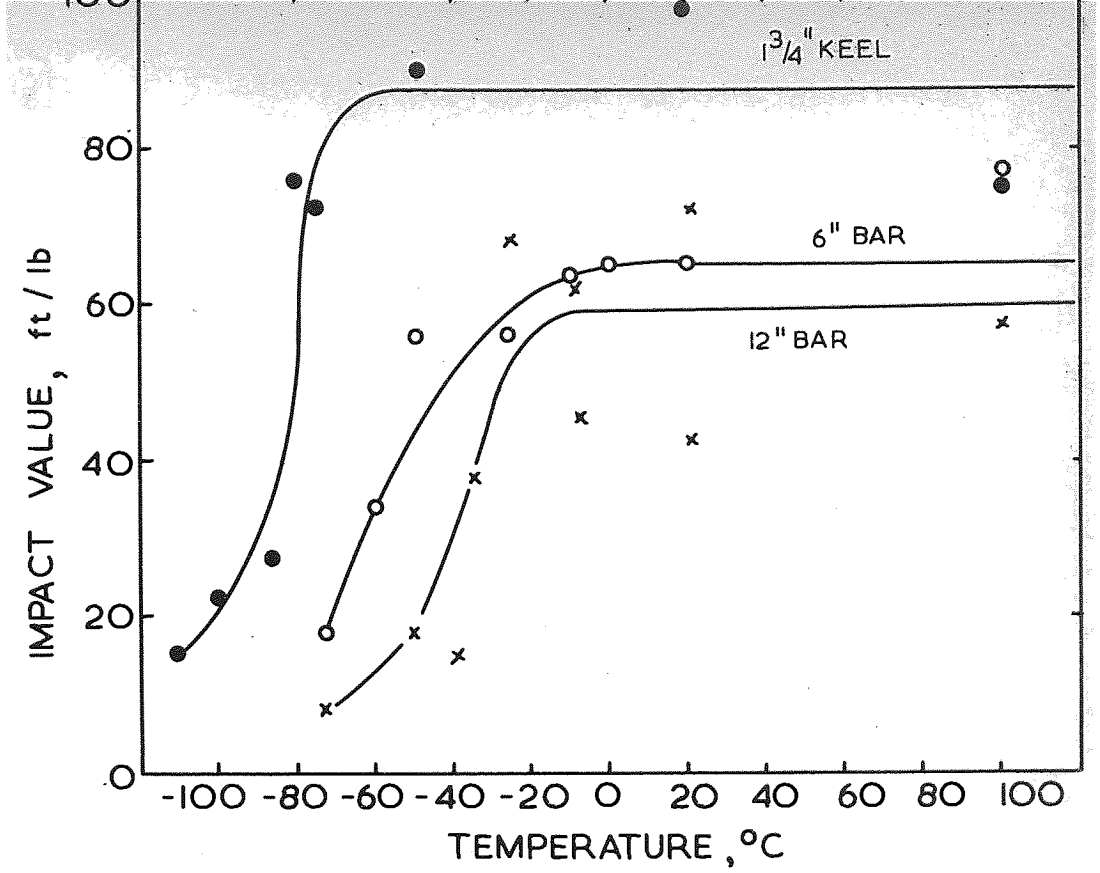

FIG. 34 Effect of section size on unnotched impact values of spheroidise annealed commercial purity material.

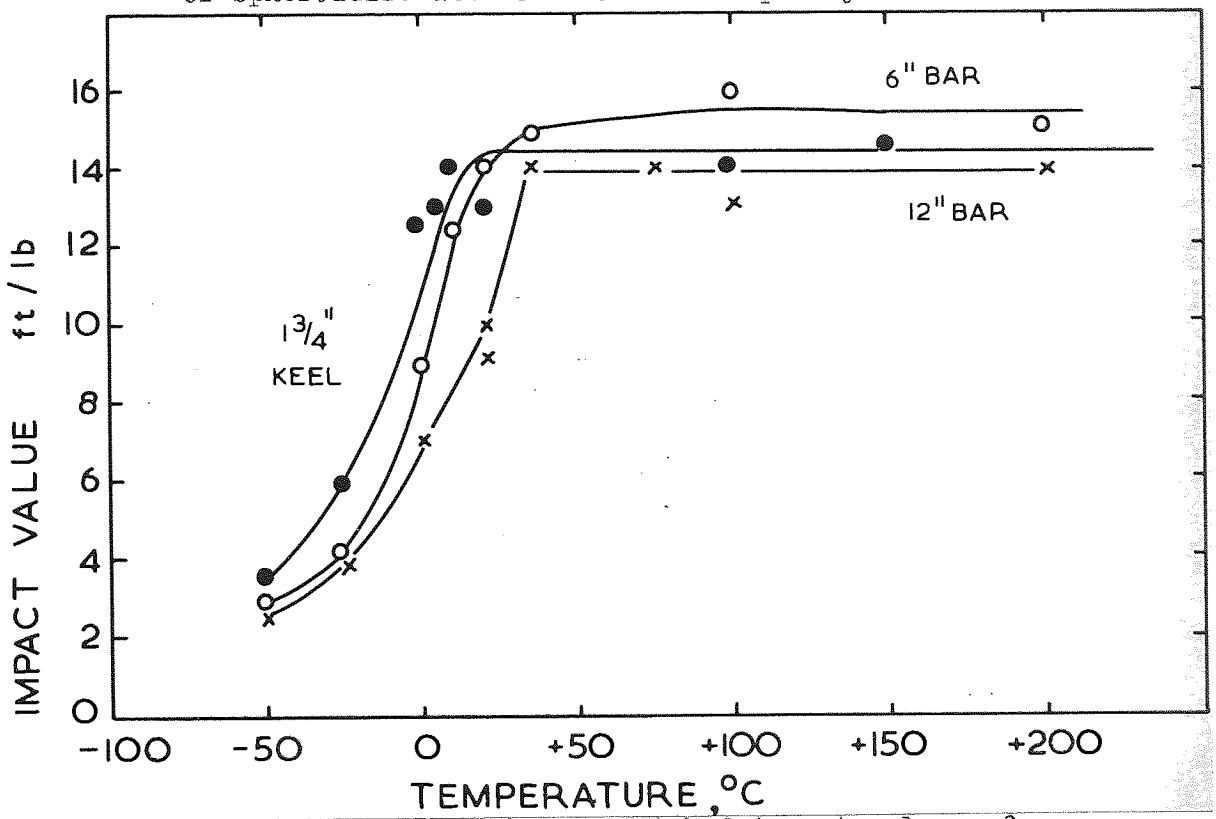

FIG. 35 Effect of section size on notched impact values of spheroidise annealed commercial purity material.

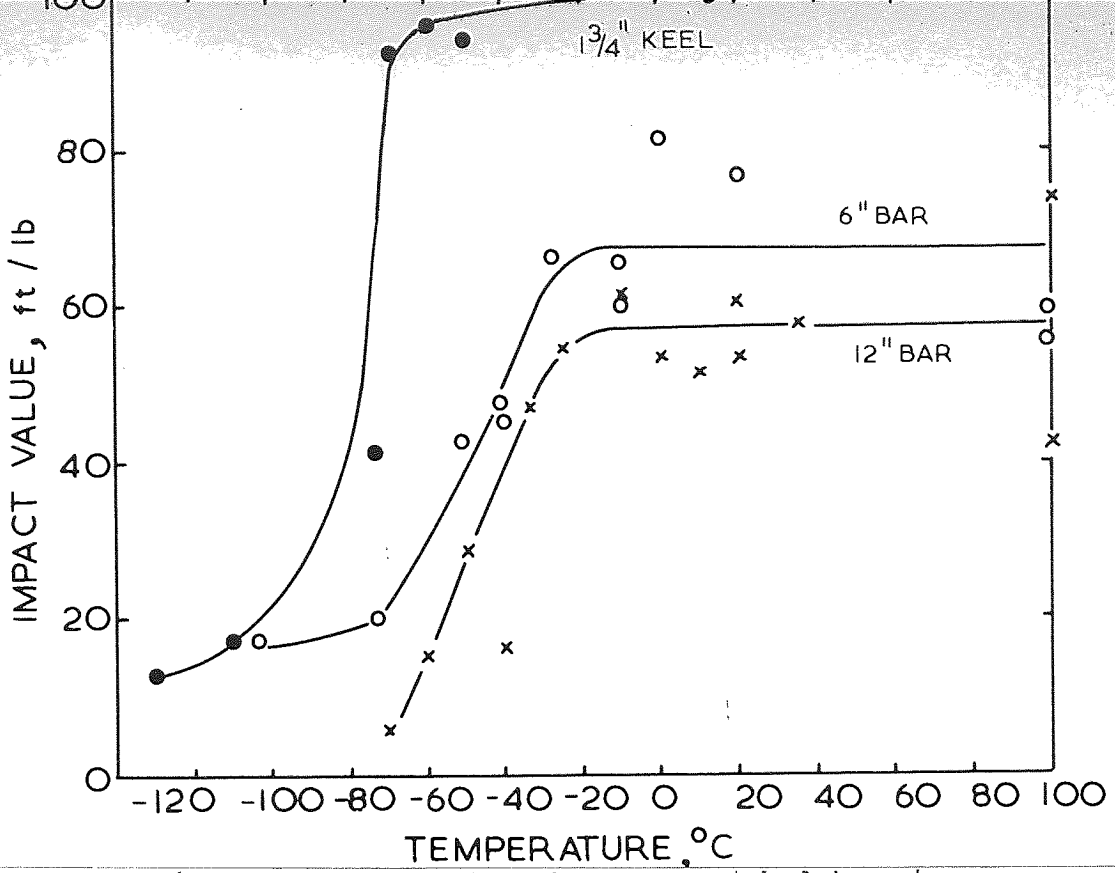

FIG. 36 Effect of section size on unnotched impact values of double annealed refined material.

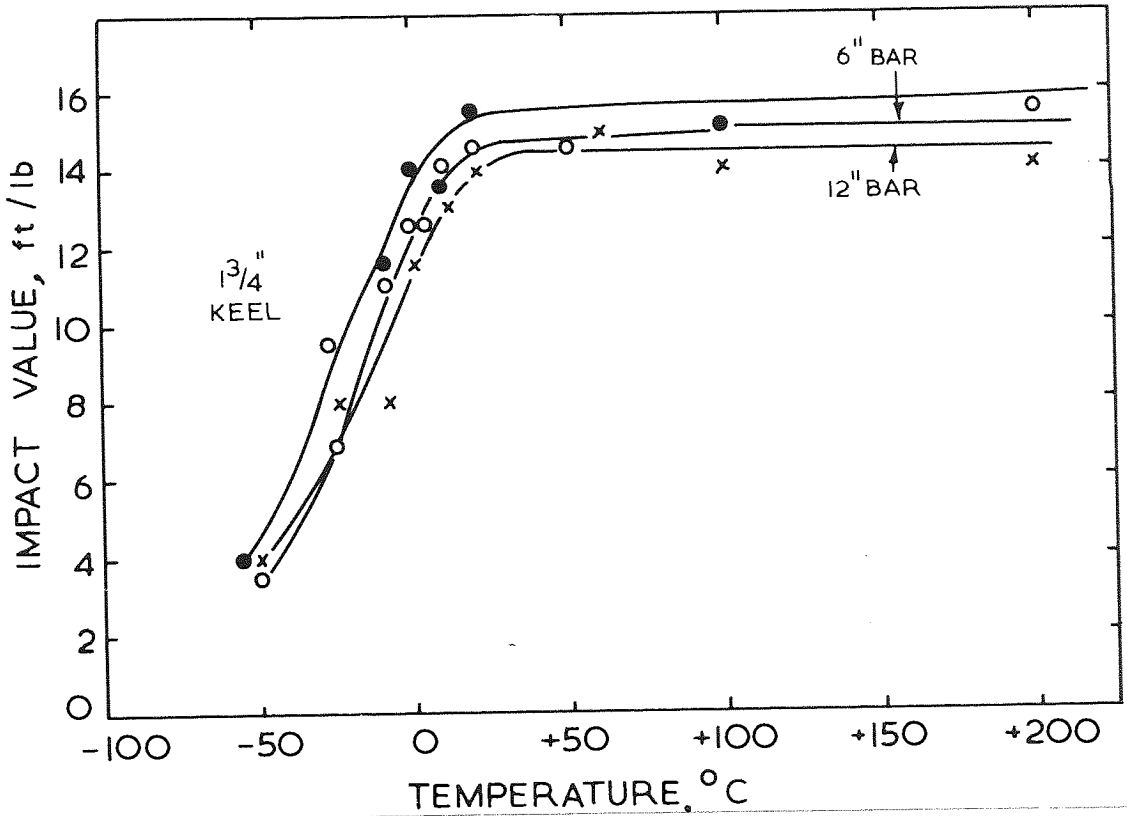

FIG. 37 Effect of section size on notched impact values of double annealed refined material.

has resulted in a decrease in the ductile impact value and an increase in the ductile-brittle transition temperature of this material. Fig. 36 shows that a similar decrease in ductile impact value with increase in section was found in the refined material. The difference in unnotched impact transition temperature between the various sections was not so marked in the purer material, however.

Fig. 33 illustrates the effect of section size on the notched impact values of the double-annealed commercial purity material. The notched ductile impact value was not influenced significantly by change in section. The notched transition temperature, however, increased with increase in section. The spheroidising anneal treatment had resulted in a lessening of the variation in transition temperature with section size as shown in Fig. 35. In Fig. 37 it can be seen that the refined material showed very little change in transition temperature with section size.

Micro-analysis Metallographic examination of the commercial purity specimens revealed segregation effects such as cell boundary carbides in the as-cast state which led to the retention of pearlite after annealing treatments. It was assumed that maximum segregation had occurred in these areas and it was thus decided to examine these regions with the micro-analyser. The results of these investigations are reported below.

Fig. 38 illustrates an electron image and X-ray photographs for different elements over the same area. The area selected

(a)

Electron Image

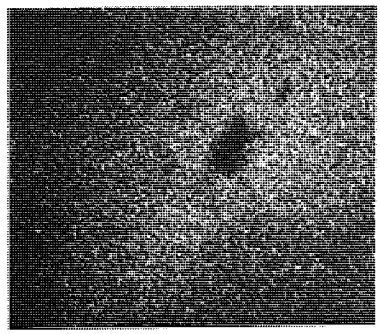

(b)

Manganese X-ray

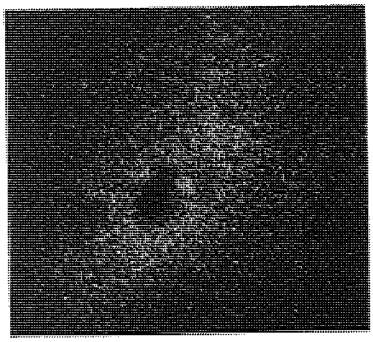

(c)

Chromium X-ray

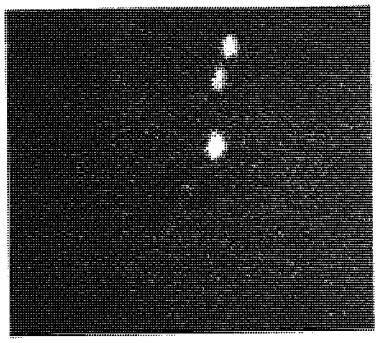

(d)

Titanium X-ray

FIG. 38 Distribution of various elements in a cell boundary carbide in commercial purity material as-cast. x 500

was a carbide phase at a cell boundary in the 12 in section and the X-ray photographs demonstrate qualitatively the manganese, chromium and titanium distribution in this region. It can be seen that manganese and chromium segregated markedly towards cell boundaries and were associated with the carbide phase. Manganese segregation is shown to have been more widespread in this area. Titanium was associated with small precipitates within the carbide phase which could be seen under the optical microscope to have a pink coloration.

In order to obtain more quantitative data concerning segregation effects in these samples it was decided to produce line scans from edge to centre of austenite graphite eutectic cells. Graphite nodules were assumed to be eutectic cell centres for this purpose and, as has been stated, the eutectic cell boundaries were delineated by segregation effects such as cell boundary carbides. The positions of nodules were easily located on the recorder chart due to the absorption of electrons in the nodules and correspondingly lower background radiation causing depressions to occur on the chart when the probe passed over a nodule. The lightness of the nodules also resulted in a low background radiation. The elements included in the curves below are the only ones which were present in sufficient quantity to be studied by micro-analysis.

Figs. 39-41 illustrate the results of line scans from the edge of a graphite nodule passing through cell boundaries in the 12 in and $1\frac{3}{4}$ in sections. The curves have been calculated from the recorder chart results, appropriate corrections having been made where necessary. The results indicate that depletions of

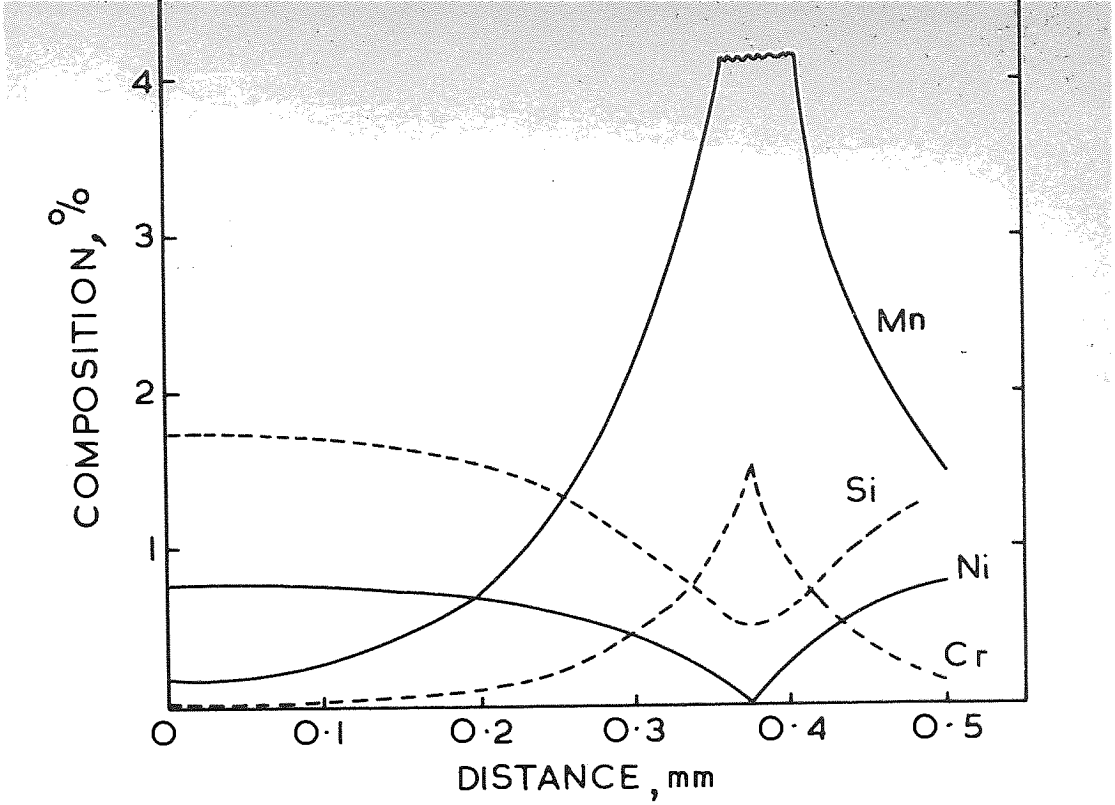

FIG. 39 Line scan from edge of a graphite nodule through a cell boundary carbide in 12 in commercial purity material as-cast.

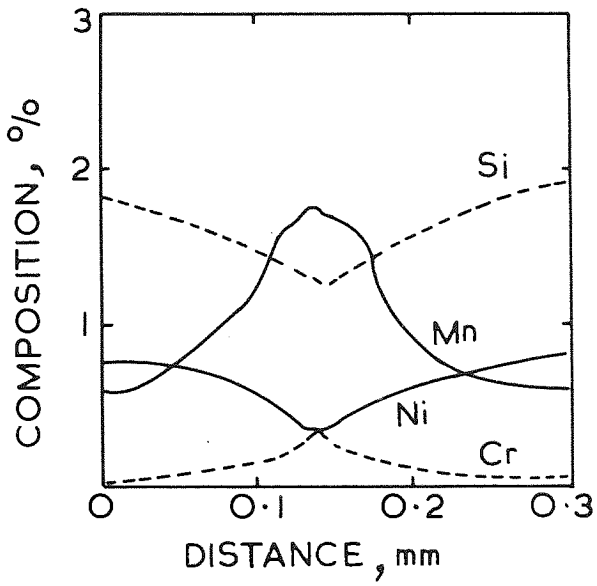

FIG. 40 Line scan from edge of a graphite nodule through a cell boundary region containing no carbide in 12 in commercial purity material as-cast.

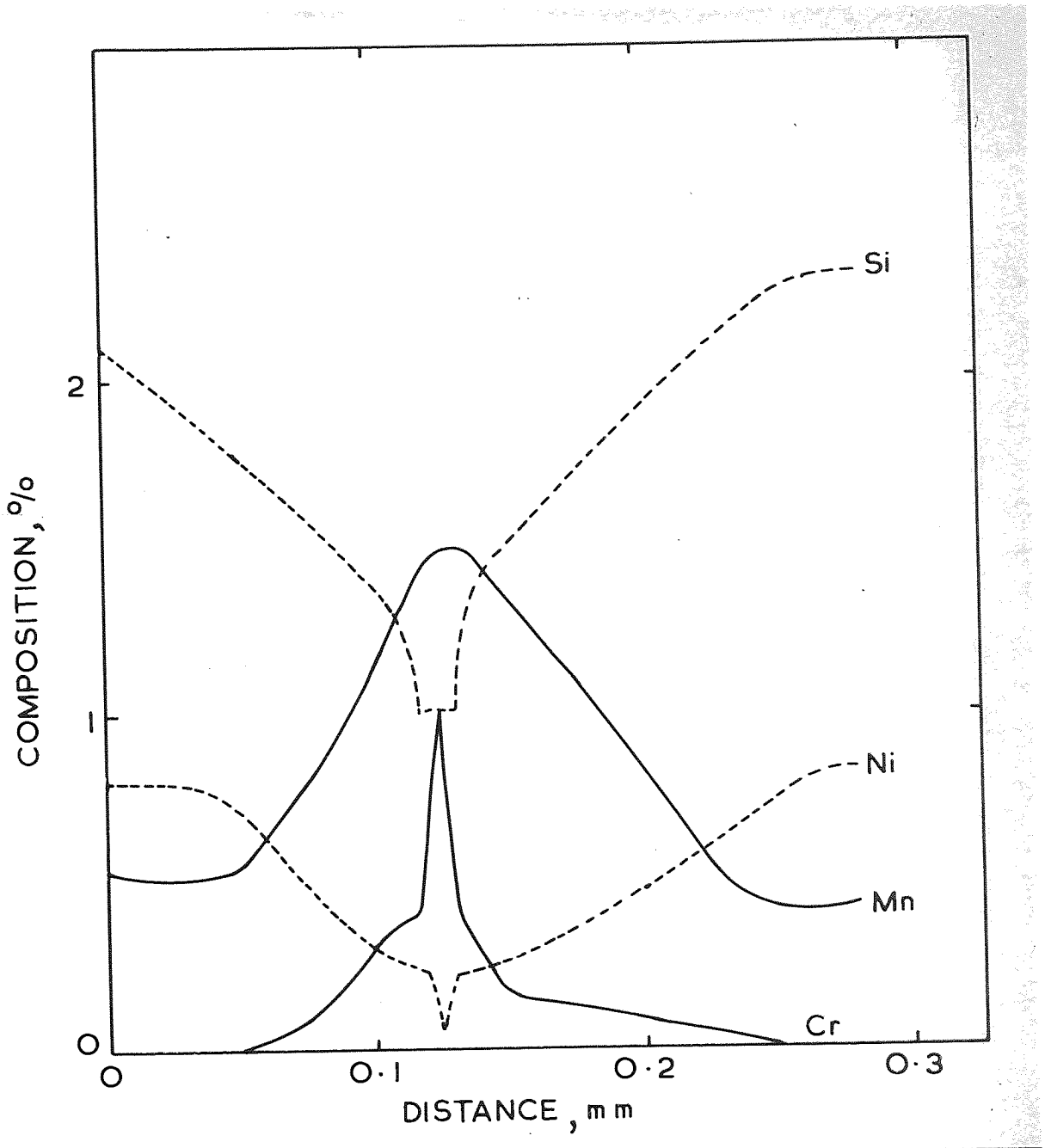

FIG. 41 Line scan from edge of a graphite nodule through a cell boundary carbide in 1.75 in section of commercial purity material as-cast.

nickel and silicon occurred at eutectic cell boundaries particularly in carbide regions. Manganese and chromium segregated towards cell boundaries and were associated with the carbide phase. Chromium was much more sharply segregated to grain boundaries than manganese which is illustrated in Fig. 41 depicting the segregation of elements across a cell boundary in the $1\frac{3}{4}$ in keel. In cell boundary regions containing no carbide but delineated by darker pearlite, manganese segregation was found to be less marked than in carbide regions (Fig. 40) and only slight chromium segregation was apparent.

Fig. 42 illustrates the segregation of manganese across an austenite graphite cell in the 12 in section which was obtained by moving the specimen under the electron probe as the microstructure was too coarse to allow a cell to be crossed by a single scan. Two nodules, depicted by chart depressions, have been crossed by the probe and were both within the segregation peaks associated with the cell boundaries. It can be seen from Fig. that more than one graphite nodule appear to be within the area bounded by cellular segregation effects which is confirmed by the micro-analytical evidence. It is difficult to show a quantitative relationship between section size and microsegregation. In the heavier sections there was a great deal more carbide around the cell boundaries and these carbides contained greater amounts of manganese, in particular, than similar carbides in smaller sections. Static spot analyses were carried out on the $\frac{1}{2}$ in chill keel in order to determine the distribution of elements

between the carbide and pearlite phases of the ledeburite eutectic. Table 6 shows the results obtained by this method.

Electron probe scans were carried out across cell boundary regions in the normalised materials. It was found that the segregation pattern had not been significantly changed (Fig. 43) by this treatment. Presumably the normalise treatment had not been of sufficient duration to cause any carbide breakdown.

Probe scans were also made across retained pearlite areas in the double-annealed commercial purity materials. It was found that the segregation of manganese and chromium had been markedly affected by the double-anneal heat treatment. Fig. 44 shows the distribution of manganese, chromium, silicon and nickel across an area of retained pearlite in the 12 in section. It is apparent that some dissolution of a cell boundary carbide has taken place although manganese and chromium are still associated with the undissolved carbide. The heat treatment had not been long enough to allow complete redistribution of manganese and chromium to take place in the matrix and a "plateau" of manganese and, to a lesser extent, chromium still remained. It was in these regions that pearlite had been retained after the heat treatment. Fig. 45 illustrates the segregation pattern across a retained pearlite area in the 12 in double-annealed sample which contained no undissolved massive carbide. Segregation of manganese was not so marked as in the previous scan and very little chromium segregation was apparent. It seems likely that this area, in the as-cast state contained a much smaller amount of cell boundary

TABLE 6

DISTRIBUTION OF VARIOUS ELEMENTS BETWEEN CEMENTITE AND PEARLITE IN $\frac{1}{2}$ IN CHILLED KEEL SPECIMEN

Element	Cementite (%)	Pearlite (%)
Manganese	0.40	0.29
Chromium	0.16	N.D.
Silicon	N.D.	3.30
Nickel	0.295	1.21
Copper	N.D.	0.07

N.D. = none detected

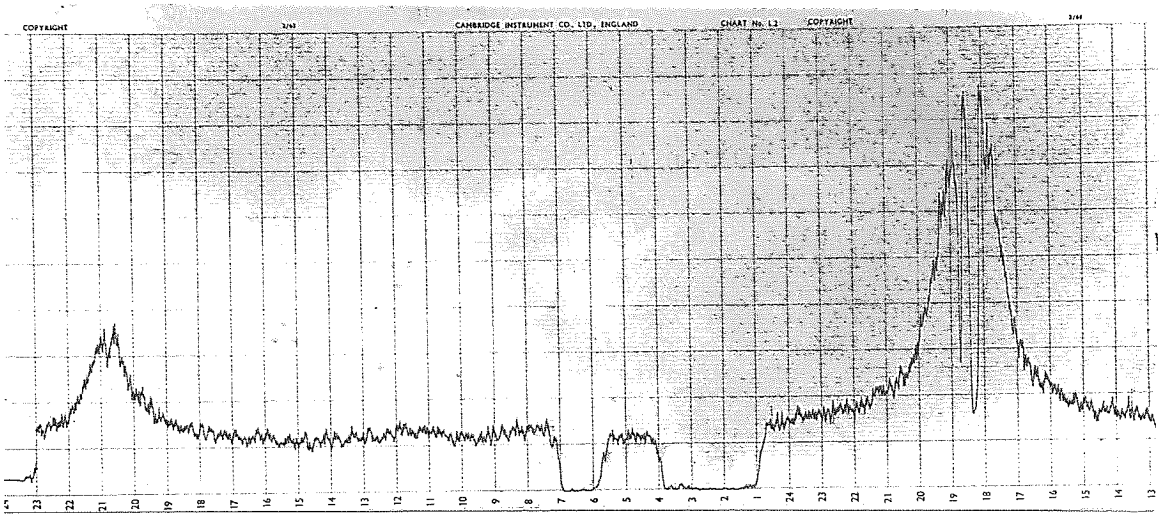

FIG. 42 Distribution of manganese across an austenite-graphite eutectic cell in 12 in section of commercial purity material as-cast.

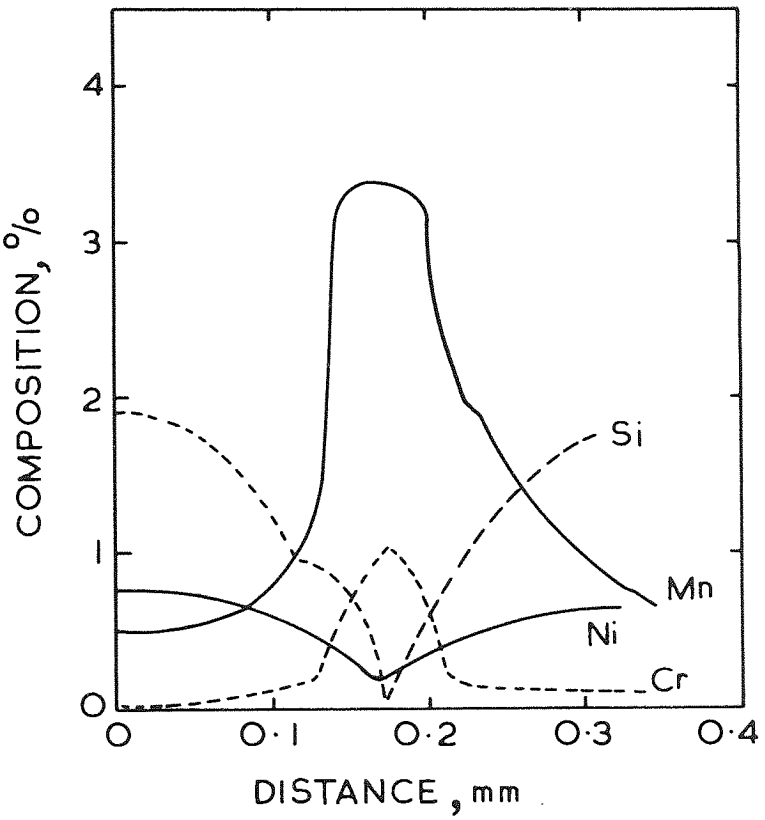

FIG. 43 Line scan from edge of a graphite nodule through a cell boundary carbide in 12 in section of commercial purity material normalised.

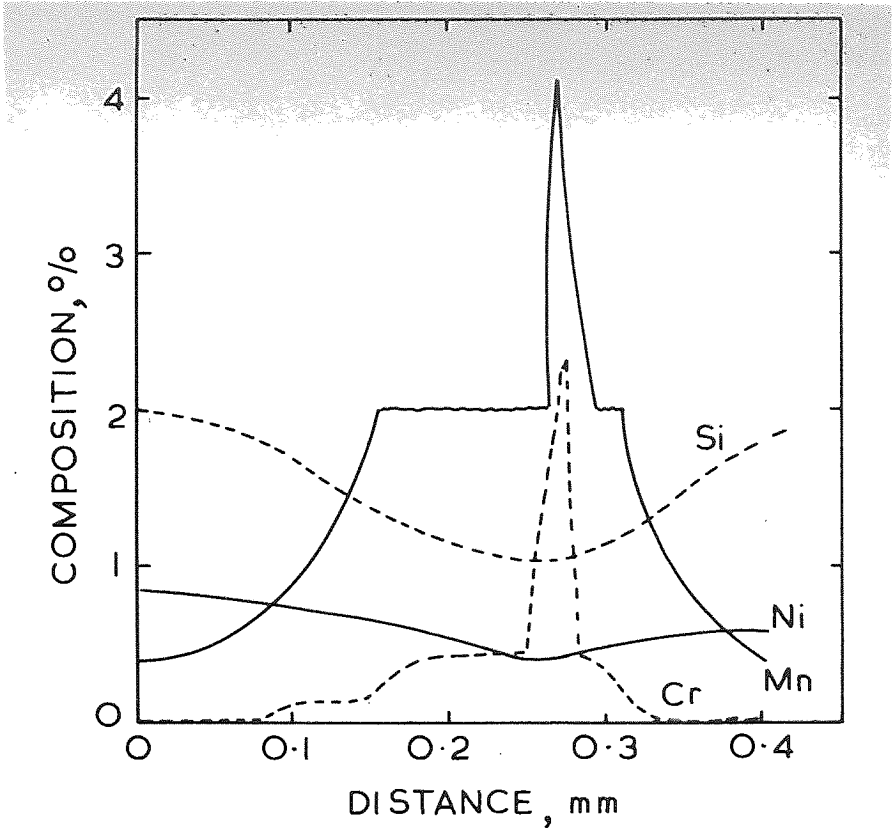

FIG. 44 Line scan from edge of a graphite nodule through a retained pearlite area containing undissolved carbide in 12 in section of double annealed commercial purity material.

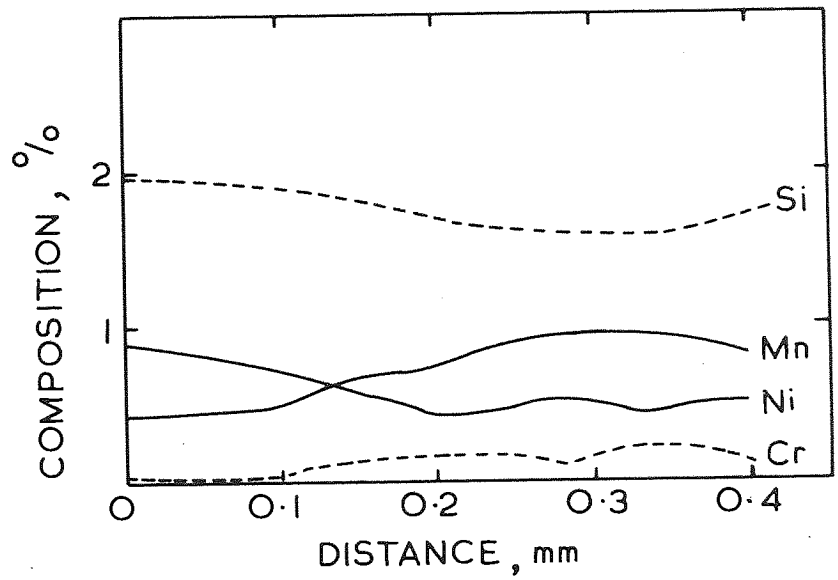

FIG. 45 Line scan through an area of retained pearlite containing no undissolved carbide in 12 in section of double annealed commercial purity material.

carbide containing correspondingly lower amounts of manganese and chromium which was dissolved but not fully redistributed by the double-anneal treatment.

Examination of the $1\frac{3}{4}$ in keel specimen in which no undissolved carbides were apparent revealed that segregation of manganese was still associated with retained pearlite areas in concentrations of over 1 per cent (Fig. 46), while chromium concentrations in the same regions were 0.3 per cent or less. No segregation of elements could be detected in the double-annealed $\frac{1}{2}$ in keel section.

Fig. 47 illustrates the distribution of manganese, chromium, nickel and silicon across a retained pearlite area in the 12 in sample which was subjected to a "spheroidise" anneal (treatment 5). Microsegregation had been minimised by this treatment although some carbide, rich in manganese and chromium but much more globular in shape, still persisted in smaller amounts than in the double-annealed sample.

The double-annealed refined material was also examined to find out if any segregation could be detected. No manganese or chromium could be detected in cell boundary regions although slight depletions of nickel and silicon occurred in these areas (Fig. 48).

The segregation patterns observed in the commercial purity single-annealed samples were very similar to those found in the double-annealed condition although somewhat more massive carbide was to be found on the single-annealed samples. No evidence of

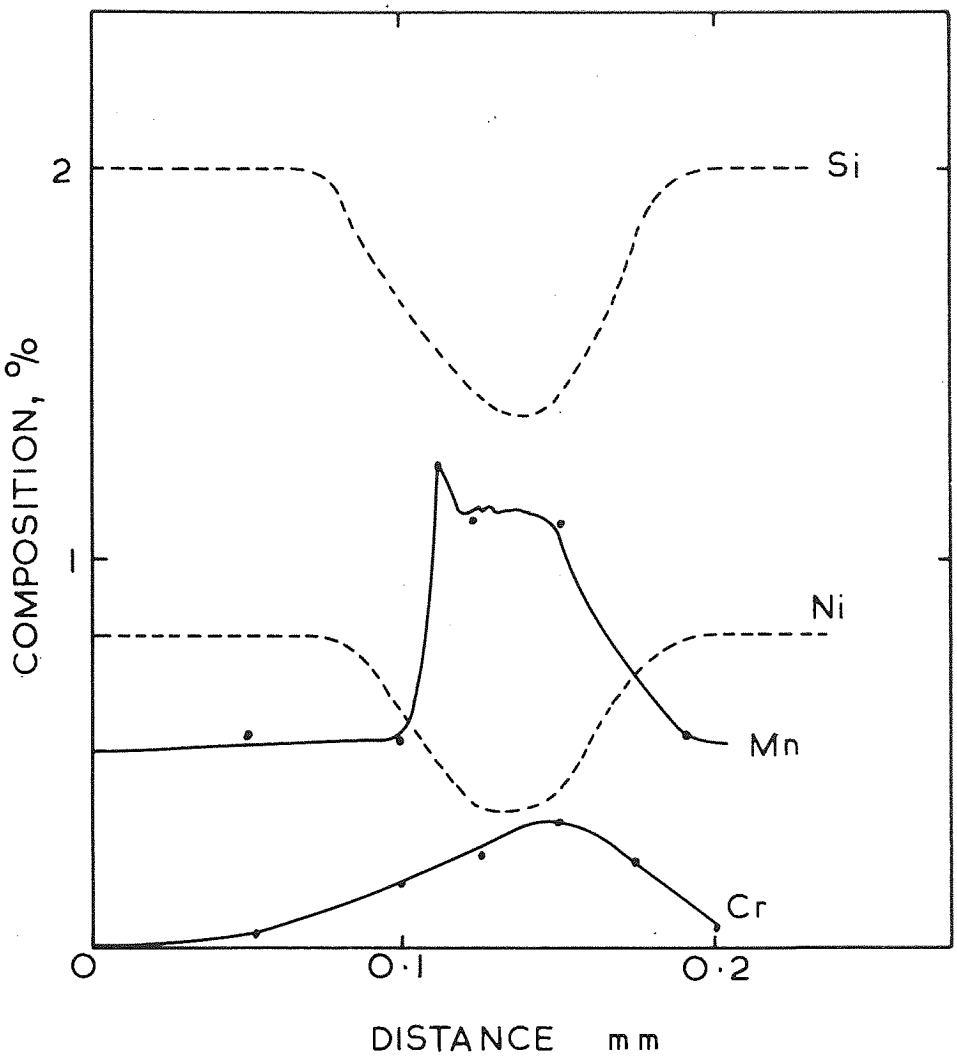

FIG. 46 Line scan from edge of a graphite nodule through a cell boundary area in 1.75 in keel section of double annealed commercial purity material.

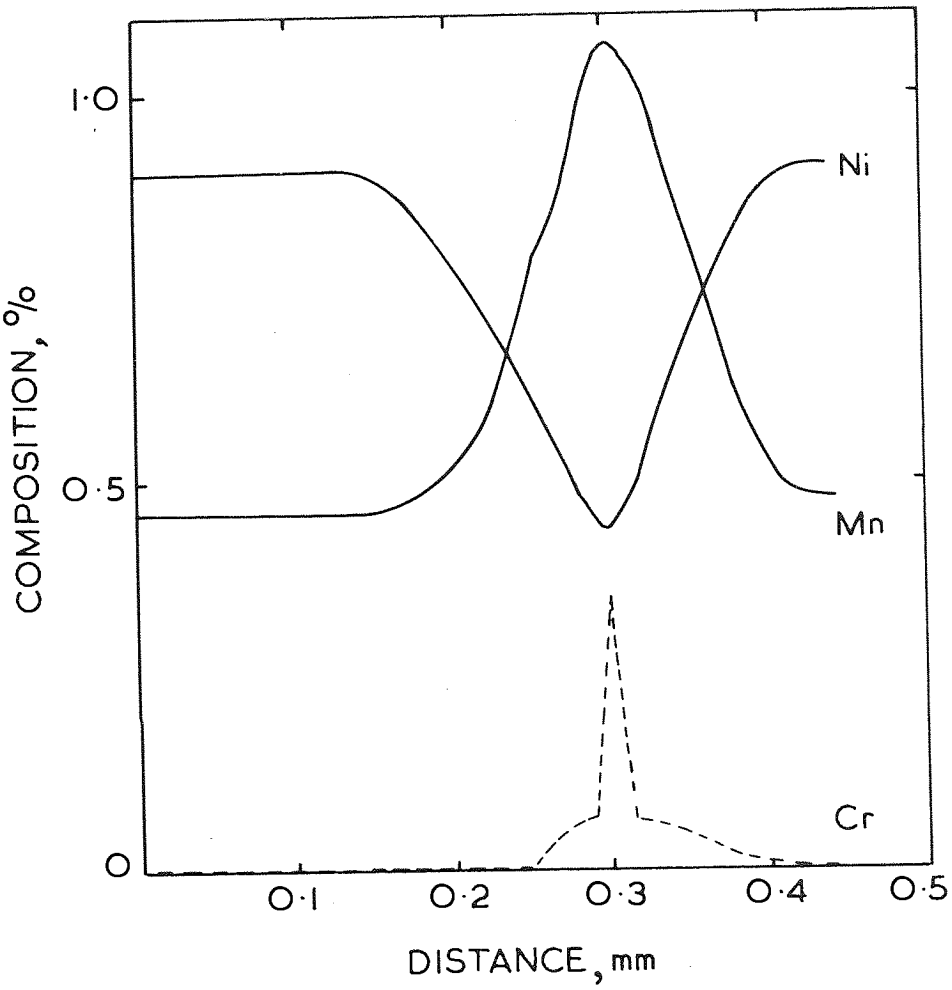

FIG. 47 Line scan across an area of undissolved carbide in spheroidise annealed 12 in section of commercial purity material.

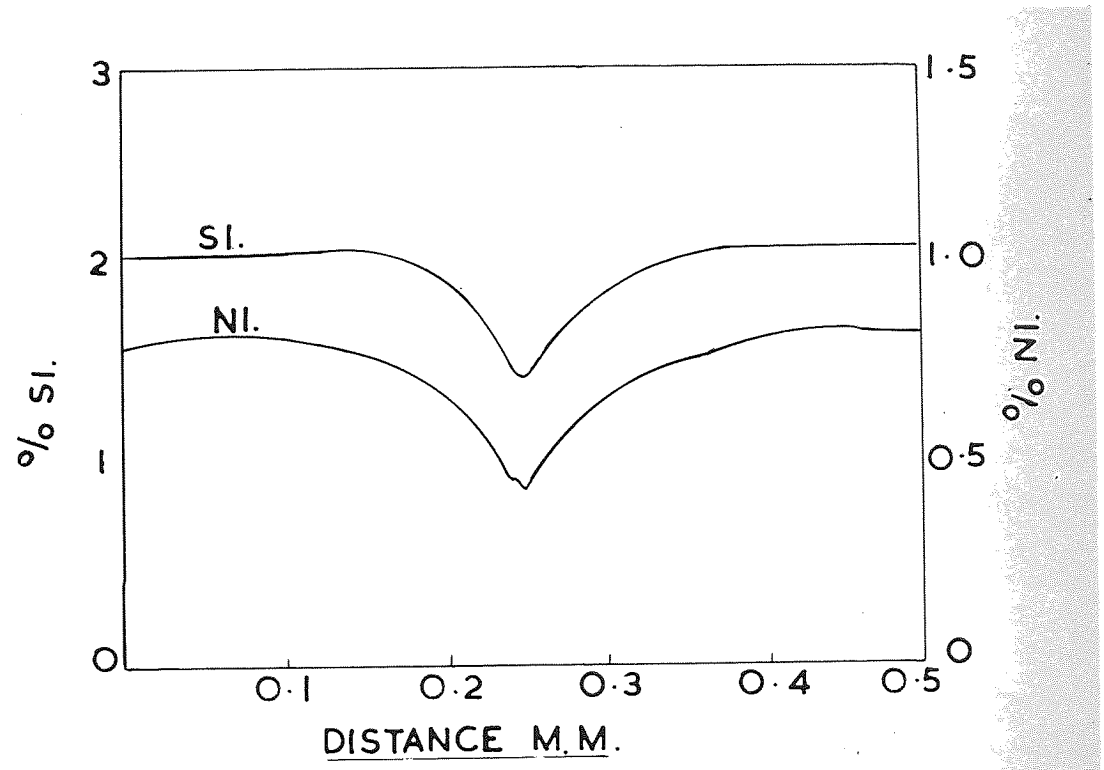

FIG. 48 Line scan across cell boundary area in refined material double annealed.

any segregation effects that could possibly be related to the presence of the undesirable ferritic sub-structure could be detected by micro-analysis.

AUSTENITIC IRONS

Metallography Figs. 49 and 50 illustrate the structures obtained in the 0.5 per cent manganese iron in the as-cast condition. The structure consisted mainly of graphite nodules in austenitic matrices. The nodule size increased while their number decreased with increase in section. A two phase carbide structure was noticed in cell boundary areas and was more widespread in heavier sections. Fig. 49 depicts an area of this carbide in the 12 in diameter bar. As with the ferritic materials the microstructures of the 6 in and 12 in bars were examined from edge to centre of these bars. In the centre of the 12 in bar, a region which had cooled very slowly, bainite was associated with these carbides (Fig. 51). The phase was assumed to be bainite rather than martensite as the Ms temperature of the material was found to be about -50°C (Fig. 53). Samples from each section were heat treated for 24 hours at 1 000°C and air cooled in an attempt to break down these carbides. (A heat treatment of holding for 1 to 5 hours at 950-1 100°C and air cooling is recommended practice[68]). The treatment caused a partial rounding of the carbides but did not remove them even from the $1\frac{3}{4}$ in section. Microhardness determinations were carried out on these carbides.

The microstructures of the 4 per cent manganese material were similar to those of the low manganese material but contained much more carbide as can be seen from Fig. 52. The presence of this carbide made the material difficult to machine and

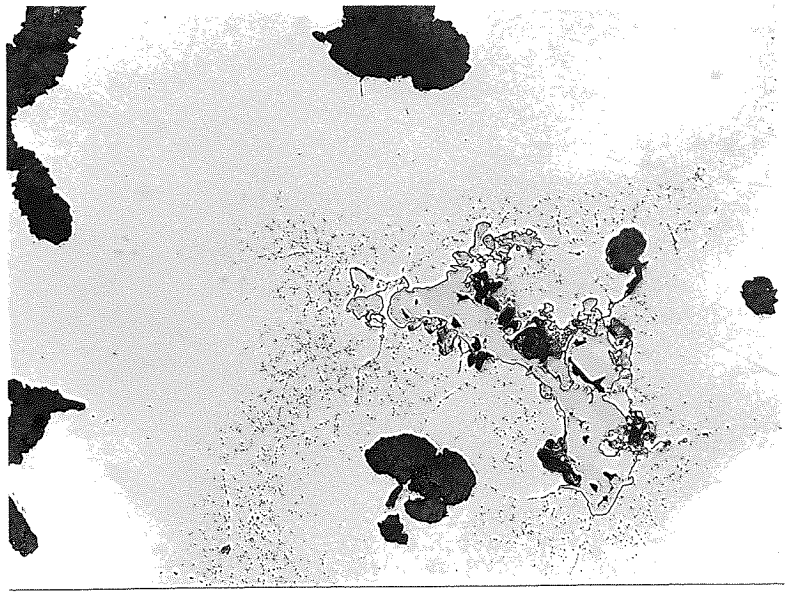

FIG. 49 12 in section of 0.5 per cent manganese austenitic iron as-cast.
Etched in 5% Nital x 100

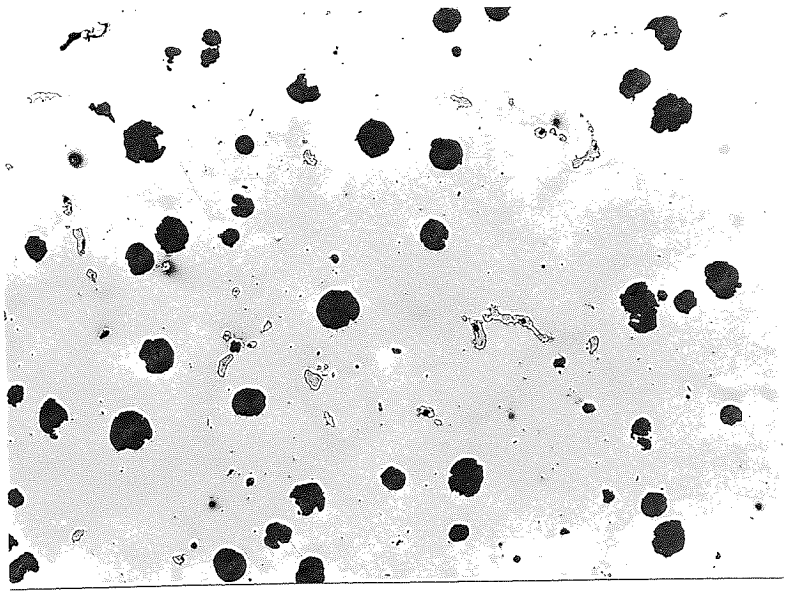

FIG. 50 1.75 in keel section of 0.5 per cent manganese austenitic iron as-cast.
Etched in 5% Nital x 100

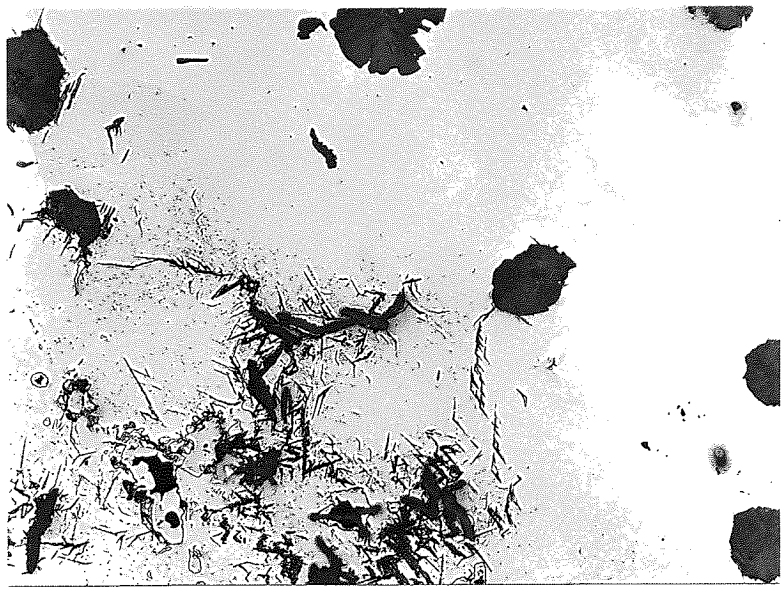

FIG. 51 Centre of 12 in section of 0.5 per cent manganese austenitic iron showing bainite near cell boundary carbides.
Etched in 5% Nital x 100

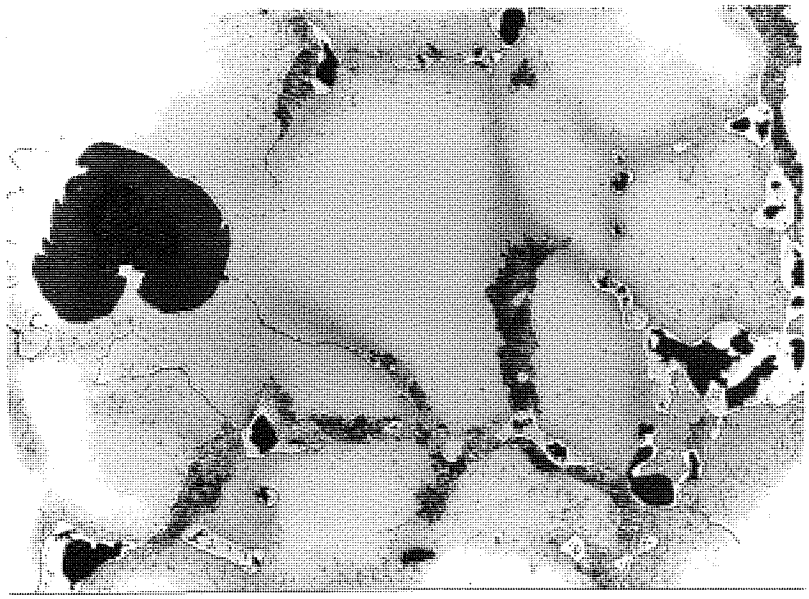

FIG. 52 12 in section of 4 per cent austenitic material as-cast.
Etched in 5% Nital x 100

so mechanical test specimens were only taken from the $1\frac{3}{4}$ in keel and the 12 in diameter bar.

Mechanical Properties Table 7 illustrates the results of tensile test determinations on various sections of the 0.5 and 4 per cent manganese material. Increase in section size in the lower manganese iron had resulted in a significant decrease in the ultimate tensile stress, elongation and hardness values while proof stress values showed no change with change in section. The effect of change in section on the 4 per cent manganese material was more marked. The $1\frac{3}{4}$ in keel sections of this material had elongation values of 40 per cent compared with 22 per cent in the 12 in sections.

Figs. 53 to 55 illustrate the results of notched and unnotched Charpy impact tests on the austenitic materials. It can be seen that apart from a slight decrease of the unnotched impact value with increase in section size there were no significant trends in the results from the low manganese material. The change from non-magnetic to magnetic properties with decreasing temperature indicates the onset of martensite formation in the material. It is shown in Fig. 55 , however, that increase in section size significantly lowered the notched impact value of the 4 per cent manganese material.

Micro-analysis Fig. 56 shows the distribution of nickel, manganese, silicon and iron in a cell boundary carbide in the 12 in section of the low manganese austenitic iron. The duplex nature of this region is evident from these results. It can be seen

TABLE 7

TENSILE PROPERTIES OF AUSTENITIC IRONS

Sample	Diameter (in)	Ultimate Tensile Strength (tons/in^2)	0.5% Proof Stress (tons/in^2)	Elongation (%)	HB 10/3000
0.5% Mn					
1.75 in keel	0.564	26.7	13.5	26	121
6 in bar	0.798	24.8	12.6	24½	117
12 in bar	0.798	23.1	12.4	21½	118
4% Mn					
1.75 in keel	0.564	29.0	14.6	40	138
12 in bar	0.798	23.9	13.5	22	119

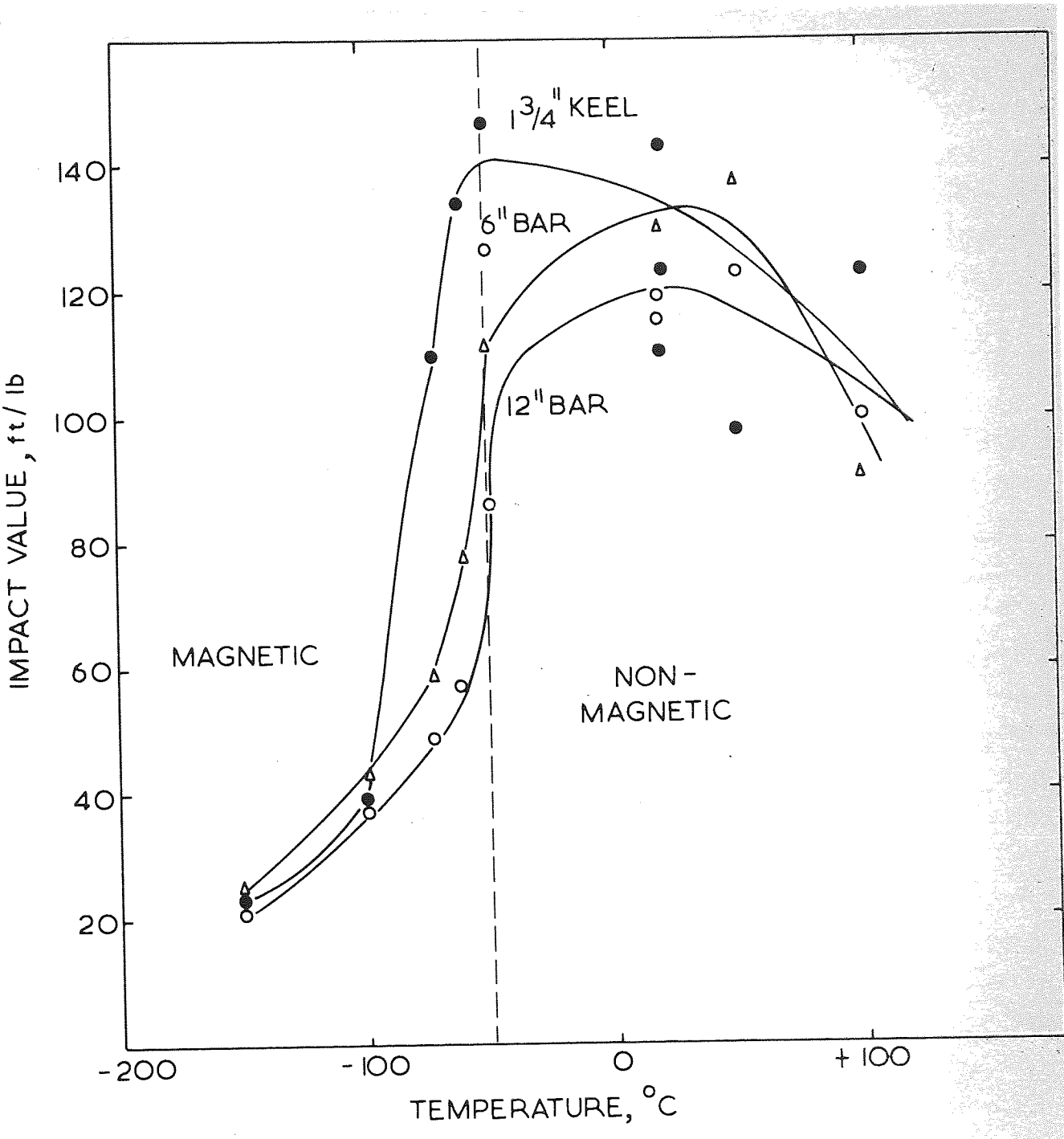

FIG. 53 Effect of section size on the unnotched impact properties of 0.5 per cent manganese austenitic material.

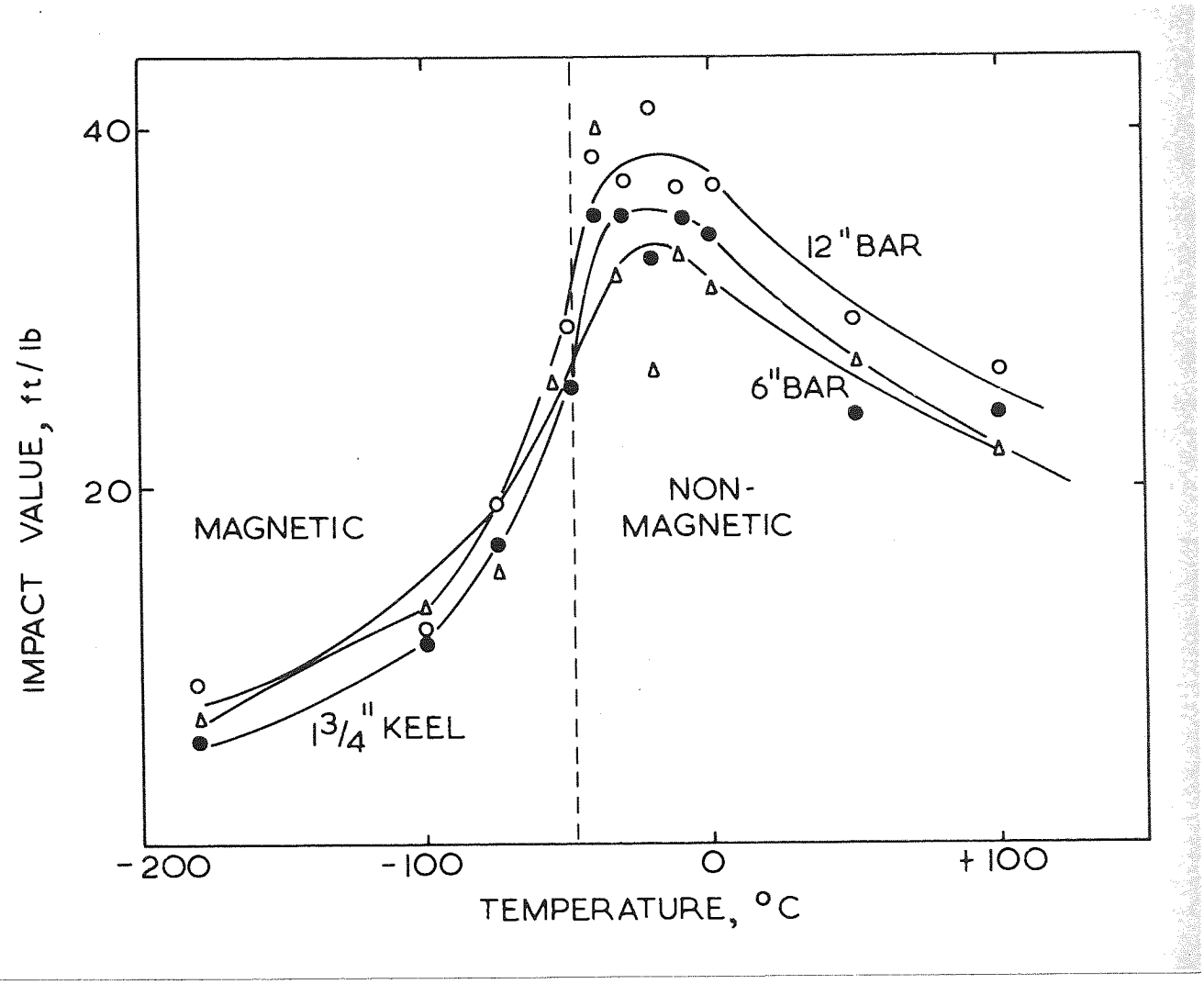

FIG. 54 Effect of section size on the notched impact properties of 0.5 per cent manganese austenitic material.

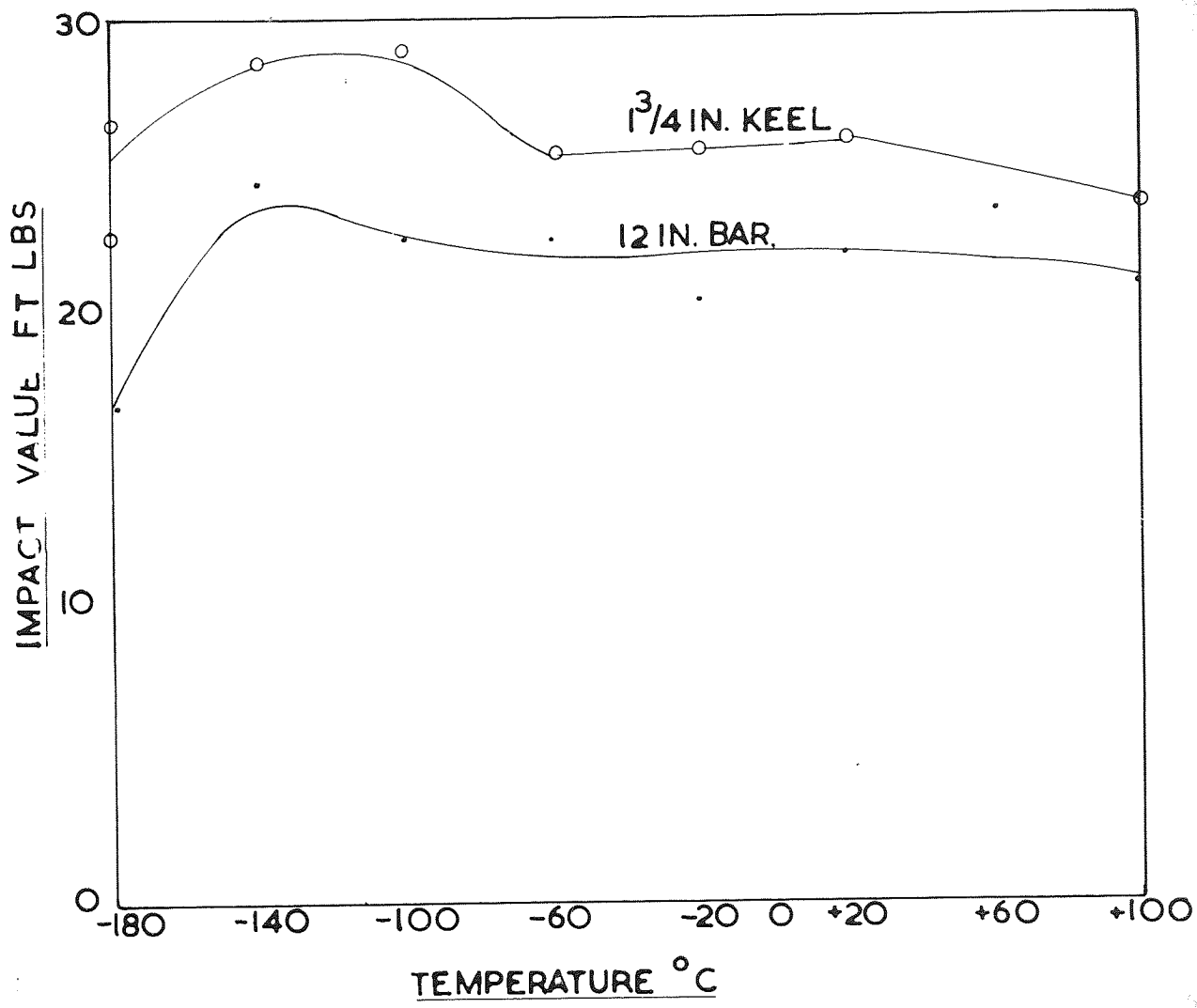

FIG. 55 Effect of section size on the notched impact properties of 4 per cent manganese austenitic material.

that the "carbide" consisted of a constituent rich in nickel and silicon and a constituent richer in manganese and iron. ~~The nickel rich constituent corresponded to the lighter etching constituent noticed under the microscope and mentioned on p.46. A quantitative static probe analysis was carried out on both constituents which yielded the results shown in Table 7.~~

Electron probe line scans were again carried out from the edges of nodules to cell boundary regions in these samples. Fig. 57 shows the distribution of manganese, nickel and silicon from the edge of a graphite nodule across a duplex carbide in the 12 in section austenitic iron. The partition of the various elements in the carbide is obvious from these curves. It is interesting to note the segregation behaviour of these elements towards the grain boundary. Manganese was concentrated towards the grain boundaries as in the ferritic irons. Nickel was depleted in grain boundary areas. It can be seen from Fig. 57 that the nickel content of the regions adjacent to cell boundary carbides contained 14 per cent nickel compared with 22.0 per cent in the matrix. Although partition of silicon occurred between the constituents of the cell boundary carbide no silicon segregation occurred in this material. The distribution of alloying elements across a cell boundary area in the 12 in section containing no carbide is shown in Fig. 58. Depletion of nickel and concentration of manganese to a somewhat lesser extent than in carbide regions can be seen to have occurred from this diagram. Fig. 59 illustrates the segregation

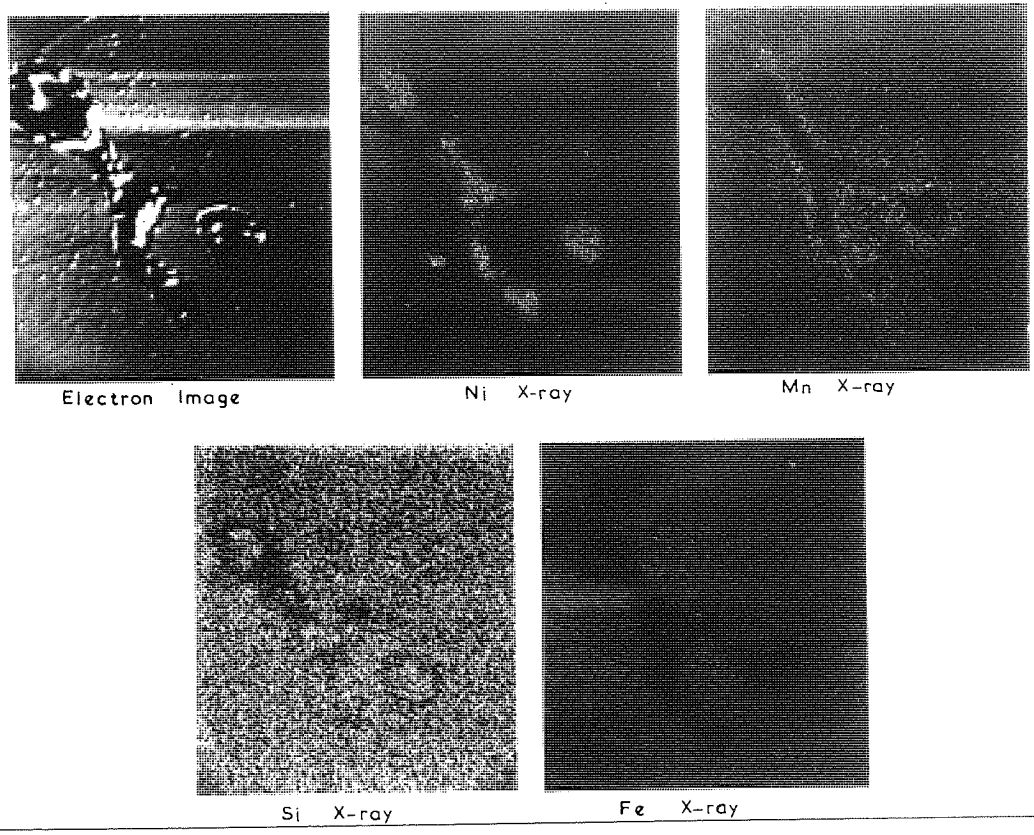

FIG. 56 Distribution of various elements in duplex grain boundary phase in 12 in section of 0.5 per cent manganese austenitic iron. x 500

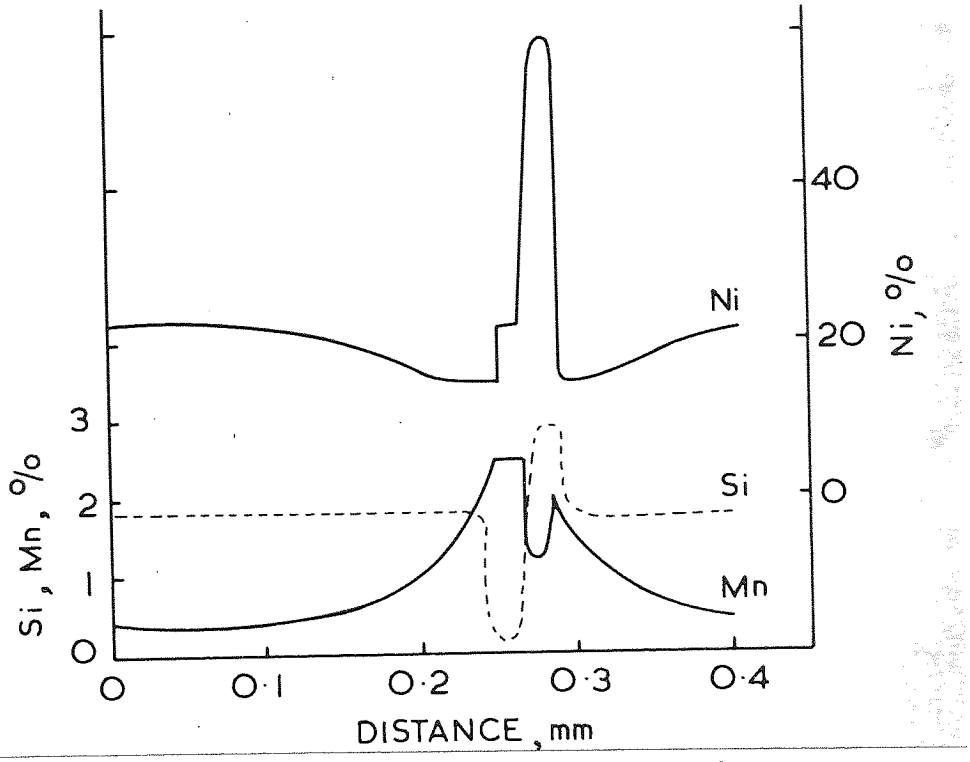

FIG. 57 Line scan from edge of a graphite nodule across grain boundary phase in 12 in section of 0.5 per cent manganese austenitic iron.

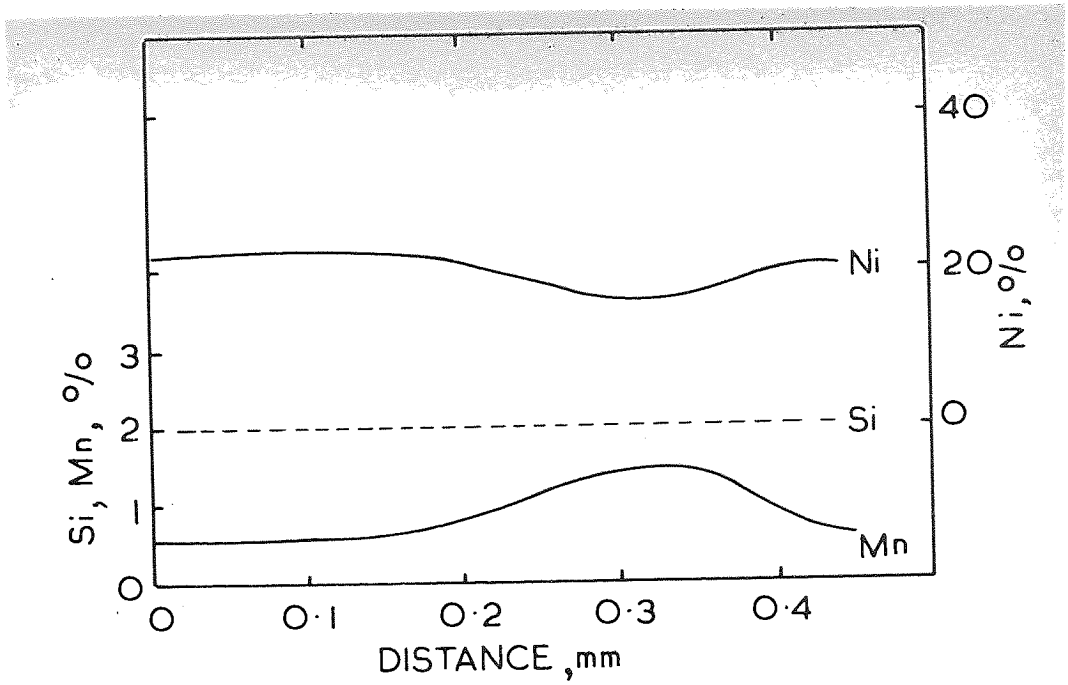

FIG. 58 Line scan across cell boundary area containing no carbide in 12 in section of 0.5 per cent manganese austenitic material.

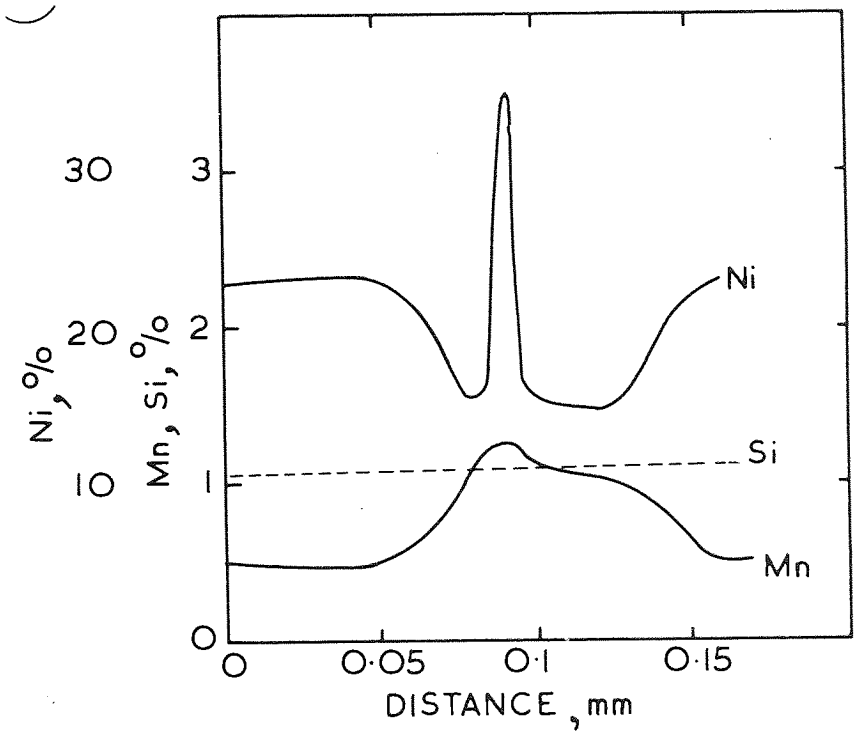

FIG. 59 Line scan across cell boundary area in 1.75 in keel section of 0.5 per cent manganese austenitic material.

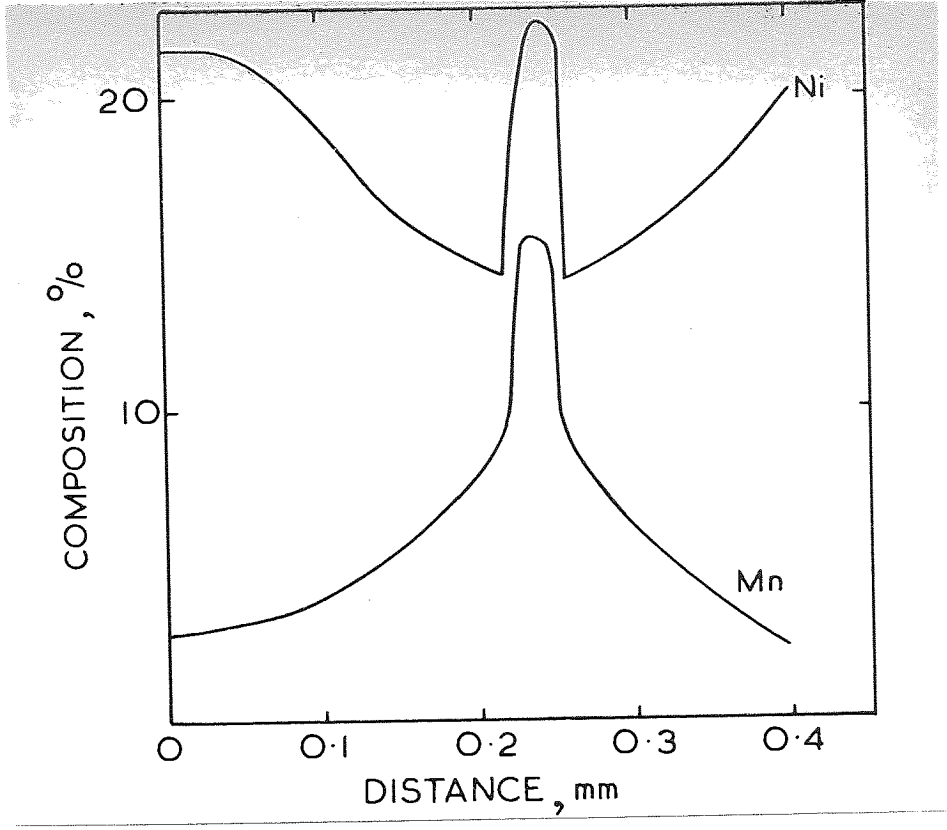

FIG. 60 Line scan across cell boundary carbide in 12 in section of 4 per cent manganese austenitic iron.

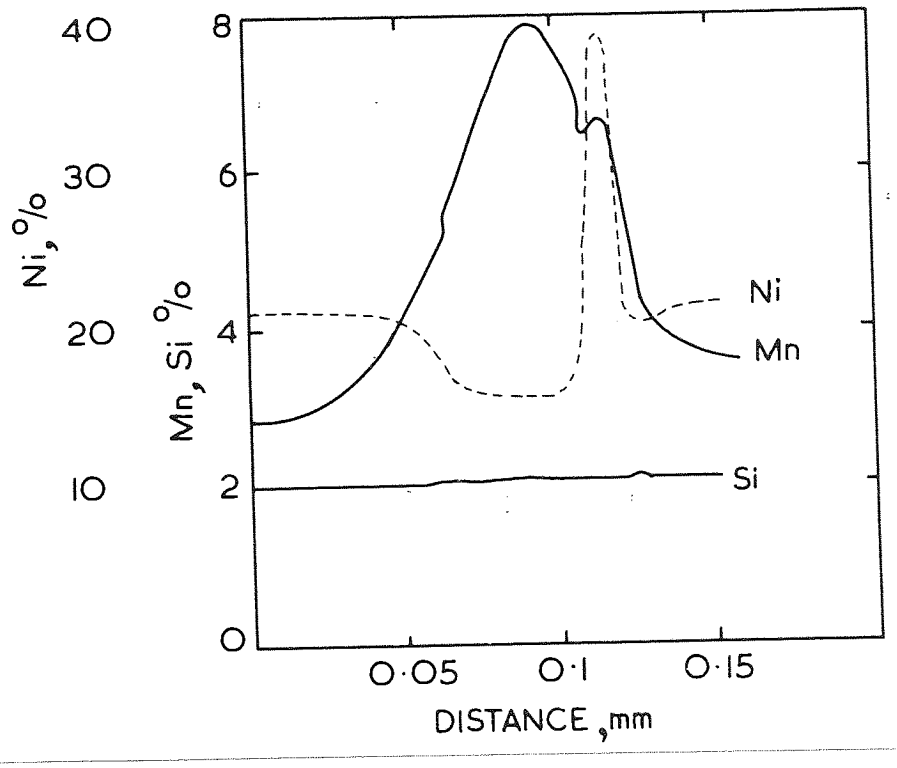

FIG. 61 Line scan across cell boundary carbide in 1.75 in keel section of 4 per cent manganese austenitic iron.

results obtained in the 1¾ in section material. Depletion of nickel occurred adjacent to cell boundary carbides, the nickel concentration being similar to that observed in similar areas in the 12 in section. Manganese concentration in grain boundary areas was noticeably less marked in the smaller section.

Similar experiments were carried out with the 4 per cent manganese material. Figs. 60 & 61 illustrate typical results from the 12 in diameter bar and 1¾ in keel sections. The large concentrations of manganese in grain boundary areas is obvious from these graphs. The main difference between the two sections was the segregation behaviour of manganese. In the 12 in section grain boundary concentrations of manganese all seem to have been much greater than in the 1¾ in section.

QUENCHING EXPERIMENTS

Fig. 62 illustrates the cooling curve obtained from the 2 in diameter bar of commercial purity nodular iron from which the holding times for five further samples were estimated at the points shown. Microstructures illustrating progressive stages of solidification are shown in Figs.63 to 67. The process of eutectic solidification may be seen to have followed the pattern described earlier. Many cell "aggregates" which probably resulted from early eutectic cell impingement contained more than one nodule and were irregular in outline. The graphite nodules were surrounded by austenite envelopes both of which increased in size as solidification proceeded. The austenite had transformed to martensite and the liquid to ledeburite as a result

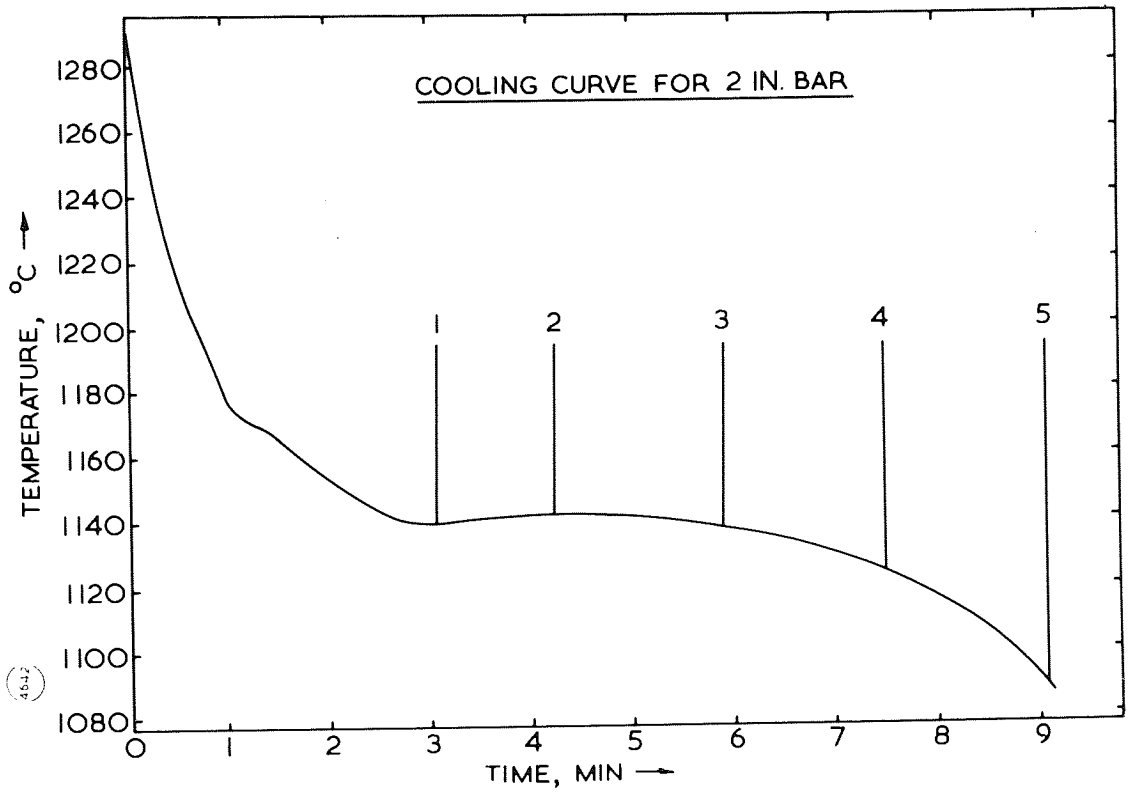

FIG. 62 Cooling curve for 2 in diameter bar of commercial purity nodular iron.

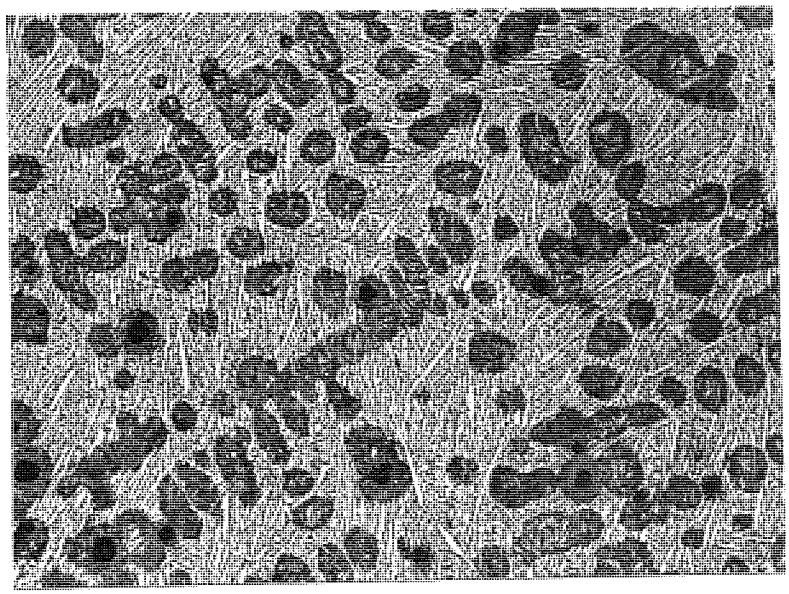

FIG. 63 Microstructure of sample 1.
Etched in 4% Picral x 100

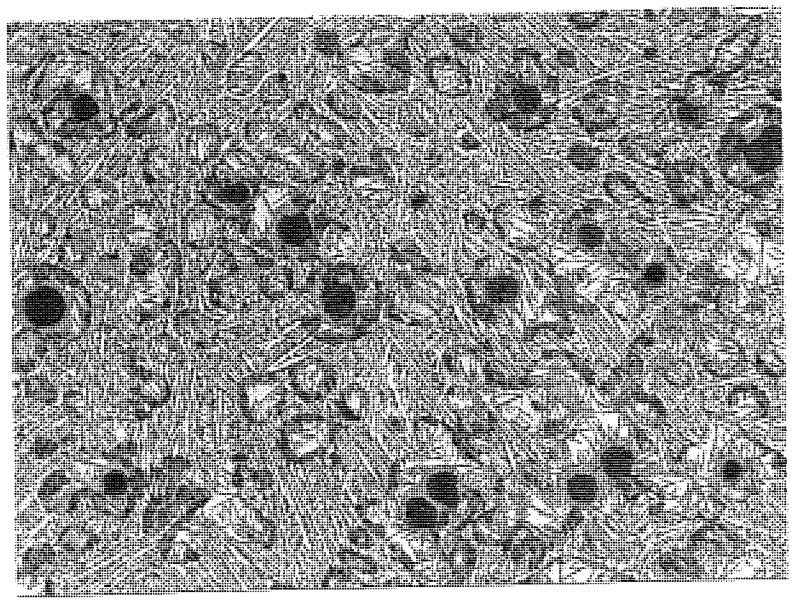

FIG. 64 Microstructure of sample 2.
Etched in 4% Picral x 100

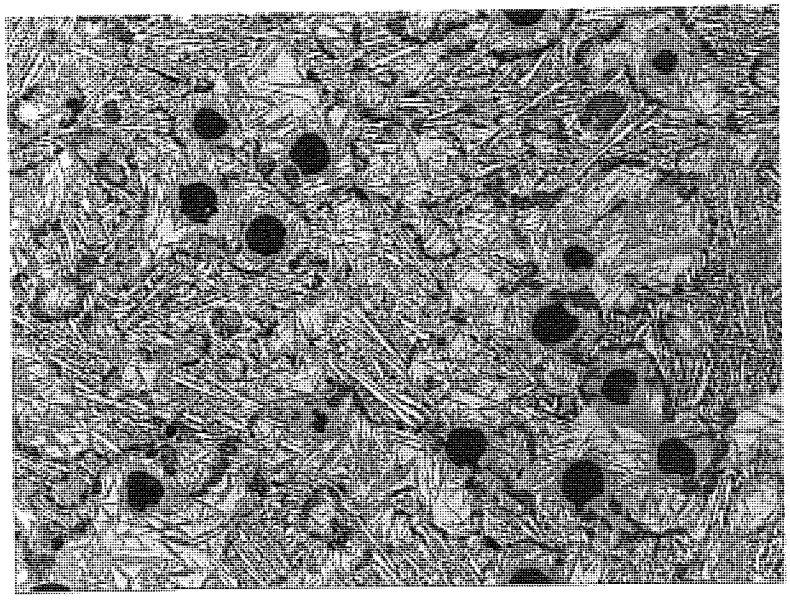

FIG. 65 Microstructure of sample 3.
Etched in 4% Picral x 100

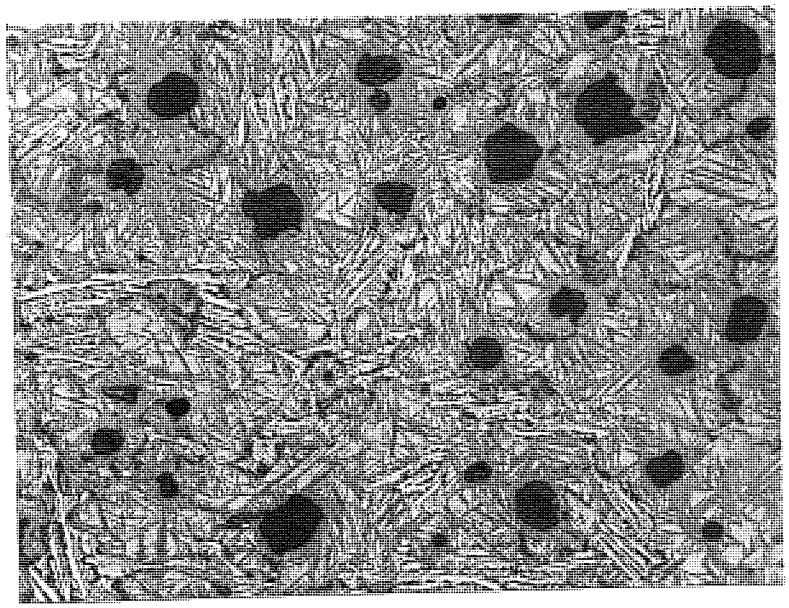

FIG. 66 Microstructure of sample 4.
Etched in 4% Picral x 100

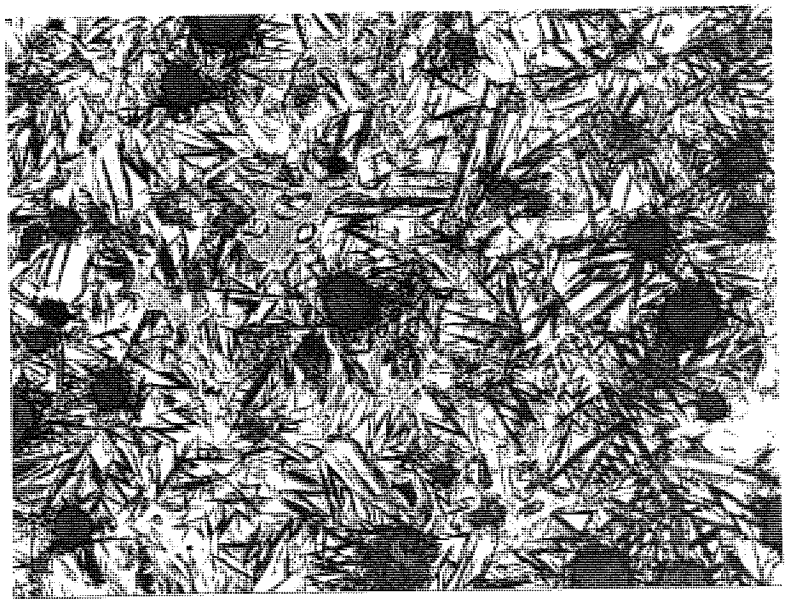

FIG. 67 Microstructure of sample 5.
Etched in 4% Picral x 100

of the quench.

Detailed examination of the microstructures revealed that many growing eutectic cells contained filaments of carbide connecting the quenched liquid and the graphite nodules. These filaments were bounded by an irresolvable transformation product which also bounded the areas of quenched liquid and separated the cementite plates of the ledeburite eutectic. Figs. 68 to 70 show examples of these carbide filaments at higher magnification.

In order to determine the nature of these filaments the samples were subjected to X-ray micro-analysis. It was found that the composition of the filaments differed from the ledeburitic areas. Fig. 71 illustrates an electron image and a manganese X-ray picture of an area containing a carbide filament connecting a region of ledeburite to a graphite nodule. It appeared that the manganese content of the filament was similar to that of the matrix while the ledeburitic area was much richer in manganese.

Heat treatment of these quenched samples produced some interesting results. Fig. 72 shows the microstructure obtained by furnace cooling a section of sample 4 from 800°C. The treatment had resulted in graphitisation of the carbide filaments while the ledeburitic areas had only been slightly spheroidised. Sections of the same sample were also treated at 1 090°C for periods of up to 1 hour and quenched. In these samples the carbide filaments and areas of ledeburite had been removed leaving behind

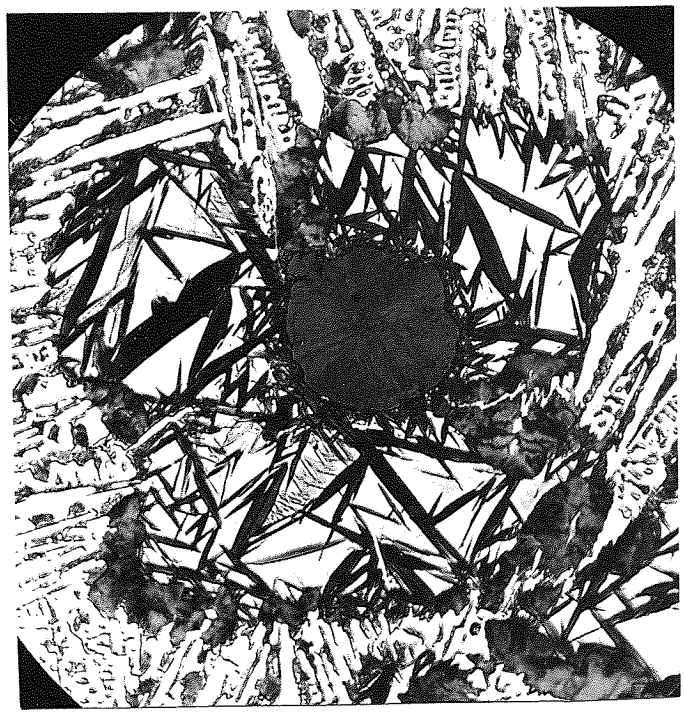

FIG. 68 Microstructure of sample 2.
Etched in 4% Picral x 600

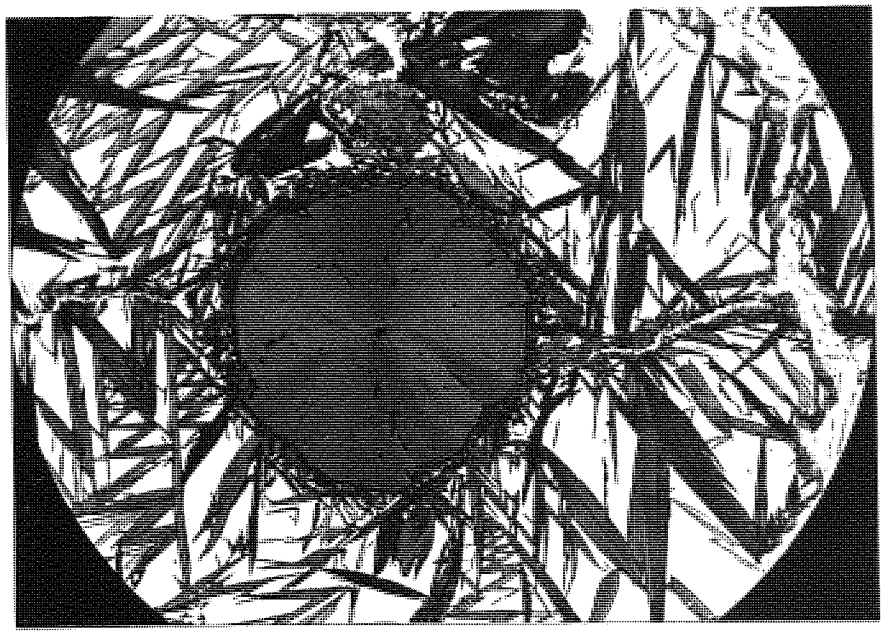

FIG. 69 Microstructure of sample 5.
Etched in 4% Picral x 600

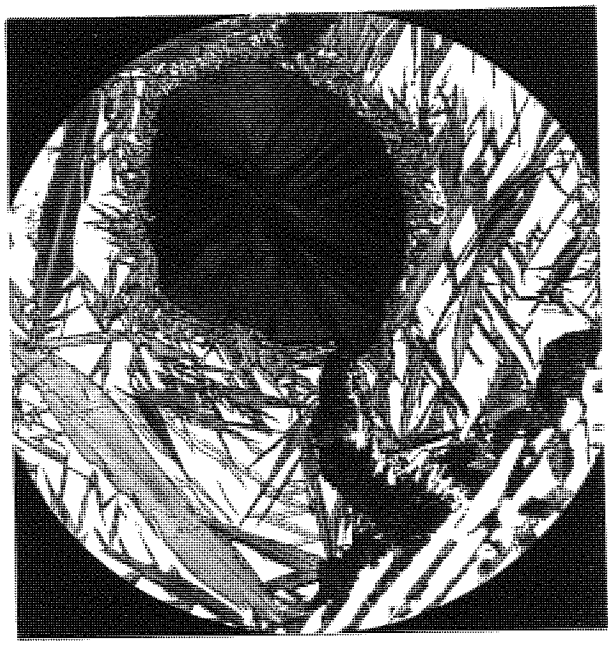

FIG. 70 Microstructure of sample 2.
Etched in 4% Picral x 1500

(a)
Electron image x 500

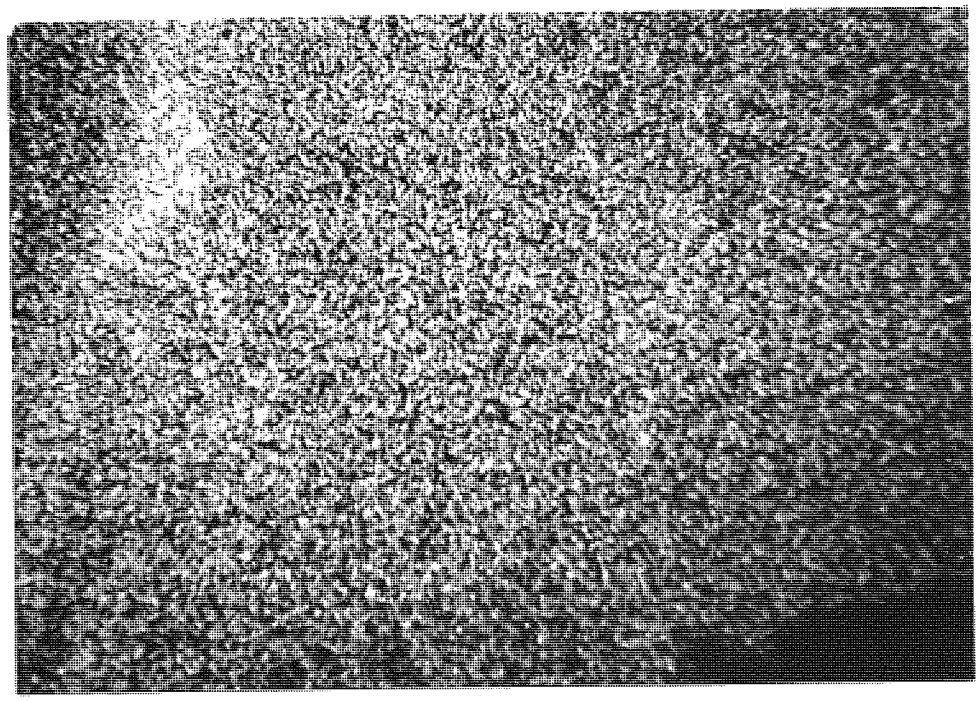

(b)
Manganese X-ray x 500

FIG. 71 Electron image and manganese X-ray pictures of an area containing a carbide filament in sample 4.

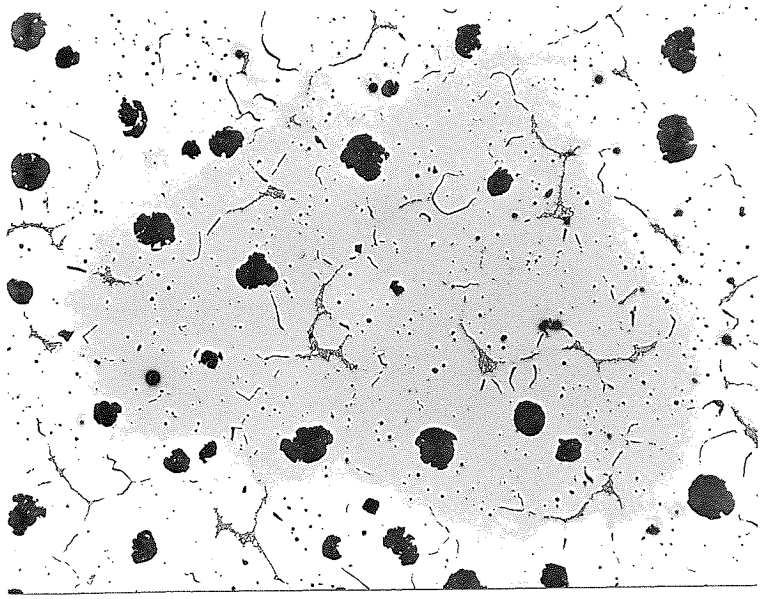

FIG. 72a Sample 4 furnace cooled from 800°C.
Etched in 4% Picral x 100

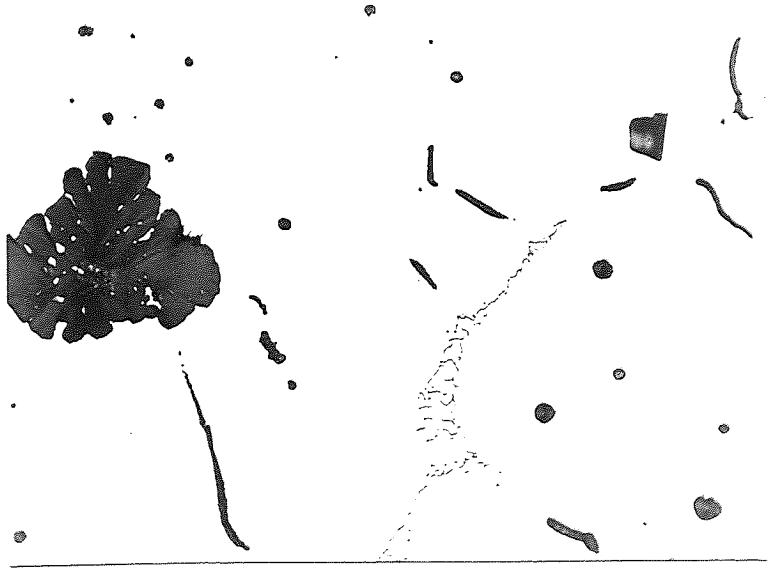

FIG. 72b Same sample at higher magnification.
Etched in 4% Picral x 600

cell boundary carbides.

Micro-analysis was carried out on the quenched samples in order to determine the distribution of various elements about the solid/liquid interface at progressive stages of the solidification process. Figs. 73 to 76 show the distribution of manganese, chromium, nickel and silicon from the centre of a cell to a position in the quenched liquid at various stages of solidification. The accumulation of manganese and chromium and depletion of nickel and silicon in the liquid is demonstrated by these curves. The irregular composition of the liquid was due to the partition of the alloying elements between the austenite and cementite phases of the ledeburite which prevents an assessment of the actual distribution of these elements in the liquid to be made. In samples 3-5 there are increasing concentrations of manganese and chromium and depletions of nickel and silicon in the solid near the solid/liquid interface which can be related to a fall in temperature on the cooling curve in Fig. 62.

The experiment was repeated with an austenitic iron which corresponded to International Nickel specification D-2C. The cooling curve obtained for this material is shown in Fig. 77. Figs. 78 and 79 show the microstructures of samples 3 and 5. The austenite envelopes were surrounded by ledeburite but because of the high manganese and nickel content had not transformed during the quench. Fig. 80 shows a carbide filament similar to those noticed in the quenched commercial purity nodular cast iron speci-

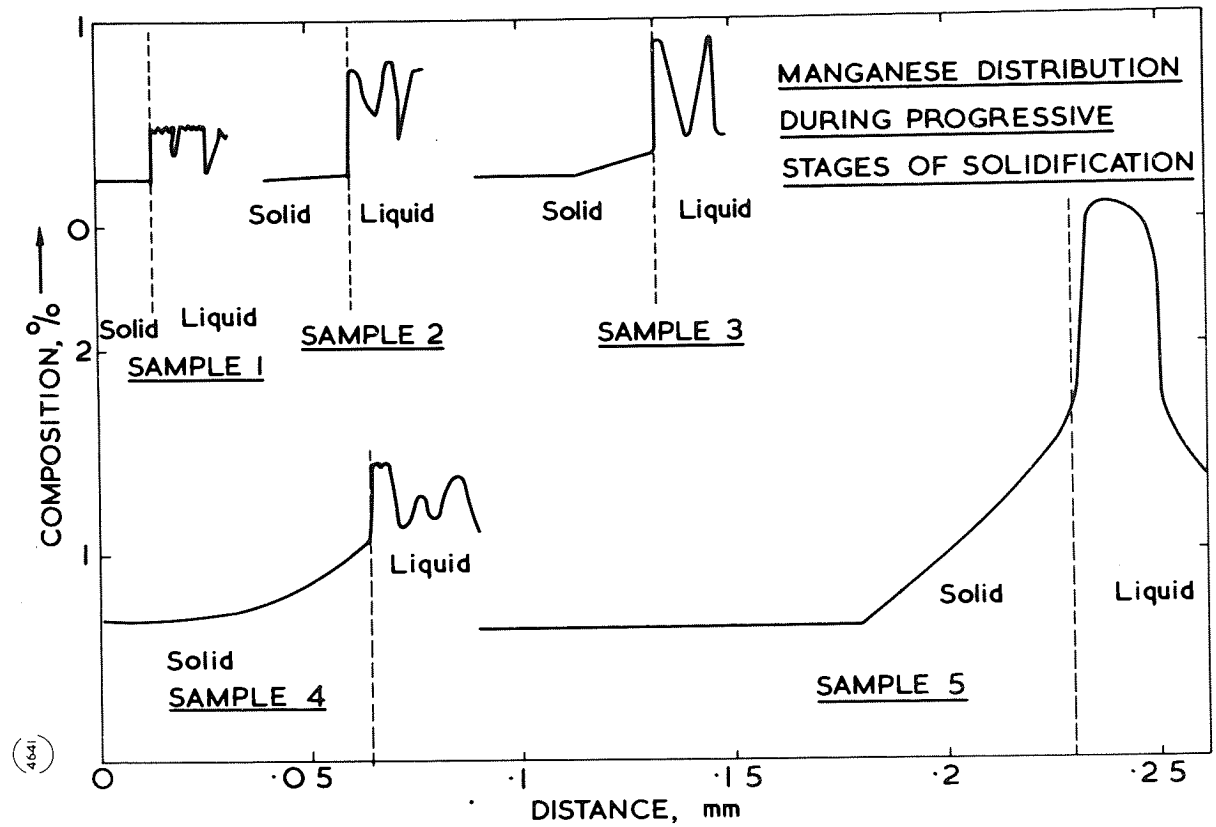

FIG. 73 Manganese distribution during progressive stages of solidification of commercial purity material.

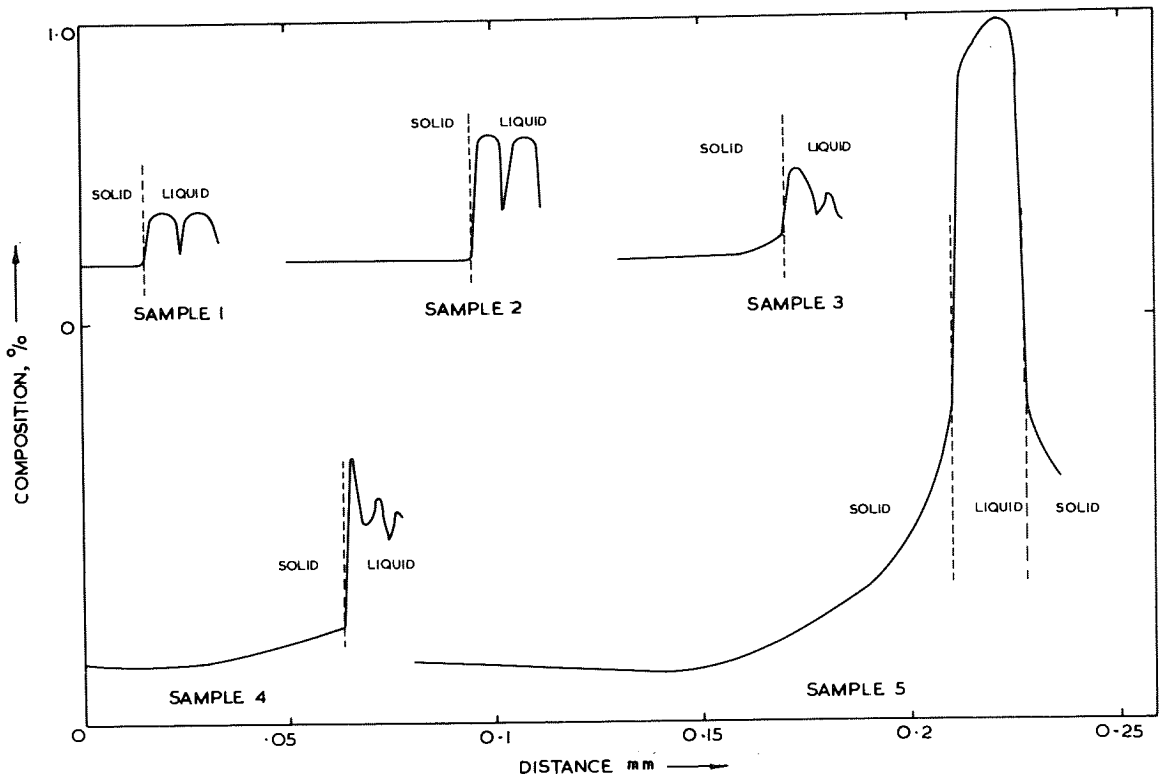

FIG. 74 Chromium distribution during progressive stages of solidification of commercial purity material.

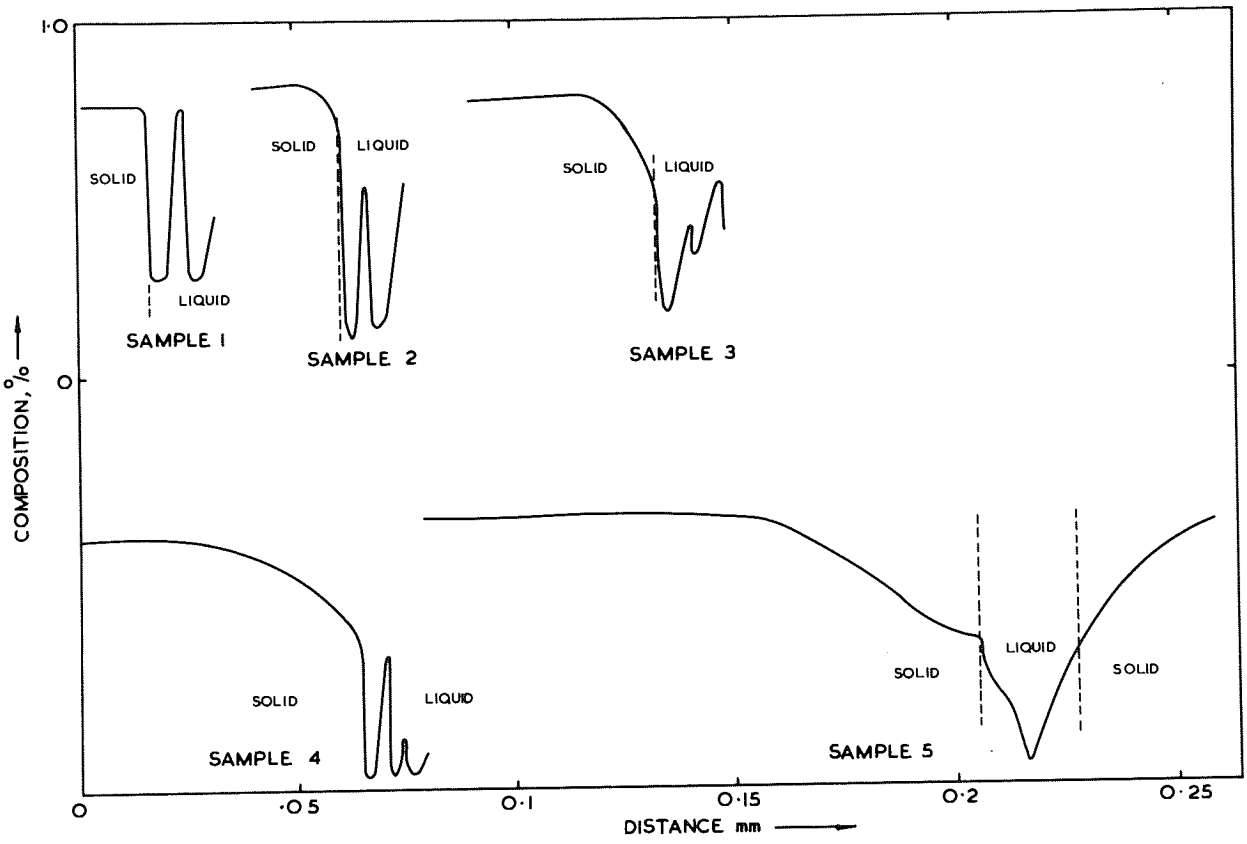

FIG. 75 Nickel distribution during progressive stages of solidification of commercial purity material.

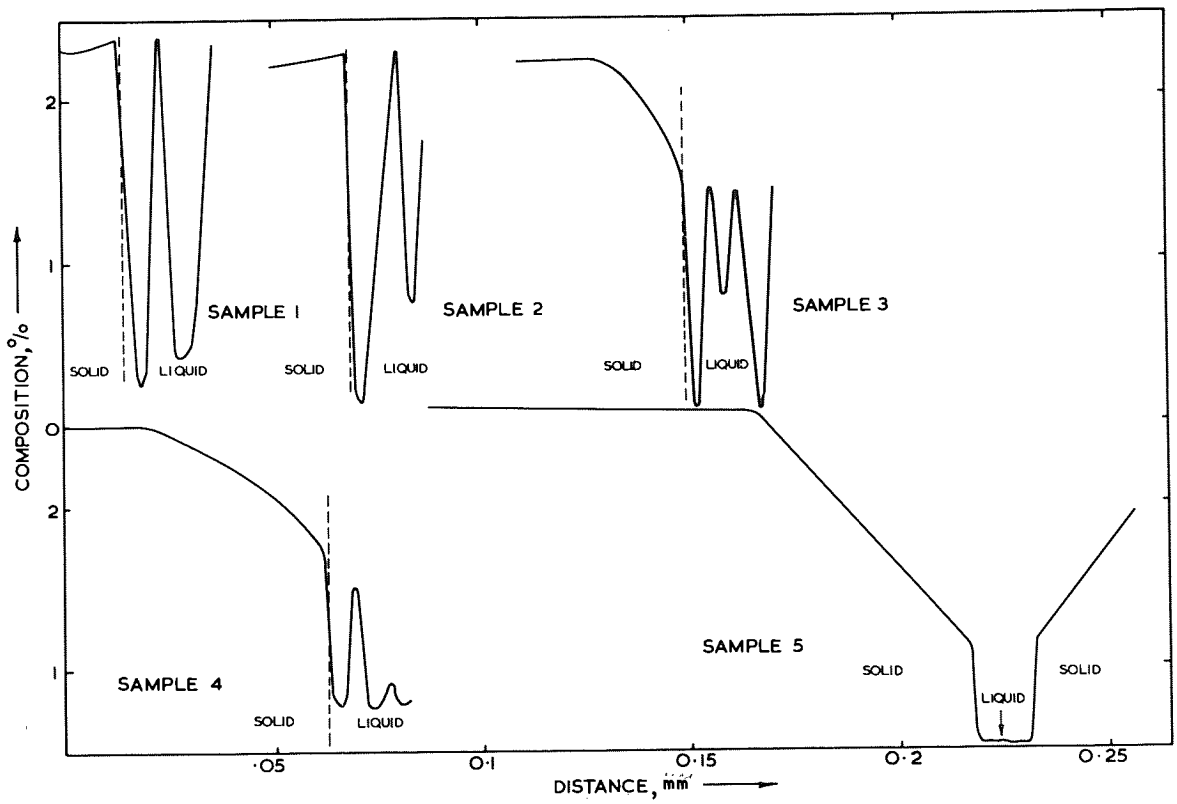

FIG. 76 Silicon distribution during progressive stages of solidification of commercial purity material.

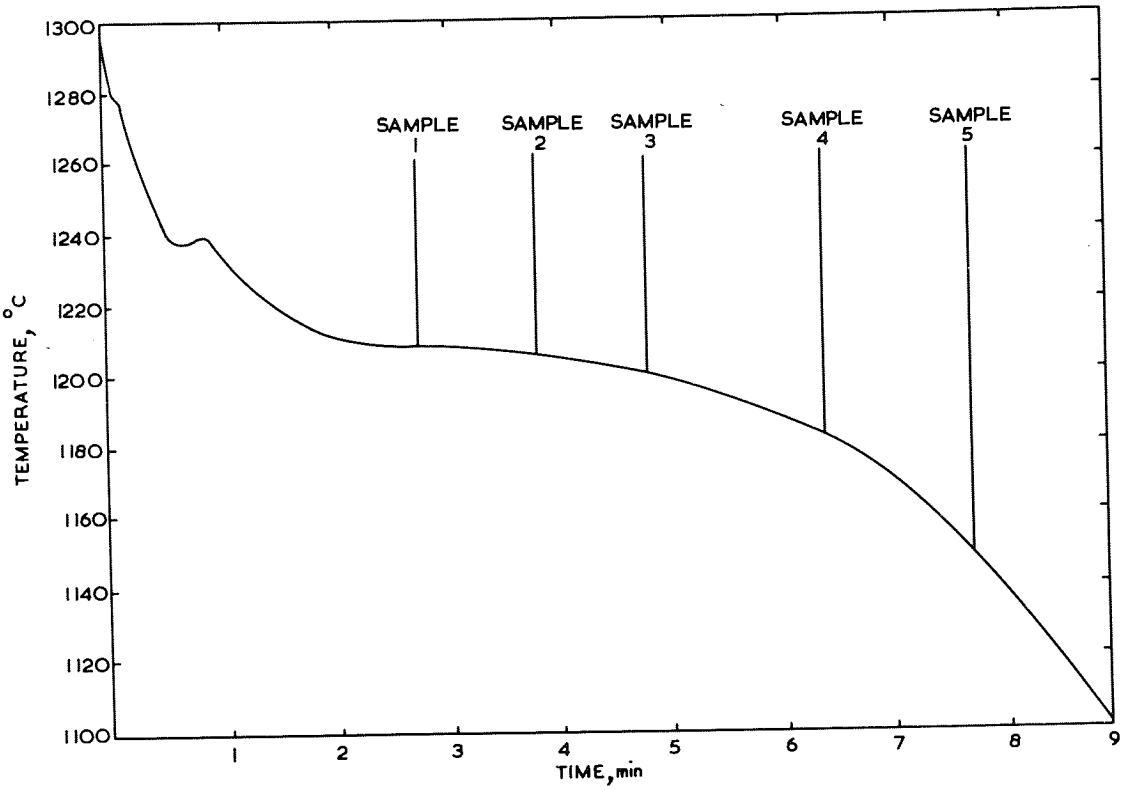

FIG. 77 Cooling curve of 2 in diameter bar of 0.4 per cent austenitic material.

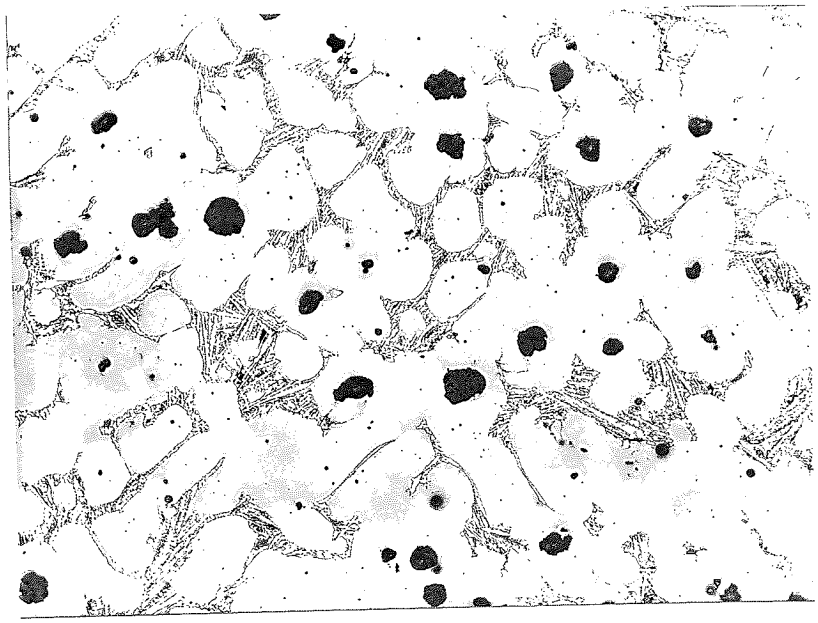

FIG. 78 Sample 2.
Etched in 5% Nital x 100

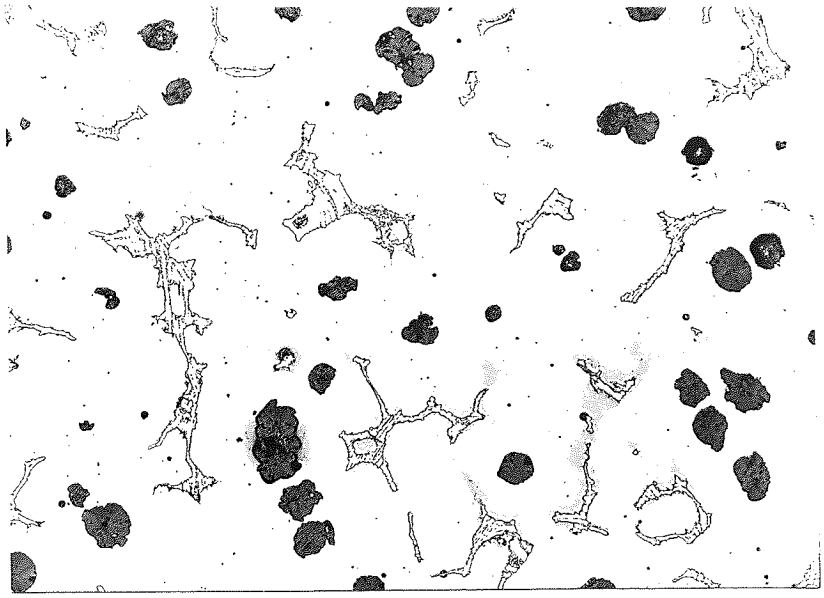

FIG. 79 Sample 5.
Etched in 5% Nital x 100

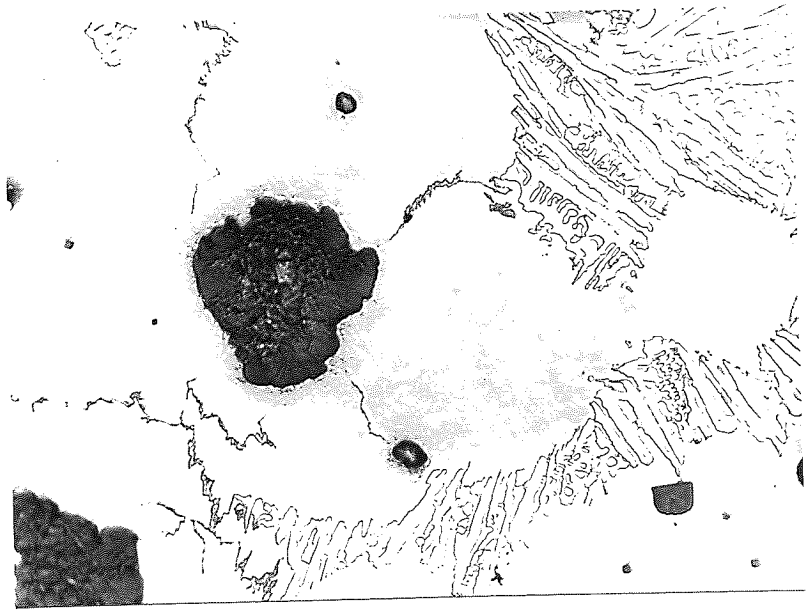

FIG. 80 Sample 3 at higher magnification.
Etched in 5% Nital x 600

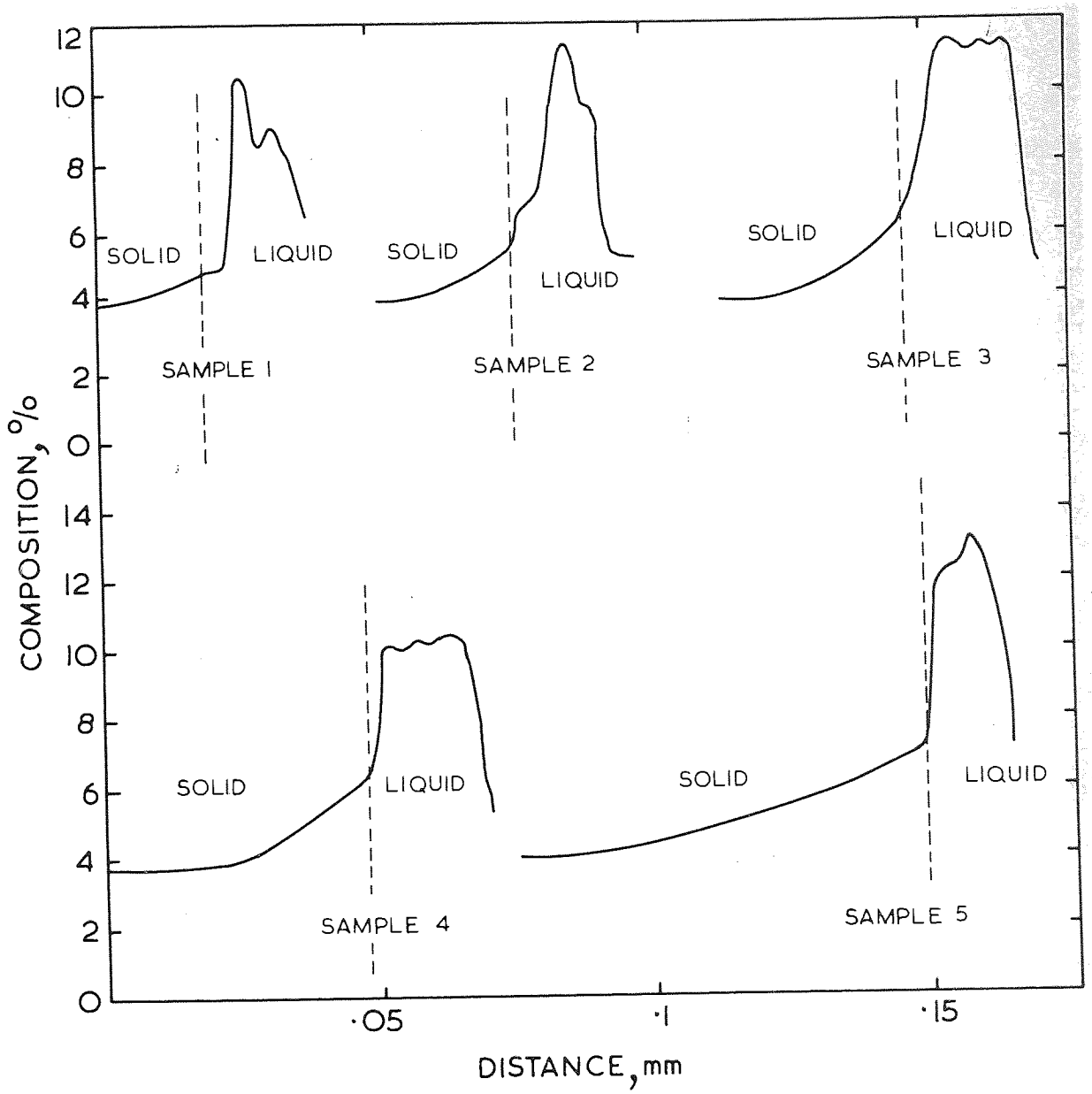

FIG. 81 Distribution of manganese during progressive stages of solidification of 4 per cent manganese austenitic material.

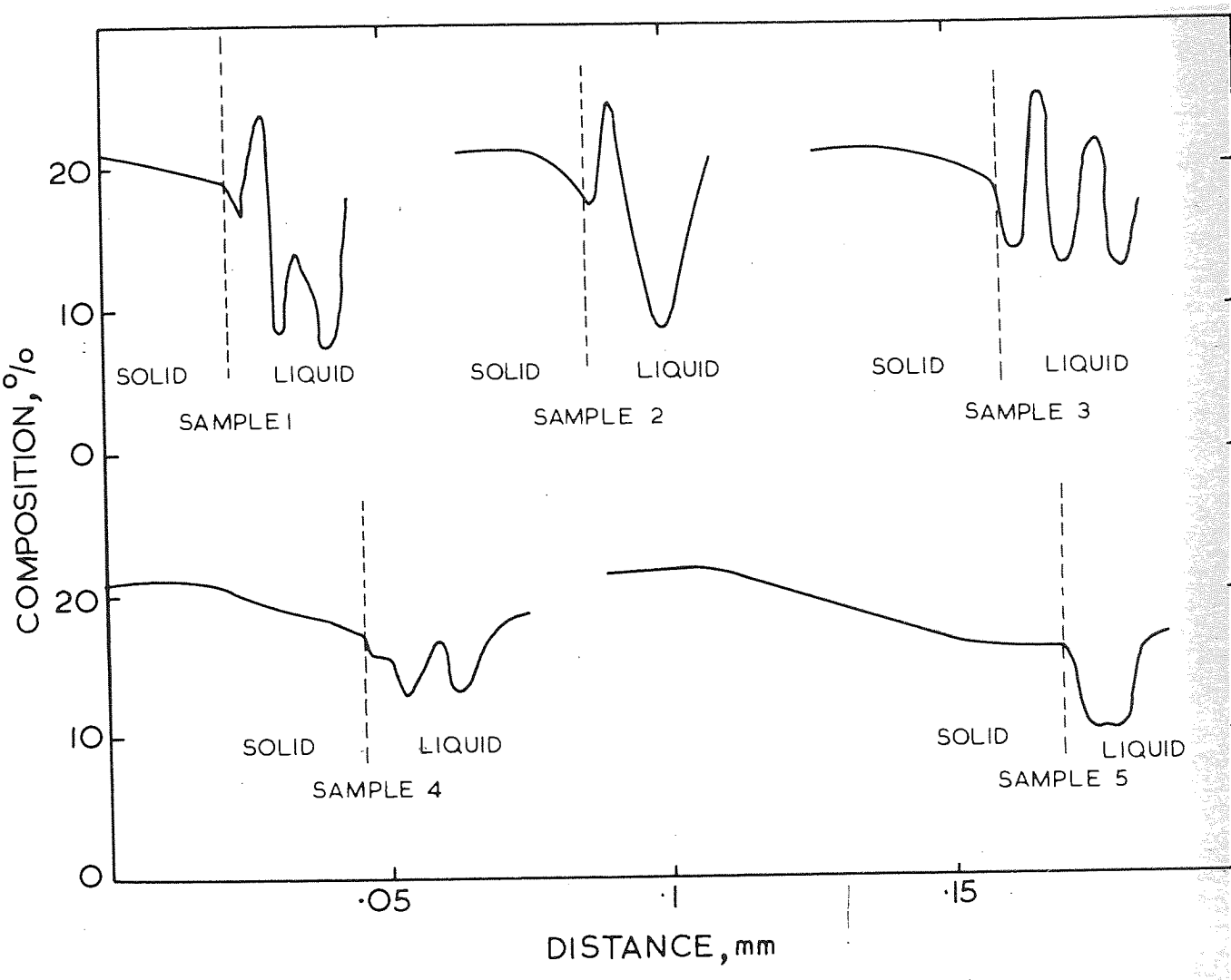

FIG. 82 Distribution of nickel during progressive stages of solidification of 4 per cent manganese austenitic material.

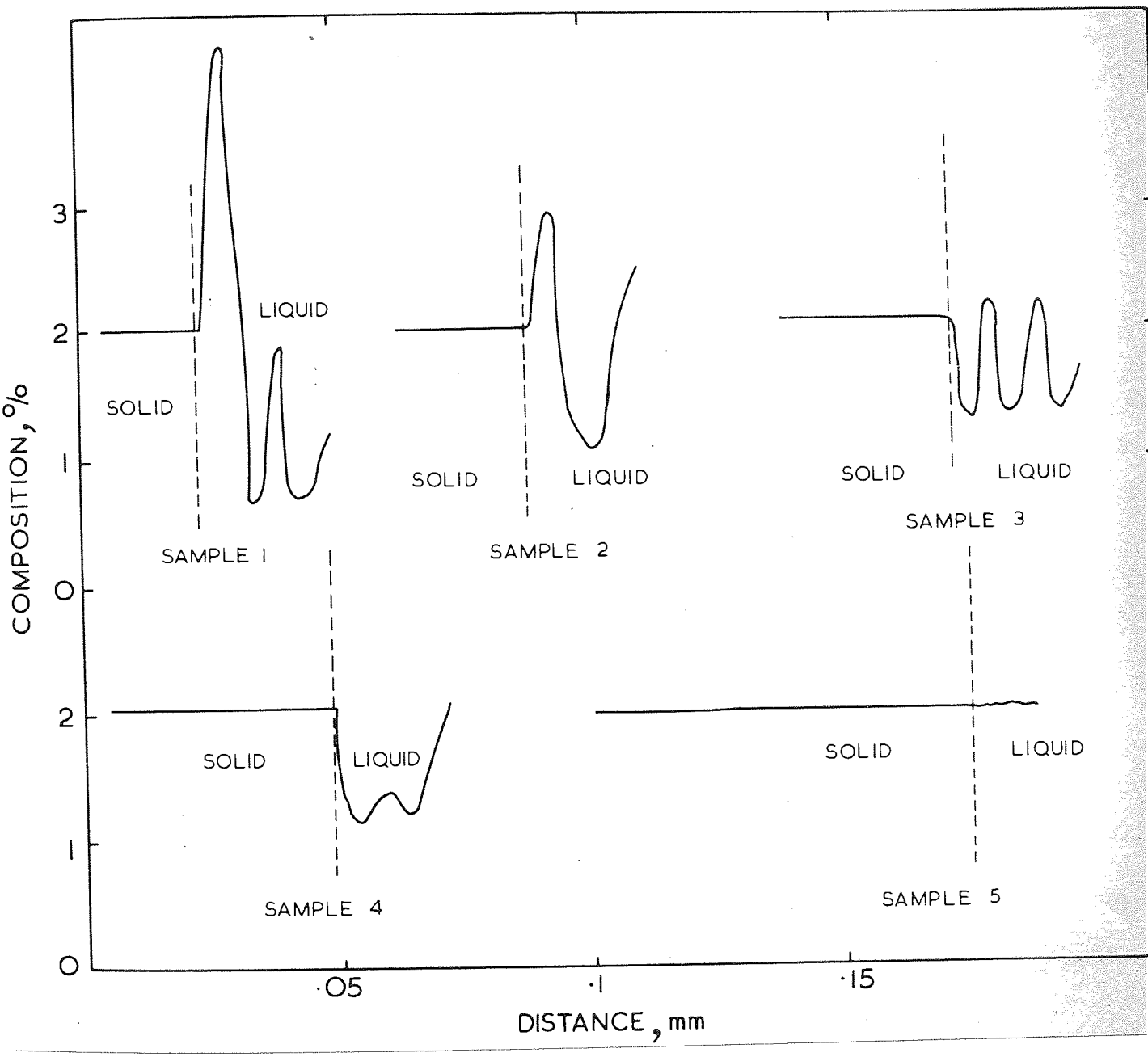

FIG. 83 Distribution of silicon during progressive stages of solidification of 4 per cent manganese austenitic material.

mens. Micro-analyser line traces were also carried out across solid/liquid interfaces in these samples. Figs. 81 to 83 illustrate the distribution of manganese, nickel and silicon during the progressive stages of the eutectic solidification process. The accumulation of manganese and depletion of nickel in the liquid is obvious from these curves. It is notable that the concentration of manganese and depletion of nickel in the solid occurred at an earlier stage than was observed in the previous material. This can be related to the cooling curve of the austenitic material which revealed an earlier fall in temperature than the curve for the commercial purity material. The silicon distribution in the solid was shown to be homogeneous but partitioning of silicon took place between the eutectic phases of the quenched liquid.

DISCUSSION

The purpose of these investigations was to study the relationship between segregation and mechanical properties in nodular cast iron. In the course of the work some interesting observations have been made in connection with the solidification process. In the following discussion the various aspects of the investigation are first treated separately and then the relationship between them is discussed.

MECHANICAL PROPERTIES An increase in section size in ferritic nodular iron has been shown to affect several variables, e.g. nodule size and number, grain size and segregation effects such as cell boundary carbides. In these investigations a study of the effect of segregation on the mechanical properties of nodular cast iron was made by casting a refined material in a series of different section sizes so that the effect of section size on a material in which a minimal amount of segregation had occurred, could be known. The role of segregation in influencing the mechanical properties of a commercial purity nodular cast iron over the same series of section sizes could then be assessed. It was found that the proof stress of the commercial purity materials was not significantly affected by change in section while the proof stress of the double annealed refined material decreased with increase in section. This indi-

cates that, in the double annealed condition at least, segregation effects tended to increase the proof stress of the commercial purity material thus removing the tendency for proof stress values to fall with increasing section. It would be expected from the work of Pellini, Sandoz and Bishop[13] that the large cell boundary carbides in heavier sections should increase the proof stress of the material.

Similar conclusions may be drawn from the ultimate tensile stress values found in these materials. Increase in section on the double annealed commercial purity material did not affect the ultimate tensile stress while the tensile strength decreased with increase in section in the refined material.

The inferior tensile strengths of the heavy section pearlitic materials, confirmed by the work of Gilbert[12], may be attributed to premature failure of these materials which is further evidenced by the low elongation values shown in Fig. 27. In any case, ultimate tensile stress and elongation values are of minor importance in pearlitic materials where proof stresses are quoted for design purposes.

The variation of elongation with section in the double annealed condition was very similar in the commercial purity and refined materials. The decrease in elongation with increasing section can be related to the larger nodule size and lower nodule number in the heavier sections. The effect of the larger amount of carbide in the heavier section on the

elongation values of this material seems to have been negligible as the refined material exhibited very similar behaviour with change in section. This is not unreasonable as the graphite nodules in nodular cast iron act as stress raisers and the introduction of a further stress raiser might not be expected to greatly influence the ductility. The variation in ferrite grain size (Table 3) was shown to be slight and would not, therefore, have a significant influence on the elongation. The variation in graphite nodule size is also likely to have caused the deterioration of the elongation values of the pearlitic materials (Fig. 27) with increase in section. However, it has been shown above that the plastic properties of pearlitic nodular irons are of minor importance in engineering design.

The effects of change in section were most obvious from the impact tests carried out on the various materials. It was shown that the ductile impact value in unnotched tests decreased with increasing section while notched ductile impact values were not significantly affected by section size. Gilbert has suggested a relationship between ductility in tension and the ductile impact value and it is well known that similar types of fracture occur in both processes, i.e. "ductile" fracture around graphite/matrix interfaces. Fig. 84 illustrates the relationship between unnotched ductile impact value and per cent elongation for the materials used in this thesis. It can be seen that there is an unmistakable relationship between unnotched ductile impact value and per cent elongation. From

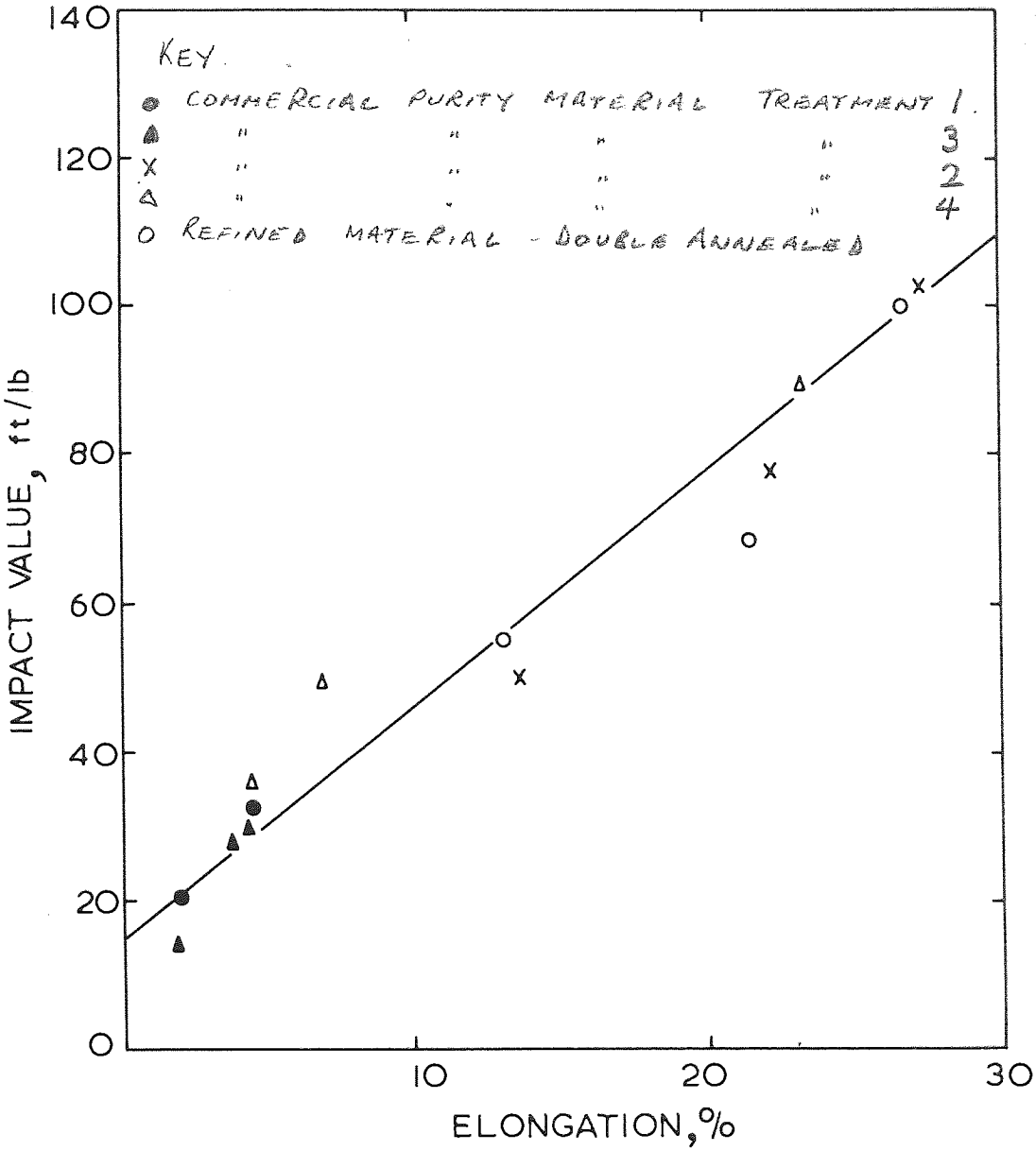

FIG. 84 The relationship between elongation and unnotched ductile impact values for materials used in this thesis.

Figs. 32 and 36 it can be seen that the effect of section size on the unnotched ductile impact value of the commercial purity material and the refined material is very similar. Thus the massive cell boundary carbides in the heavy section commercial purity material have not significantly affected the unnotched ductile impact or the elongation values for the same reasons.

It is felt that the most important effect of segregation was shown in the impact transition values. In the unnotched tests a wide difference in impact transition was found between different sections of the commercial purity material in the as-cast state and after each heat treatment. Gilbert[10] has shown that nodule size and number will affect the transition temperature. The effect of section size on the unnotched impact transition temperature of the refined material (Fig. 36) demonstrates the effect of nodule size and number on the impact transition. This effect can be seen to be smaller than in commercial purity materials. It is felt that segregation is responsible for the greater effect in commercial purity material as this is the only additional variable. The effects of segregation are more noticeable from the notched impact results. Tests on the double annealed refined material showed that change in section size had no significant effect on the notched impact properties (Fig. 37) while increasing the section size of the commercial purity material in the double annealed condition resulted in a significant increase in the transition temperature (Fig. 33). A prolonged anneal (treatment 5) which spheroidised and partially

removed the cell boundary carbides in the commercial purity material slightly lessened the transition difference between the various sections (Fig. 35). These results show that segregation effects such as cell boundary carbides can exert a significant effect upon impact transition properties in nodular cast iron but that these effects can be partially removed by lengthy heat treatment. The theory of brittle fracture discussed in the Literature Survey indicated the manner in which carbides could influence the impact transition temperature, by acting as stress raisers, and this is further confirmed by the above results.

Table 6 shows the effect of section size on the tensile properties of the two austenitic irons which were studied. It can be seen that a significant reduction of ultimate tensile stress, proof stress and elongation occurred with increase in section size. The effect of section size on the ultimate tensile stress, and elongation of the 4 per cent manganese austenitic material was shown to be more drastic. It is difficult to assess the role of nodule size and number on the above results in the absence of similar results from a carbide free austenitic material. However, since graphite nodule size and number have already been shown to account for the difference in tensile properties with section in the ferritic irons a similar effect would be expected in austenitic irons. In the 4 per cent manganese material much larger amounts of carbide appeared in the microstructure of the 12 in section. As carbide has

been stated to reduce the mechanical properties of austenitic irons[40] it is suggested that the drastic loss of tensile properties with increasing section in this material is partly related with a large increase in the carbide content although it is realised that graphite nodule size, shape and number also exert an influence. Graphite nodule size, shape and number have already been shown to exert no influence on the notched ductile impact values of ferritic nodular cast iron. Figs. 54 and 55 show that while no change of notched impact value with increase in section occurred in the low manganese material a significant reduction in impact value was noticed with increasing section size in the 4 per cent manganese iron. It is suggested that this latter effect was related with the increased carbide content of the 12 in section of the higher manganese iron.

SOLIDIFICATION OF NODULAR CAST IRON

From the results obtained in these investigations some modifications to the existing theory for nodular cast iron may be proposed. It was shown in Figs. 15 and 42 that there is some evidence to suggest that a eutectic cell of nodular cast iron, certainly in heavy sections, may contain more than one nodule. In heavier sections where the rate of solidification is likely to be slow growing eutectic cells of nodular cast iron may well impinge at an early stage in the solidification process. Thus solidification would proceed by the growth and eventual impingement of growing austenite-graphite aggregates. The

process is illustrated in Fig. 85. Segregation effects would then occur at the boundaries of these cell aggregates.

Metallographic examination of the samples quenched during solidification has provided circumstantial evidence which may also be used to propose further modifications to the accepted theories of nodular iron solidification. The established theory involving solid state diffusion of carbon has been criticised recently as was shown above (p.22). Since Hillert[52] showed that diffusion of carbon in the liquid is 20 times faster than diffusion in solid austenite at the same temperature it was realised that liquid diffusion of carbon would occur if it was at all possible. However, the amended proposals of Tiller[53] discussed in the literature survey (p.22) can be refuted from the results of the present investigation.

The cooling curve in Fig. 62 shows a pronounced eutectic arrest from which the duration of solidification can be seen. Between samples 1 and 5 most of the latent heat of solidification has been evolved and therefore a substantial proportion of solid has been formed. This strongly suggests that the austenite envelopes in Figs. 63 to 67 are present before quenching. Furthermore the segregation patterns seen in Figs. 73 to 76 and 81 to 83 are characteristic of solute rejection at a growing solid/liquid interface. It is extremely difficult to imagine this type of segregation from the area of low carbon liquid mentioned by Tiller.

Figs. 63 to 67 show that considerable growth of graphite

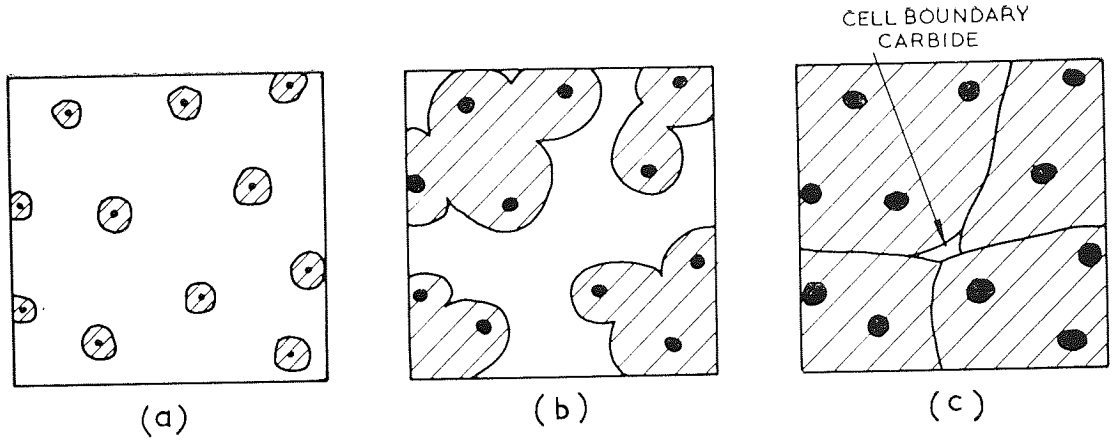

FIG. 85 Schematic diagram of the growth from the liquid of a heavy section of nodular cast iron showing carbide formation at austenite-graphite aggregate boundaries.

nodules occurs between samples 1 and 5 concurrent with growth of the austenite envelopes. Tiller's other statement that graphite nodules are close to their maximum size before austenite formation occurs now seems unlikely in the light of this evidence.

It is assumed from this evidence that the quenched microstructures are representative of the actual solidification process and that graphite nodules and their surrounding envelopes of austenite grow concurrently during solidification.

The presence of carbide filaments in the austenite envelopes could be used to suggest that carbon diffusion had occurred along preferred paths. There are two explanations for the formation of these carbides:

(1) that the carbides had formed from pre-existing liquid filaments;

(2) that the carbides were pro-eutectoid carbides formed by rejection of carbon from a super saturated austenite.

It can be seen that if the former explanation were correct some extensive modifications to the existing hypothesis of solidification of nodular iron could be proposed. The presence of liquid channels connecting the graphite nodules and the liquid would mean that growth of the nodules could proceed by liquid diffusion of carbon to the nodules from the liquid along preferred sites which would satisfy the criticisms levied against the solid state diffusion theories on the basis of Hillert's work. The evidence that can be compiled in this thesis is of a circum-

stantial nature and all the individual points are discussed below.

1. It was shown that heat treatment of quenched samples at 1 090°C removed these carbide filaments. If the filaments were formed by a solid state reaction on quenching a super saturated austenite they may be expected to be present after quenching from 1 090°C. However, it is possible that the heat treatment had removed inhomogeneities which had caused the carbide formation.

2. These carbide filaments were noticed in quenched austenitic iron specimens. Pro-eutectoid carbides are not normally seen in austenitic irons.

3. Experiments on quenching flake graphite cast irons during solidification[67] did not result in the formation of carbide filaments. Growth of flake graphite iron during solidification occurs by carbon deposition on growing flakes which project into the liquid[68]. Carbide filaments formed from liquid channels would not therefore be expected in these samples. On the other hand, the conditions for pro-eutectoid carbide formation from an inhomogeneous, super saturated austenite are similar to the nodular iron case. However, it is well known that carbide formation is more frequently found in nodular cast iron.

The difference in composition between the filaments and the quenched liquid (figs. 71 and 72) which has been established by heat treatment and micro-analysis is consistent with the fila-

ments being pro-eutectoid carbide. However, the diffusion of manganese and chromium in liquid iron is much slower than that of carbon[69] and if the solidification of nodular cast iron were being controlled by the diffusion of carbon atoms through liquid channels the manganese and chromium rejected at the solid/liquid interface may not have sufficient time to diffuse into the liquid channels.

Thus it can be seen that there is circumstantial evidence to support the theory that carbide filaments are formed from the liquid but there is some need for a critical experiment to establish this fact. At the moment it is very difficult to suggest the possible nature of such an experiment.

In recognition of the possibility of liquid channels a simple model for the growth of an austenite-graphite eutectic cell containing one nodule was constructed and is shown in Fig. 86. The diagram shows a nodule surrounded by six lobes of austenite at the interstices of which are the proposed sites for liquid diffusion of carbon to the nodule. Sectioning of this model can produce a variety of structures. A section along the plane AA' is shown in the sketch and shows a marked resemblance to the microstructure in Fig. 68.

The mechanism of carbon redistribution at the surface of the growing nodule is not evident from these results. Two possibilities are either by solid state diffusion over the austenite-graphite interface or diffusion through a thin film at the nodule surface. Kellerman and Loper[70] have shown that

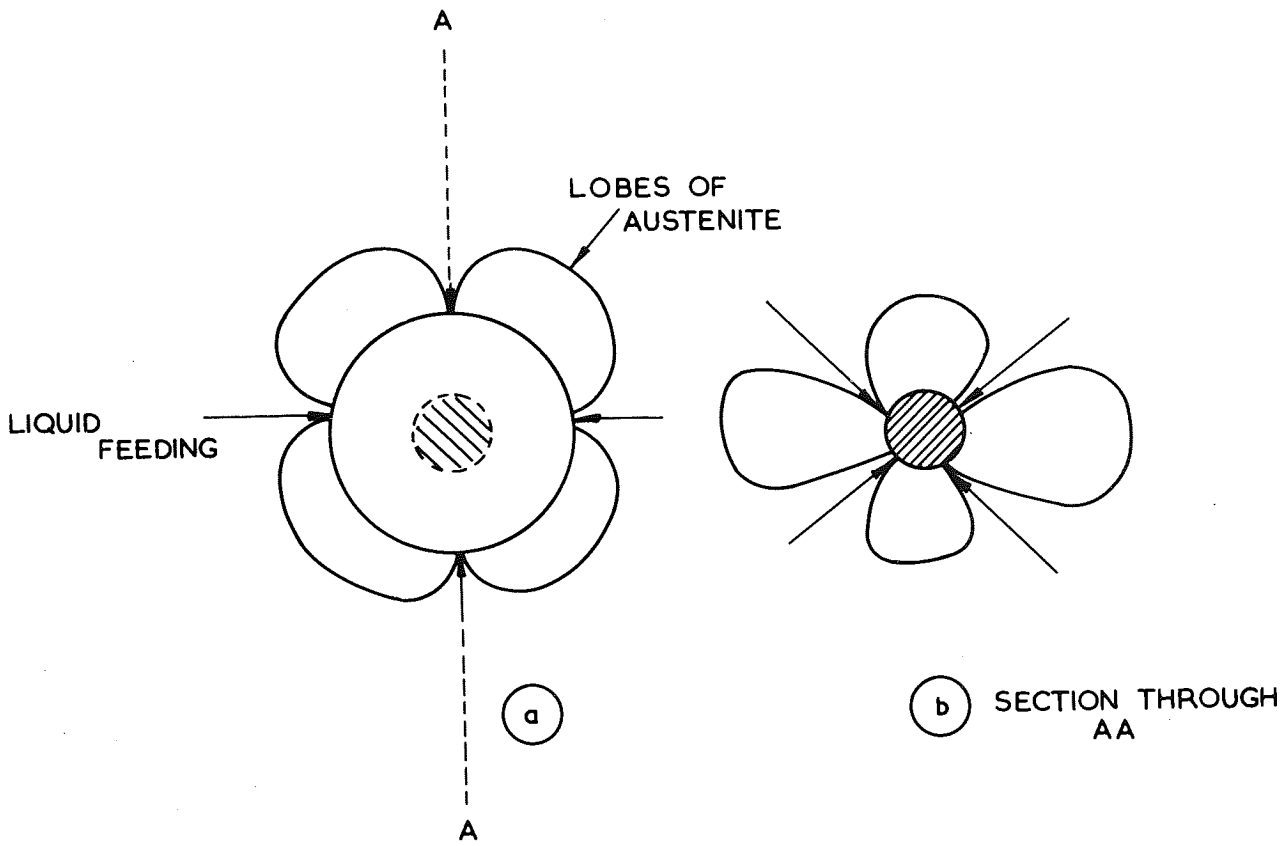

FIG. 86 Simple model for solidification of the nodular graphite eutectic by liquid diffusion of carbon.

when a sample of nodular cast iron is heated near to the eutectic temperature, melting first occurs at the graphite-austenite interface. They suggested that the degenerate graphite structures sometimes found in heavy section nodular iron castings were caused by re-melting at the austenite-graphite interface during the relatively slow solidification process, the liquid then re-solidifying as flake graphite. It does not seem unreasonable, therefore, to suggest that a liquid film exists around the graphite nodule during the solidification process. Solidification could then proceed by continuous re-melting of austenite adjacent to the graphite-austenite interface and carbon deposition on the surface of the growing graphite nodule. However, no evidence of a liquid film around the nodule could be seen from the microstructures even at high magnification but it has been shown by Hillert that liquid diffusion of carbon is thermodynamically preferable to solid state diffusion.

The revised hypothesis for nodular cast iron solidification, therefore, involves liquid diffusion of carbon along preferred sites to the graphite nodule in a fashion depicted by Fig. 86. Carbon deposition at the nodule surface takes place from a thin film of carbon rich liquid around the nodule. This theory satisfies the results of the present investigation and also the objections to the solid state diffusion model of eutectic solidification. Much of the evidence is circumstantial, however, and it is realised that more critical experiments are necessary before the exact nature of nodular cast iron solidi-

fication can be firmly established.

SEGREGATION IN NODULAR CAST IRON

Before discussing the results of these investigations a brief introduction to the theory of segregation in binary alloys is appropriate.

Theory of Segregation The mathematical treatments of the re-distribution of solute during solidification involve several assumptions, many of which are invalid in practice. A brief discussion of these treatments is appropriate, however, in order to attain an understanding of the variables involved. In the following cases the interface is assumed to be planar and moving at a constant speed.

The three cases normally considered are as follows:

(i) Equilibrium maintained at all times;

(ii) Mixing in the liquid by diffusion only; no diffusion in the solid;

(iii) Complete or partial mixing of the liquid; no diffusion in the solid.

If an alloy possesses an equilibrium diagram of the form shown in Fig. 87 the first solid to form (at temperature T) has a composition C'_S and the ratio C'_S/C'_L is known as the equilibrium distribution coefficient, K_O, which is constant over the freezing range assuming that the liquidus and solidus lines are straight. During the solidification process the layer of solid being formed at any instant has the composition C_S given by the equation $K_O = \frac{C_S}{C_L}$ where C_S and C_L are the portion on the

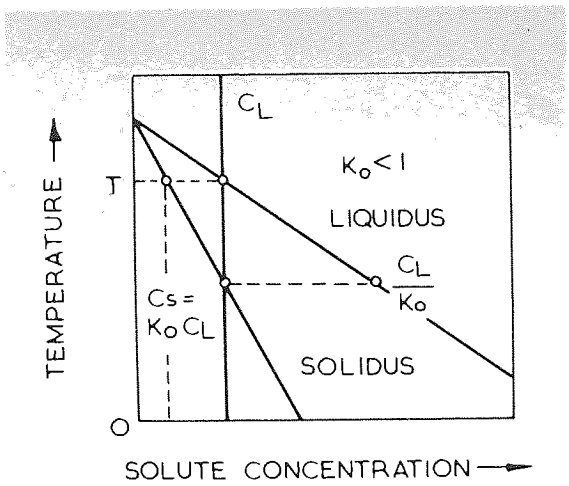

FIG. 87 Portion of the equilibrium diagram of a binary alloy where the freezing point of the solvent is lowered by the solute.

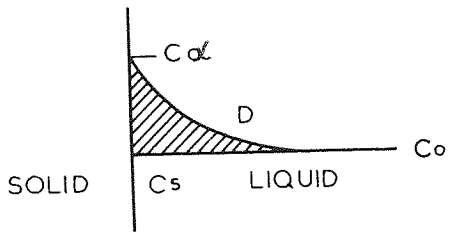

FIG. 88 Distribution of solute in the liquid where mixing takes place by diffusion only.

solidus and liquidus corresponding to the temperature at that instant.

If equilibrium is maintained at all times this does not result in any inhomogeneous distribution of solute but the conditions necessary for this case are never satisfied in practice due to the relative difficulty of solid state diffusion.

In the second case of mixing in the liquid by diffusion only, the diffusion in the solid is ignored being much slower than liquid diffusion. It is necessary in this case to consider the rate of advance of the interface R. The distribution of the solute in the liquid takes the form shown in Fig. 88. The ratio C_S/C is equal to K_0. The effective distribution coefficient, K_e is equal to C_S/C_0 where C_0 is the initial composition of the liquid. The solute rejected at the interface diffuses into the liquid and is represented by the curve D. When the amount of solute rejected at the interface is balanced by the amount of solute diffusing away into the liquid, a steady state will exist when solid of composition C_0 is formed. It has been deduced by Tiller et al[71] that if the composition of the solid is C_0 then C must be C_0/K_0 and the expression for C_L during the steady state is as follows:

$$C_L = C_0 \left[1 + \frac{1-K_0}{K_0} \exp\left(-\frac{R}{D} X'\right)\right]$$

where D is the diffusion coefficient of solute in the liquid and X' is the distance from the interface at which the concentration is C_L. This relationship shows that the liquid distribution is

exponential with a characteristic distance of $\frac{D}{R}$, i.e. the distance in which the concentration falls to $\frac{1}{e}$ of C . This distance and hence the segregation behaviour is influenced by the rate of growth, R, of the solid/liquid interface and is shown in Fig. 89. The steady state will thus proceed while R remains constant and diffusion of solute away from the interface can proceed unhindered. Towards the end of solidification the second condition is obviously not fulfilled when cell boundaries begin to impinge and the concentration of the solid formed rises above C_0 in order to accommodate the excess solute. The first solid to form from a liquid of composition C_0 will be K_0C_0 and the steady state will not be reached until a substantial amount of solute has been rejected. The distribution of solute during the solidification of an alloy with $K < 1$ according to this theory would be as shown in Fig. 90.

In the third case of complete or partial mixing of the liquid it has been shown by Pfann[72] that the concentration, C_S, of the solid is given by

$$C_S = K_E C_0 (1 - g)^{K_0 - 1}$$

where g is the fraction of the liquid that has solidified. The variation of C_S/C_0 with g is shown in Fig. 91 for values of K_E from 0.01 to 5. It can be seen that there is no steady state on any of these curves.

It is very difficult to apply the above formulae to a practical case of solidification. It has been shown that the

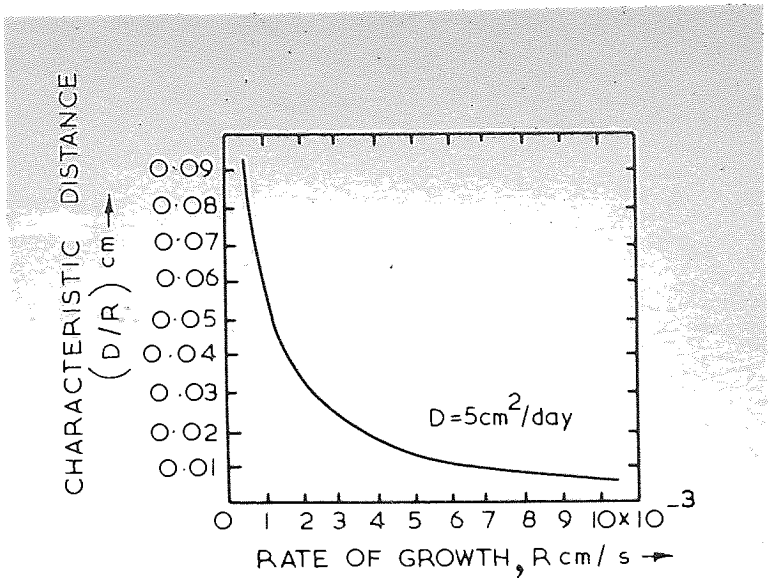

FIG. 89 Thickness of diffusion zone as a function of temperature.

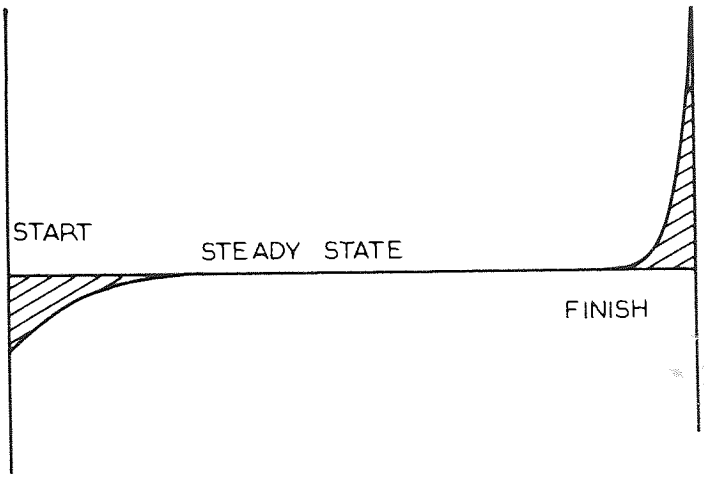

FIG. 90 Solute concentration during the solidification of an alloy with K < 1.

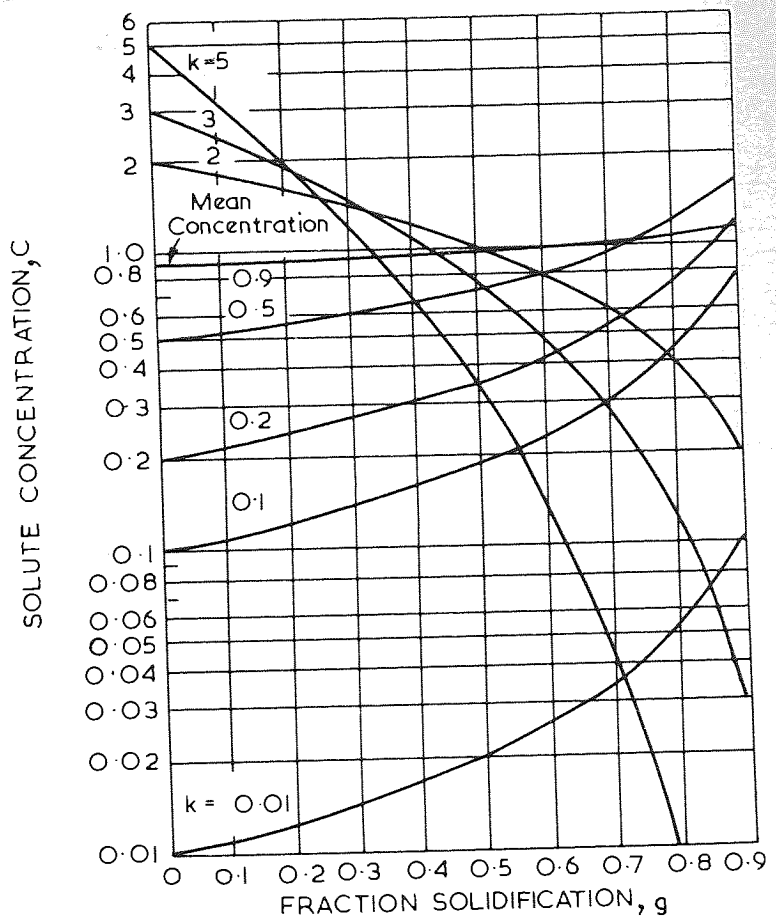

FIG. 91 The variation of solute concentration with the fraction of liquid solidified, g, after Pfann[72].

various equations have been formulated for a planar interface undergoing uniaxial solidification. In practice the interface is not planar and in the case of nodular cast iron, is spherical. Furthermore, solidification under conditions of constant heat abstraction proceeds by evolution of latent heat at a constant rate, i.e. a constant weight of solid is formed per unit time. This means that the growth rate R in cm/s decreases as solidification proceeds and the analysis of Tiller et al[71] becomes invalid. However, Kohn and Philibert[73] showed that the distribution of solute in the liquid was of the type predicted in Fig. 88 by X-ray micro-analysis of samples of an aluminium copper alloy quenched during solidification.

Malinochka[74] has recently forwarded some ideas on the reasons for microheterogeneity which differ from the established views described above. He relates segregation with the type of cooling curve of a binary alloy. Consider the cooling of an alloy of composition C_0 in Fig. 92 which has a cooling curve similar to the one illustrated, the first solid to form at temperature T_1 is of composition n'. The latent heat evolved heats the alloy to a certain temperature T at which the rate of heat extraction balances the rate of evolution of latent heat. During this steady state the composition of the deposited solid is n. Because the liquid is becoming enriched with solute the diffusion of A atoms becomes sluggish which slows down the rate of growth of the solid. Therefore the tempera-

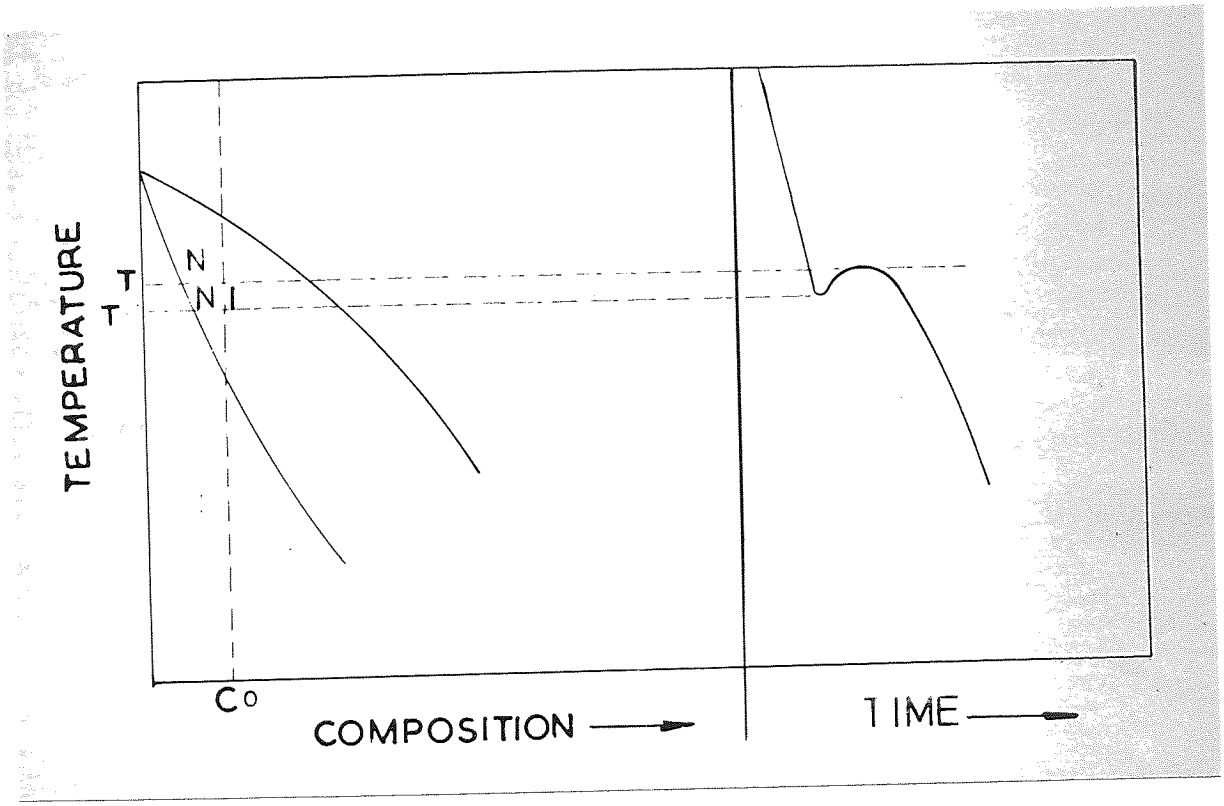

FIG. 92 Diagram taken from the work of Malinochka[74].

ture falls as is shown on the cooling curve. The composition of further deposited solid therefore follows the solidus line n n' until solidification is complete.

Although nodular cast iron is a eutectic alloy it has been shown previously that solidification of the austenite-graphite eutectic involves the growth of a sphere of austenite in contact with the liquid. Hence segregation will occur in the alloy in a similar fashion to that expected from solidification of a solid solution.

Quenching Experiments Having reviewed the theories of segregation it is now possible to discuss the results obtained from micro-analysis of the nodular iron specimens quenched during solidification. Figs. 73 to 76 show the results obtained from the commercial purity nodular iron. It is unfortunate that the solute distribution of the liquid prior to the quench is very difficult to assess due to the partitioning of solute elements between the ledeburite eutectic phases. However, it can be seen that the distribution coefficients of manganese, chromium and titanium in nodular cast iron is less than 1 while nickel and silicon have K_0 values of > 1. It is also noticeable that there is an initial steady state during solidification when the solute distribution in the solid is constant (samples 1 and 2) but the solute level of deposited solid begins to change from sample 3 onwards until solidification is complete. The cooling curve in Fig. 62 shows that during solidification of the 2 in bar the temperature arrest is maintained until the time at which

sample 3 was taken and then begins to fall from which it can be assumed that the rate of evolution of latent heat is at first constant and then slows down. The photomicrographs in Figs. 63 to 67 show that the linear growth rate of the eutectic cells is also much slower from sample 3 onwards. This change in growth rate is to be expected from the nature of solidification of nodular cast iron whereby the diffusion distance for carbon increases as the austenite envelope thickens.

There are no mathematical relationships to describe the predicted segregation behaviour in a growth sphere of solid solution with a varying growth rate. However, the explanation forwarded by Malinochka would account for the observed segregation behaviour of nodular cast iron as the solute content of the solid can be related to the cooling curve of the 2 in bar of nodular cast iron. Unfortunately there are no accurate equilibrium diagrams for this rather complex material from which the segregation behaviour of the various solute elements in a carbon-saturated austenite could be predicted.

It can be seen from the micro-analysis results that the distribution coefficients of manganese, chromium and titanium are less than unity and decrease in that order. The last liquid to solidify is rich in these elements, all of which are carbide stabilisers and therefore cell boundary carbide is formed in these areas.

The segregation results of the austenitic quenched samples provide an interesting comparison. The cooling curve obtained

from the austenitic 2 in bar (Fig. 77) did not show a temperature arrest similar to the one on the commercial purity nodular iron cooling curve but the temperature dropped increasingly faster from the start to the end of solidification. Figs. 78 to 80 show the distributions of nickel, manganese and silicon across the solid/liquid interfaces in samples quenched from various positions on the cooling curve of the austenitic bar. It can be seen from these curves that the solute content of the solid began to change at a much earlier stage of the solidification process in these specimens and only a very small portion of the first solid to form possessed a constant level of solute. This can be explained using Malinochka's arguments. The pattern of segregation in both materials examined can be seen to be related to the type of cooling curve exhibited by the material. In the austenitic material the diffusion of carbon in the liquid would be hindered by the high solute content of the liquid, e.g. Fig. 78 shows that at an early stage of solidification the liquid contains an appreciable quantity of manganese. This would mean that the growth rate of the solid would be hindered and that possibly the rate of evolution of latent heat of fusion would not balance the rate of heat extraction causing the temperature to fall. The distribution of the solute in the solid would thus show a corresponding change during solidification for reasons described above. Similarly, in the case of the "ferritic" nodular iron where a steady temperature arrest was maintained during the

initial stages of solidification a more pronounced region of constant solute composition was found.

Fig. 80 shows that no segregation of silicon occurred in the austenitic material which would suggest that in this material the equilibrium diagram is such that the distribution coefficient of silicon is unity.

Effect of Section Size and Heat Treatment Before discussing the effect of section size and heat treatment on microsegregation two important findings of these investigations will be dealt with. It has been stated[49] that the differential etching effect noticed at the grain boundaries in as-cast nodular irons is caused by cellular segregation and that a normalising treatment removes this effect by homogenizing the segregated as-cast structure[20]. It has been shown in this thesis that the segregation pattern of the as-cast material was unaffected by normalising although the differential etching effects were removed by this treatment. Metallographic examination of the as-cast pearlite revealed that the pearlite in the cell boundary regions was much finer than the rest of the matrix which caused it to appear darker at lower magnification. It is therefore suggested that in cell boundary regions due to the relatively large amounts of segregated elements the pearlite lammelae in the as-cast state are closer together than in the rest of the matrix and that a normalising treatment in refining the rest of the pearlitic matrix apparently removes this effect but does not re-distribute the segregated elements.

Gilbert[19] has suggested that the sub-boundary ferrite structure found in single annealed nodular iron specimens could be related to segregation of solute elements. It has been shown that no segregation that could be associated with these sub-boundary structures could be detected by micro-analysis in single annealed samples but this does not eliminate the possibility of microheterogeneities on too fine a scale to be detected by micro-analysis. However, the photomicrographs shown in Fig. 23 suggest a relationship between the structure of as-cast pearlite and the sub-boundary ferrite structure. It is difficult to provide an explanation of the formation of these structures in the as-cast state but it is obvious that a treatment in the austenitic range will remove them. It is felt therefore that this problem will not be solved by micro-analysis in its present state of development.

From the results of the quenching experiments it was concluded that a relationship exists between microsegregation and the type of cooling curve arrest. The effect of change in section on microsegregation has been demonstrated in the results where it was shown that an increase in section size resulted in increased segregation effects, particularly manganese segregation. This can be related to the larger austenite-graphite eutectic cell aggregates in thicker sections. Solidification in heavier sections is slower and involves fewer eutectic cells per unit volume. The cell boundary regions will therefore be much further apart than in smaller sections but greater amounts

of solute elements will accumulate in these regions as a result of the solidification process. This is apparent from the microstructures of the various sections of as-cast material where cell boundary carbides were much larger in the heaviest sections, particularly in the 4 per cent manganese austenitic iron where cell boundary carbides were much more pronounced in the 12 in section. Removal of segregation effects by heat treatment was more difficult in the heavier sections where carbides were larger and contained greater quantities of carbide stabilising elements. Hence in the 12 in section of commercial purity nodular iron undissolved carbides were still present in the microstructure after the spheroidise annealing treatment while no carbides were apparent in the $1\frac{3}{4}$ in keel specimens after the normal double anneal heat treatment.

RELATIONSHIP BETWEEN SEGREGATION AND MECHANICAL PROPERTIES

The results of these investigations show that segregation effects can influence the mechanical properties of ferritic nodular cast iron. The only property which is significantly affected is the ductile/brittle transition temperature and all other observed effects were caused by section variation rather than segregation behaviour. It has been shown that some segregation can be tolerated in smaller sections of nodular iron without any significant deterioration in mechanical properties. In heavier sections where segregation effects are more marked cell boundary carbides tend to lower the ductile/brittle transition of the material. Fig. 35 reveals a difference of

50°C between the notched impact transition temperatures of the $1\frac{3}{4}$ in keel specimens and 12 in bar specimens of double annealed commercial purity iron. This is the most significant influence of segregation upon mechanical properties in this material.

In the austenitic materials segregation was more apparent. In these irons large amounts of carbide were noticed in the heavier sections particularly in the D-2C "modified" specimens. It is difficult to say whether this carbide influenced the mechanical properties in the 0.5 per cent manganese material in the absence of a comparison with carbide free material. The drastic decrease in elongation with increasing section in the 4 per cent manganese iron, however, would seem to be related to the relatively large carbide content of this material.

It has been shown that segregation is a feature of the solidification process of nodular cast iron and it is difficult to prevent its occurrence in impure or alloyed materials. However, it has also been shown that extensive segregation only occurs towards the end of solidification. If the graphitic solidification of a nodular iron were interrupted in the early stages and the rest of the liquid solidified white to produce a mottled iron, it will be appreciated that this white iron would contain far less concentrations of carbide forming elements than the normal cell boundary carbide and would thus be easier to break down by heat treatment. However, it is

realised that white iron solidification introduces shrinkage problems which may offset the advantage of producing carbide free material.

CONCLUSIONS

1. Increase in section size results in a decrease in elongation and unnotched impact values of pearlitic and ferritic nodular cast iron. In the ferritic condition, at least, this has been shown to be related to change in graphite nodule size, shape and number with change in section.

2. Increase in section size results in a decrease in the elongation values of austenitic nodular cast irons. This was thought to be due, in part, to a change in graphite nodule shape, size and number but in higher manganese material an increased carbide content in heavier sections was thought to be partly responsible for these effects.

3. In as-cast nodular cast iron of commercial purity concentrations of chromium and manganese and depletions of nickel and silicon occur at austenite graphite cell boundaries and are often associated with carbides in these regions. These effects are shown to be due to microsegregation during the solidification process. Segregation effects are only partially removed by two-stage annealing heat treatments of 16 hours at 900°C followed by 48 hours at 690°C.

4. A normalising treatment of 6 hours at 900°C followed by air-cooling does not cause any significant redistribution of as-cast microsegregation but produces a more uniform microstructure due to its refining action on the pearlitic matrix.

5. A sub-boundary structure exists in the pearlitic matrix of as-cast pearlitic nodular cast irons. It is suggested that this structure is related to the sub-boundary ferrite structure obtained after sub-critically annealing as-cast pearlitic nodular irons.

6. In austenitic nodular cast irons manganese has been shown to concentrate into the liquid during solidification while nickel concentrates into the solid. Carbides formed from the last liquid to solidify as a result of microsegregation.

7. It has been shown that classical mathematical treatments of solute distribution cannot be applied to the segregation results obtained in this thesis. However, segregation in nodular cast irons can be related to the type of cooling curve of a given alloy in a manner which has been described.

8. Recent criticisms of the information obtainable from nodular iron samples quenched during solidification can be refuted from results obtained in this thesis. It has been shown that these samples are representative of the solidification sequences.

9. Graphite nodules and austenite envelopes have been shown to grow concurrently during the solidification of the nodular graphite eutectic.

10. A revised hypothesis for the solidification of the nodular graphite eutectic by liquid diffusion of carbon has been suggested from the results presented in this thesis. The revised model satisfies recent theoretical criticisms of the present solid state diffusion theory but is based on circumstantial evidence only.

ACKNOWLEDGMENTS

The author wishes to express his gratitude to the Director and Council of the British Cast Iron Research Association for making the facilities of the Association available and for financial assistance during the course of this thesis. Thanks are also due to Professor I. G. Slater of the Metallurgy Department, The University of Aston in Birmingham for allowing the use of the department's electron probe micro-analyser for this work.

The author is also grateful to Dr. J. A. Belk, Senior Lecturer in Physical Metallurgy at The University of Aston in Birmingham, who supervised this project, for his helpful guidance and encouragement and to Mr. I. C. H. Hughes, Assistant Director of the B.C.I.R.A. for his interest and valuable discussion.

Thanks are due to all members of the routine and investigations staff of the B.C.I.R.A. who assisted the author and to Mrs. R. Tarver for typing this thesis.

APPENDIX

MICRO-ANALYSIS CORRECTION FACTORS

Birks' Absorption Correction In this correction an intensity function $f(\chi)$ is plotted against χ which is defined by the formula

$$\chi = \mu \operatorname{cosec} \theta$$

where μ is the X-ray mass absorption coefficient and θ is the take off angle for X-rays.

The count ratio, K_A, is defined as

$$K_A = \frac{I_A}{I_{(A)}}$$

where I_A is the intensity of a particular X-ray line in the alloy under investigation and $I_{(A)}$ is the intensity of the line from the pure metal standard.

Birks' correction is applied as follows:

Consider the measurement of element A in a binary alloy of A and B.

The mass absorption coefficient for A radiation in pure A $= \mu_{AA}$.

" " " " " " " " " B $= \mu_{AB}$.

" " " " " " " "alloy AB $= \mu_{AX}$.

$$\mu_{AX} = \mu_{AA} W_A + \mu_{AB} W_B$$

where W_A and W_B are the respective weight fractions of A and B in the alloy.

$$\chi_{AA} = \mu_{AA} \operatorname{cosec}$$

$$\chi_{AX} = \mu_{AX} \text{ cosec } \theta$$

If values of W_A and W_B are known, or assumed, then values of χ_{AA} and χ_{AX} can be determined and hence values of the intensity function $f(\chi_{AA})$ and $f(\chi_{AX})$ can be read off a curve produced by Birks[61].

This method was used, in this thesis, to determine the absorption correction for nickel in iron as is shown below.

A weight fraction of 1 per cent nickel in iron is assumed as this is approximately the level of nickel in the ferritic materials.

$$W_{Fe} = 99\% \quad W_{Ni} = 1\%$$

For Ni Kα ..... $\mu_{Ni} = 61^*$ $\mu_{Fe} = 397^*$

* Values obtained from table produced by Phillips Scientific Equipment Ltd.

$\therefore$ μ alloy = 0.99 x 397 + 0.01 x 61 = 394

$$\text{cosec } \theta = 2.92$$

$\therefore$ $\chi_{Ni} = 61 \times 2.92 = 178$

χ alloy = 394 x 2.92 = 1147.6

$\therefore$ From Birks' curve $F_{Ni} = 92$ F alloy = 64.

$\therefore$ I calc = $W_{Ni} \times \frac{64}{92} = 0.695$

$\therefore$ To correct for absorption the recorded intensity must be divided by 0.695

Atomic number correction For silicon determinations in cast iron some correction must be made for the difference in atomic number between silicon and the base metal, iron. The correction used in this work is Castaing's second approximation which states

$$K_A = \frac{W_A \alpha_A}{W_A \alpha_A + W_B \alpha_B}$$

Therefore assuming a 2 per cent silicon alloy we have:

$$K_A = \frac{2 \times 8.04^*}{2 \times 8.04^* + 98 \times 7.08^*}$$

* Values obtained from information published by Poole and Thomas[64].

$$= 2.27$$

∴ To correct for atomic number the count ratio must be multiplied by $\frac{2.00}{2.27} = \underline{\underline{0.88}}$

Philibert's Absorption Correction Birks' $f\chi$ curve cannot be used for silicon corrections and hence the absorption correction devised by Philibert was used. Philibert has shown that $f\chi$ can be related to χ by the following formula:

$$\frac{1}{f\chi} = \left(1 + \frac{\chi}{\sigma}\right)\left(1 + \frac{h}{1+h} \times \frac{\chi}{\sigma}\right)$$

where $h = 1.2 \frac{A}{Z^2}$ A = atomic weight

Z = atomic number

The correction factor then required to relate the count ratio K_A with the weight fraction W_A is given by:

$$W_A = K_A \frac{f\chi_{AA}}{f\chi_{AX}}$$

where χ_{AA} refers to the pure metal and χ_{AX} to the alloy.

For the purpose of these investigations a weight fraction of 2 per cent silicon was assumed and the calculation was determined as follows;

$\underline{f\chi_{Si}}$

$$\mu_{Si} = 315 \times 2.92 = 920$$

$$\frac{1}{f\chi_{Si}} = \left(1 + \frac{920}{2550}\right)\left(1 + \frac{3}{1.3} \times \frac{920}{2550}\right)$$

(values of σ in these calculations have been obtained from tabulated data produced by Philibert).

$$\therefore \quad \frac{1}{f\chi_{Si}} = \underline{1.78}$$

$$\frac{1}{f\chi_{FeSi}} = \left(1 + \frac{5850}{2550} \right) \left(1 + \frac{0.26}{1.26} \times \frac{5850}{2550} \right)$$

$$= \underline{1.23}$$

$$W_A = K_A \frac{f\chi_{Si}}{f\chi_{FeSi}}$$

$\therefore$ for a 2 per cent silicon alloy.

$$2 = K_A \quad \frac{1.23}{1.78}$$

$$\therefore \quad K_A = .69$$

$\therefore$ Absorption correction factor $= \frac{2}{0.69} = \underline{2.9}$

$\therefore$ all count ratios must be <u>multiplied</u> by 2.9 to correct for absorption.

$\therefore$ <u>The correction factor for absorption and atomic number for a 2 per cent silicon alloy will be 2.9 x .88 = 2.55</u>

REFERENCES

1. MORROGH (H.) and WILLIAMS (W. J.)
   Journal of the Iron & Steel Institute, 1948, v.158, March, pp.306-322.

2. PFEIL (L. B.)
   Discussion to above paper, ibid., v.160, September, p.21.

3. WICKENDEN (T. H.)
   Transactions of the American Foundrymen's Society, 1948, v.56, p.88 (discussion).

4. MORROGH (H.)
   BCIRA Journal of Research & Development, 1952, v.4, April, pp.292-314.

5. CASTAING (R.)
   Ph.D Thesis, University of Paris, 1951. Publ. O.N.E.R.A. No. 55.

6. GILBERT (G. N. J.)
   BCIRA Journal of Research & Development, 1954, v.5, December, pp.470-472.

7. GILBERT (G. N. J.)
   BCIRA Journal, 1964, v.12, March, pp.170-193.

8. GILBERT (G. N. J.)
   BCIRA Journal of Research & Development, 1956, v.6, December, pp.430-435.

9. REYNOLDS (C. C.), ADAMS (C. M.) and TAYLOR (H. F.)
   Transactions of the American Foundrymen's Society, 1953, v.61, pp.510-515.

10. GILBERT (G. N. J.)
    BCIRA Journal, 1964, v.12, November, pp.791-807.

11. BARTON (R.)
    BCIRA Journal, 1961, v.9, September, pp.668-686.

12. GILBERT (G. N. J.)
    BCIRA Journal, 1964, v.12, November, pp.759-793.

13. PELLINI (W. S.), SANDOZ (G.) and BISHOP (H. F.)
Transactions of the American Society for Metals, 1954, v.46, pp.418-445.

14. REYNOLDS (C. F.) and TAYLOR (H. F.)
Transactions of the American Foundrymen's Society, 1952, v.60, pp.687-713.

15. HODGSON (C. C.) and FAIRHURST (W.)
Metallurgia, 1952, v.45, June, pp.283-288.

16. GILBERT (G. N. J.)
BCIRA Journal of Research & Development, 1953, v.4, February, pp.458-478.

17. CARR (A. C.) and STEVENS (W.)
International Foundry Congress, Paris, 1953, Paper No. 3, 20 pp.

18. VANDERBECK (R. W.) and GENSAMER (M.)
Welding Journal, 1950, v.29, January, pp.37s-48s.

19. GILBERT (G. N. J.)
BCIRA Journal of Research & Development, 1955, v.6, August, pp.11-15.

20. GILBERT (G. N. J.) and PALMER (K. B.)
BCIRA Journal of Research & Development, 1957, v.6, February, pp.498-504.

21. PETCH (N. J.)
Journal of the Iron & Steel Institute, 1953, v.174, March, pp.25-28.

22. COTTRELL (A. H.)
Paper presented at U.K.A.E.A. Conference on Brittleness in Metals, 1957.

23. SPENCER (C. W.) and WERNER (F. E.) editors
"Iron and its Dilute Solid Solutions", 1963, New York, Interscience Publishers. See especially: CONRAD (H.) pp.315-339.

24. JOHNSTON (W. G.) and GILMAN (J. J.)
Journal of Applied Physics, 1959, v.30, February, pp.129-144.

25. CONRAD (H.) and SCHOECK (G.)
Acta Metallurgica, 1960, v.8, November, pp.791-796.

26. AVERBACH (B. L.) et al editors
Fracture, 1959, New York, Wiley. See especially: KAZINCZY (F. de), BACKOFEN (W. A.) and KAPADIA (B.), p.65 (discussion).

27. PETCH (N. J.)
Paper presented at U.K.A.E.A. Conference on Brittleness in Metals, 1957.

28. ZENER (C.)
Fracturing of Metals, 1948, American Society for Metals, p.3.

29. STROH (A. N.)
Advances in Physics, 1957, v.6, p.418.

30. AVERBACH (B. L.) et al
Fracture, 1959, New York, Wiley. See especially: COTTRELL (A. H.), pp.20-44.

31. GILMAN (J. J.)
ibid., pp.51-53 (discussion).

32. HULL (D.)
Acta Metallurgica, 1960, v.8, January, pp.11-18.

33. HONDA (R.)
Journal of the Physical Society of Japan, 1961, v.16, July, pp.1309-1321.

34. COTTRELL (A. H.)
Transactions of the Metallurgical Society of A.I.M.E., 1958, v.212, April, pp.192-203.

35. AVERBACH (B. L.) et al
Fracture, 1959, New York, Wiley. See especially: PETCH (N. J.), pp.54-64.

36. PUGH (H. Ll. D.), CHANG (S. S.) and BORWICK (G. R.)
National Engineering Laboratory, 1959, October, Plasticity Report No. 154.

37. KRAFT (R. W.) and FLYN (R. A.)
1951, Cleveland, Ohio, American Society for Metals, 25 pp.

38. SEFING (F. G.)
New York University, Course on Ductile Iron, June 29 - July 3 1959, preprint of Lecture No. 25. Typescript 32 pp.

39. FRANSON (I. A.) and SCHELLENG (R. D.)
Transactions of the American Foundrymen's Society, 1962, v.70, pp.1095-1100.

40. RICKARD (A. J.)
Paper discussed at a Symposium on the Austenitic Cast Irons on October 25th 1962. 1963, London, International Nickel Co. (Mond) Ltd., 11 pp.

41. STEVEN (W.) and HAYNES (A. C.)
Journal of the Iron & Steel Institute, 1956, v.183, August, pp.349-359.

42. ABBOTT (W. K.) and COLOGGI (R. W.)
Transactions of the American Foundrymen's Society, 1962, v.70, pp.1196-1209.

43. HUGHES (I. C. H.)
Foundry Trade Journal, 1952, v.93, September 25, pp.349-356; October 2, pp.385-391; October 9, pp.417-420, discussion, pp.420-423.

44. MORROGH (H.)
Journal of the Iron & Steel Institute, 1954, v.176, April, pp.378-382.

45. LOPER (C. R.) Jr. and HEINE (R. W.)
Transactions of the American Society for Metals, 1963, v.56, March, pp.135-152.

46. DUNPHY (R. P.) and PELLINI (W. S.)
Foundry, 1952, v.80, January, pp.82-86, 195-196, 198-200.

47. GITTUS (J. H.) and HUGHES (I. C. H.)
BCIRA Journal of Research & Development, 1955, v.5, February, pp.537-554.

48. PARTHASARATHI (M. N.), SRIKANTIAH (B. S.) and NIJHAWAN (B. R.)
Transactions of the Indian Institute of Metals, 1951, v.5, pp.227-242; discussion p.243.

49. WITTMOSER (A.)
Foundry Trade Journal, 1953, v.94, May 14, pp.547-555.

50. VASCHENKO (K. I) and SOFRONI (L.)
Magnievii chugun (Magnesium Cast Iron), 2nd revised edition, 1960, Moscow & Kiev, State Scientific Publishing House, 485 pp. See especially: pp.1-81.

51. SY (A. de)
Foundry, 1953, v.81, November, pp.100-103, p.210, p.212, p.218, p.220.

52. HILLERT (M.)
Paper presented at Cast Iron Seminar, June 1964, Detroit.

53. TILLER (W. A.)
Gray and Ductile Iron Founders Society, Cast Iron Seminar, Cleveland, Autumn, 1964.

54. GILBERT (G. N. J.) and WHITE (D. G.)
BCIRA Journal, 1963, v.11, March, pp.199-222.

55. LÜDERING (H.)
Archiv für das Eisenhüttenwesen, 1964, v.35, February, pp.153-158. In German with summaries in English and French.

56. CHARBONNIER (J.) and MARGERIE (J. C.)
Fonderie, 1963, May, pp.161-175. In French.

57. CHARBONNIER (J.) and MARGERIE (J. C.)
Fonderie, 1963, November, pp.412-420. In French.

58. TURNER (R. W.)
BCIRA Journal, 1960, v.8, March, pp.238-246.

59. CAMBRIDGE INSTRUMENT CO. LTD.
Microscan X-ray analyser.

60. MARTON (L.) and MARTON (C.) editors
"Advances in Electronics and Electron Physics", 1960, New York and London, Academic Press, v.13, pp.317-386.

61. BIRKS (L. S.)
Journal of Applied Physics, 1960, v.31, pp.1297-1298.

62. PHILIBERT (J.)
Journal of the Institute of Metals, 1962, v.90, pp.241-252.

63. BELK (J. A.)
Birmingham College of Advanced Technology Technical Note Met/21/1964.

64. POOLE (D. M.) and THOMAS (P. M.)
Journal of the Institute of Metals, 1962, v.90, pp.228-233.

65. BELK (J. A.)
Birmingham College of Advanced Technology Technical Note Met/23/1964.

66. DUNCUMB (P.)
X-ray Optics and X-ray Analysis. Proc. Stanford Conference 1963.

67. ENSOR (T.)
Unpublished work at BCIRA.

68. SY (A. de)
Transactions of the American Foundrymen's Society, 1959, v.67, pp.486-492.

69. GRACE (R. E.) and DENGE (G.)
Transactions of the Metallurgical Society of A.I.M.E, 1958, v.212, June, pp.331-337.

70. KELLERMAN (C. R.) and LOPER (C. R.)
Transactions of the American Foundrymen's Society, 1964, v.72, pp.417-425.

71. TILLER (W. A.), JACKSON (K. A.), RUTTER (J. W.) and CHALMERS (B.)
Acta Metallurgica, 1953, v.1, July, pp.428-437.

72. PFANN (W. G.)
Zone Meeting, 1958, New York, Wiley, 236 pp.

73. KOHN (A.) and PHILIBERT (J.)
Les Mémoires Scientifiques de la Revue de Métallurgie, 1960, v.57, pp.291-312.

74. MALINOCHKA (Ya. N.)
Russian Castings Production, 1963, October, pp.473-476.